UNIVERSIDAD DE VALLADOLID

ESCUELA DE INGENIERIAS INDUSTRIALES

GRADO EN INGENIERÍA MECÁNICA

EVALUACIÓN DEL POTENCIAL DE IMPLEMENTACIÓN SISTEMAS DE CONCENTRACIÓN SOLAR EN MALTA

Autor

Ortega Recio, Diego

Responsable de Intercambio en la Uva

Dr. Francisco Javier Rey Martínez

Universidad de destino

University of Malta (UoM)

Valladolid, Febrero 2021.

TFG REALIZADO EN PROGRAMA DE INTERCAMBIO

TÍTULO:	**INVESTIGATING THE POTENTIAL OF IMPLEMENTING SOLAR CONCENTRATED SYSTEMS IN MALTA**
ALUMNO:	**DIEGO ORTEGA RECIO**
FECHA:	**12/02/2021**
CENTRO:	**INSTITUTE FOR SUSTAINABLE ENERGY**
UNIVERSIDAD:	**UNIVERSITY OF MALTA**
TUTOR:	**Dr. CHARLES YOUSIF**

Resumen

Este TFG evalúa la posibilidad de implementar sistemas de concentración solar en Malta para aumentar la producción de energía renovable. Aunque Malta tiene un espacio limitado, todavía hay múltiples espacios infrautilizados, como rotondas, donde pueden instalarse estos sistemas de energía renovable de alto rendimiento, aprovechando las condiciones climáticas tan favorables para ello.

Con el software ArcGIS se lleva a cabo un análisis espacial de Malta, mapeando e identificando todos los lugares posibles y determinando su potencial de radiación solar. Además, se realiza una búsqueda de los sistemas de concentración solar disponibles en el mercado, despuntando los sistemas CPV, y mediante el software PV F-Chart se modela la operación de estos bajo las condiciones climáticas de Malta, obteniendo la producción eléctrica de cada uno de ellos.

Finalmente, se comparan los sistemas y se calculan los resultados de su instalación, como número de casas alimentadas con su producción, emisiones de CO_2 evitadas...

Palabras Clave: Malta, CSP, CPV, ArcGIS, PV F-Chart.

Abstract

This thesis evaluates the potential of implementing solar concentrated projects in Malta to improve the renewable energy share. Although Malta has limited space, there are still a number of under-utilised sites that can be used for installing high revenue renewable energy systems such as solar concentrators, while taking advantage of the favourable climate conditions in the whole country for it.

The dissertation uses state-of-the-art ArcGIS software to map and identify all sites suitable for such installations. A spatial analysis of the solar radiation potential was also carried out, considering topographical features, which may impact the solar resources.

Meanwhile, a search for existing solar concentrator technologies in the market was carried out, which lead to the favourable consideration of CPV systems.

Specialised software such as PVF-Chart was used to model the output of these earmarked CPV systems, which lead to the calculation of the potential renewable energy production and the results of their installation.

Key Words: Malta, CSP, CPV, ArcGIS, PV F-Chart.

INVESTIGATING THE POTENTIAL OF IMPLEMENTING SOLAR CONCENTRATED SYSTEMS IN MALTA

Diego Ortega Recio

Institute for Sustainable Energy

University of Malta

B.Sc.   February 2021

INVESTIGATING THE POTENTIAL OF IMPLEMENTING SOLAR CONCENTRATED SYSTEMS IN MALTA

by

Diego Ortega Recio

Supervised by Dr. Ing. Charles Yousif

Co-supervisor Dr. Therese Bajada

A dissertation presented at the

Institute for Sustainable Energy of the University of Malta (UoM), Marsaxlokk-Malta

in partial fulfilment of the requirements for the degree of

Bachelor of Mechanical Engineering

at the

Universidad de Valladolid (UVa), Spain,

under the Erasmus Plus Student Exchange Programme 2020/21.

DECLARATION

No portion of the work referred to in the dissertation has been submitted in support of

an application for another degree or qualification of this or any other university or other

institute of learning.

Signature of Student   Name of Student

                                                                        Diego Ortega Recio

_____   _____

ABSTRACT

The drive to generate locally produced renewable energy has been the most favourable option for the European Union to achieve its renewable energy targets for 2020 and beyond. Malta has failed to achieve its 10% renewable energy share by the end of 2020 and now it must purchase additional renewable energy from other Member States to cover this deficit on an annual basis.

This dissertation has been motivated by the fact that although Malta has limited space to install renewable energy systems, there are still a number of under-utilised sites that can be used for installing high revenue renewable energy systems such as solar concentrators, while taking advantage of the favourable climate conditions in the whole country for this type of technology.

To fulfil this purpose, the dissertation has embarked on an extensive research approach using state of the art ArcGIS software to map and identify all possible sites along arterial roads, which may be suitable for such installations. A spatial analysis of the solar radiation potential has also been carried out, taking into consideration all existing topographical features, which may impact the availability of the solar resources, for example due to shading in all of the earmarked sites.

Over 170 potential sites were found in Malta, which were then reduced to 40 best sites for further application. Meanwhile, an extensive search for adaptable and existing solar concentrator technologies were carried out, which lead to the elimination of Stirling Engine solar concentrators and the favourable consideration of concentrated photovoltaic systems.

Specialised software such as PVF-Chart was used to model the output of these earmarked CPV systems, which eventually lead to the calculation of the potential renewable energy production of at least 5,725 MWh/year, which covers the needs of 519 dwellings, and contributing by 0.311% of the total electrical energy consumption in 2018. The resulting carbon dioxide emissions avoidance potential is that of 3440 tonnes per year. This will contribute to towards achieving Malta's commitment to further its renewable energy portfolio.

KEY WORDS - Malta, Solar concentration, CSP, CPV, ArcGIS, PV F-Chart.

TABLE OF CONTENTS

ACKNOWLEDGEMENTS

First and foremost, my heartfelt thanks goes to my supervisor Dr. Ing. Charles Yousif for providing me with this project's idea about renewable energies and especially for his continuous kindness, dedication, commitment and encouragement, especially during the COVID-19 pandemic. His valuable advice and guidance are greatly appreciated.

I also wish to express my deepest gratitude to my co-supervisor Dr. Therese Bajada, for her expert advice on ArcGIS, without which this dissertation would not have been completed successfully.

Secondly, I would like to recognize my parents, family and friends for the invaluable assistance and support that they all provided me during my whole Bachelor's degree and especially during this period in Malta.

Last, I would like to thank both, the University of Valladolid (UVa) and the University of Malta (UoM) for allowing me to come to study-abroad during a whole semester under the ERASMUS+ programme, which has been an enriching experience not only academically, but also in many other aspects of my personal life.

LIST OF FIGURES

LIST OF TABLES

X

LIST OF ABBREVIATIONS

C

CF	Capacity Factor
CS	Coordinate System
CPC	Compound Parabolic Concentrator
CSP	Concentrated Solar Projects
CTR	Central Tower Receiver

D

DNI	Direct Normal Irradiation
DPS	Dense Particle Suspension
DSM	Digital Surface Model
DTIRC	Dielectric Totally Internally Reflecting Concentrator

E

EU	European Union

F

FLC	Fresnel Lens Collector
FMSC	Fixed Mirror Solar Concentrator
FPC	Flat Plate Collector

G

GCS	Geographical Coordinate System
GDP	Gross Domestic Product

H

HCPV	High Concentrated Photovoltaics
HFC	Heliostat Field Collector
HTF	Heat Transfer Fluid
HTM	Heat Transfer Model
HSC	Hyperboloid Solar Concentrator

L

LCOE	Levelized Cost Of Electricity
LCPV	Low Concentrated Photovoltaics
LFR	Linear Fresnel Reflector

M

MCPV	Medium Concentrated Photovoltaics
MITA	Malta Information Technology Agency
MS	Member State

N

NIR	Near-Infrarred

O

OSM	Open Street Map

P

PSA	Almeria Solar Platform
PTC	Parabolic Trough Concentrator
PV	Photovoltaics

R

RE	Renewable Energy
RF	Radio Frecueny

S

SBS	Spectral Beam Splitting
SET	Strategic Energy Technology
STE	Solar Thermal Electricity

T

TES	Thermal Energy Storage
TIR	Total Internal Reflection

W

WGS	World Geodetic System
WRC	World Radiation Centre

CHAPTER 1: INTRODUCTION

By 2050, the Sun could be the main source for energy surpassing other fossil fuel sources. This will be supplemented with other alternative sources such as wind, hydro biomass and nuclear power. Concretely, solar thermal concentrated power systems would generate up to 10% of the total energy production worldwide and this would avoid the emission of millions of tonnes of carbon dioxide (CO_2) each year [1].

The European Union (EU) is committed to reach zero CO_2 and greenhouse gas emissions by 2050 [2], with an intermediate target of 40% reduction by 2030 [3]. To achieve this objective, the EU through its Strategic Energy Technology (SET) Plan is impelling research, development and innovation of non-nuclear and low carbon energies to achieve "safe, clean and efficient energy" [4]. In doing so, it will support the transition to a profitable, sustainable, competitive and reliable energy system through the cooperation of all Member States (MS) and in so doing, bring the EU to the forefront as a world leader in utilising and exporting low carbon emission technologies.

The outgoing EU Directive 2009/28/EC has stipulated specific objectives to be achieved by the EU by the end of 2020, namely [5]:

- 20% of total EU energy amount must proceed from renewables.
- Energy efficiency should be improved in 20% from 2005 levels.
- Greenhouse gas emissions should be cut at 20% from 1990 levels.

For achieving this purpose, each MS had a different target to achieve in terms of renewable energy contribution, which depended on a number of factors such as the gross domestic product (GDP) and the renewable energy penetration levels in 2005 in that particular country. With reference to Malta, the percentage targets were set as [6]:

- Greenhouse gas emissions cannot increase more than 5% from 1990 levels.
- Total energy consumption coming from renewables should be around 10% from 2005 levels.
- Energy efficiency should be improved in 27% from 2005 levels.

Initially, 10% RE contribution could seem a poor target but to understand this digit it is necessary to consider a few points. Malta is an archipelago composed of five islands located in the middle of Mediterranean Sea between north Africa coast and Italia. This

condition makes it the smallest EU MS not only in population with a total amount of 514,564 inhabitants but also in area with an overall span of 316 km^2. Conversely, it is the highest densely populated country in the EU with 1,633 inhabitants per km^2.

One of the main economic activities of the country is related to tourism with total incoming tourists equivalent to triple the total current population, most of whom arrive during the summer months. This directly impacts on energy services and infrastructure, and this is one of the reasons why the electricity generation infrastructure is designed to be oversized and flexible. The maximum power generation in Malta has been reported as reaching 465 MW (August 2018) [7] but the total installed power, including a 200-MW undersea cable connection to Sicily, Malta, is close to 737.8 MW, i.e. an oversizing of more than 1.5 [8]. With regards to flexibility, the new power station comprises of four different power stations that can be run according to demand.

Taking a look at Figure 1 which shows the percentage of energy consumed by sector in 2018, it is clear how the tourism activity affects the consumption of energy, making transport and commercial and public services the two foremost consumers [9]. In fact, energy demand is increasing every year at the rate of 2.23% as shown in Figure 2 and Malta has registered the highest increase in energy consumption last year, when compared to other European MS [10].

Energy consumption by sector in 2018.
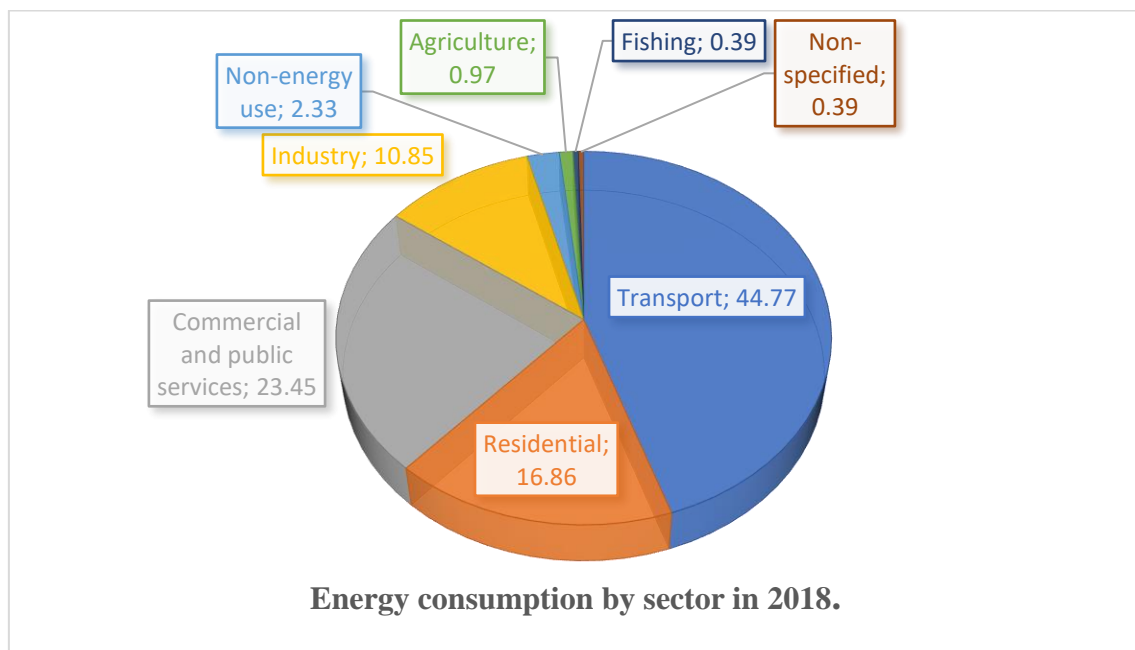
Figure 1: Percentage share of energy consumed by sector in 2018 at Malta [data from 9].

2
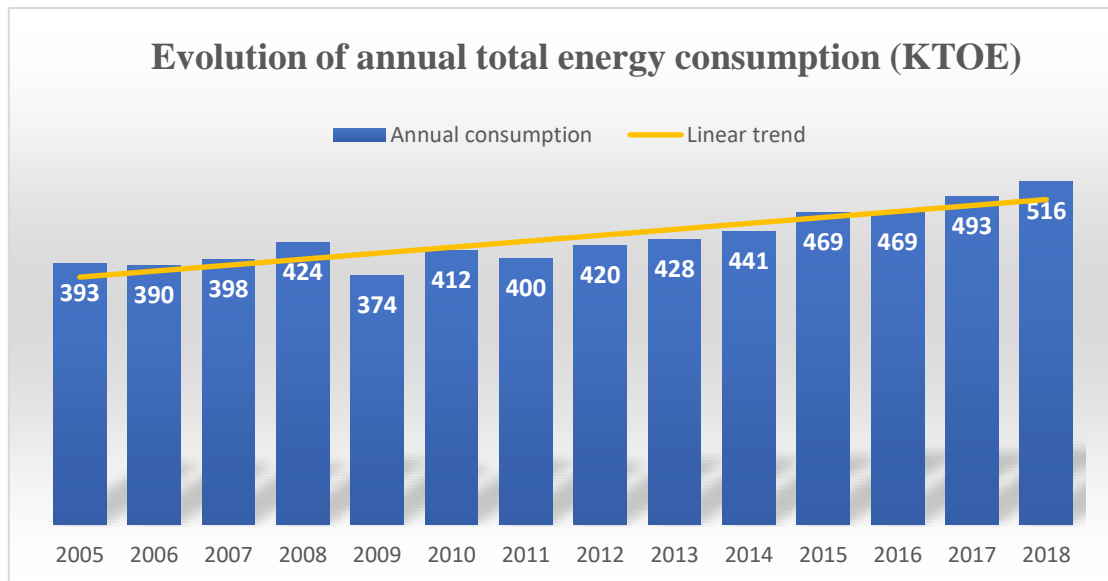
Figure 2: Evolution of annual total energy consumption in Malta [data from 9].

Other factors that weigh down on the energy system in Malta is the lack of a gas pipeline interconnection and distribution network and lack of indigenous fossil fuels resources. Therefore, the level of energy vulnerability of Malta is very high, as reported by the World Energy Council's Trilemma Index. In 2020, Malta scored the lowest rank of D for energy security [11].

However, improvement to energy security has been made in recent years. For example, the share of renewable energy and in particular, solar photovoltaics has been steadily increasing over the years and is reported to have reached 8% of the total energy consumption in 2018. Also, given that new power stations burn natural gas, the overall efficiency has doubled, which means that the fuel consumption in these power stations has dropped, as shown in the Figure 3 [9].
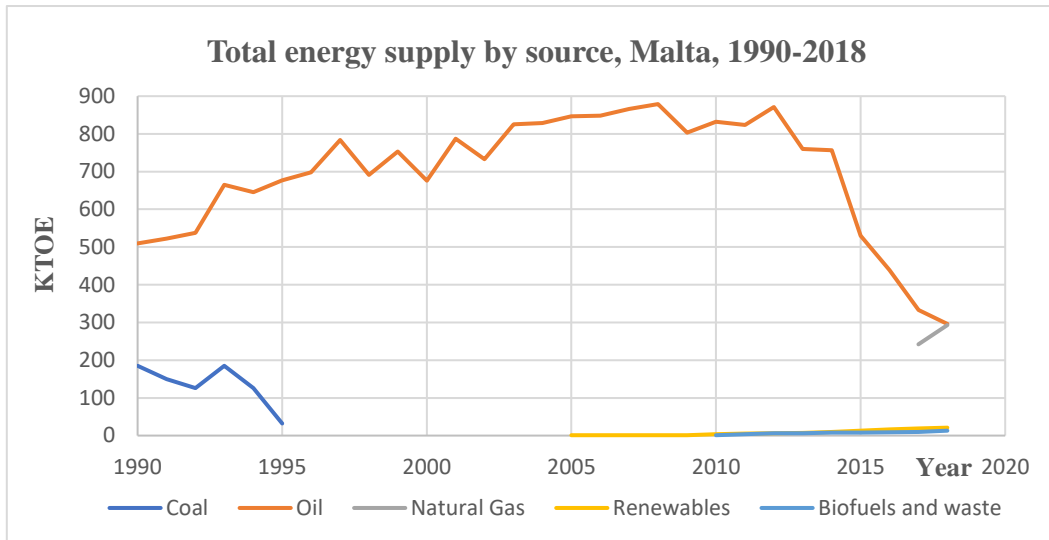
Figure 3: Total energy supply for power generation by source in Malta (1990-2018) [data from 9].

Most of the solar photovoltaic installations are rooftop systems mounted on private residential roofs and several commercial and public spaces like car parks, commercial centres or disused quarries. PV technology has become popular by time, especially due to the strong incentives offered by the Maltese Government, part-financed by EU funds. A total production of 217.3 GWh have been achieved in 2018, which has been generated by 151,473.9 kWp installed PV systems [12]. Figure 4 shows the total installed PV systems in kWp by locality. It is seen that the highest installations are in the localities of Marsa, Qormi, Naxxar, Mosta, Zejtun and Birzebbugia, followed by localities in the south-west and Gozo.
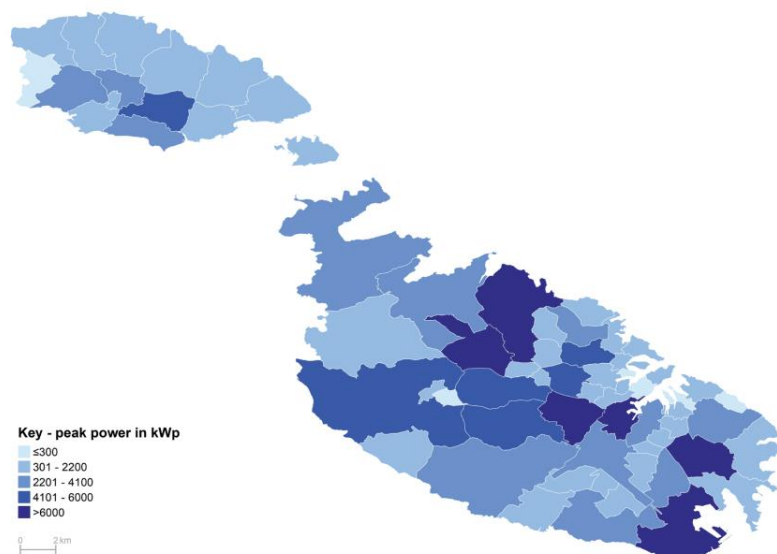
Figure 4: Total kWp of PV systems installed by locality in Malta in 2019. [12]

The installation of PV systems is also popular because Malta is one of the countries with the highest solar radiation potential across Europe, as shown in Figures 5 and 6, which is at the same level as that in Almeria, the South of Spain and the coastal regions of Cyprus.
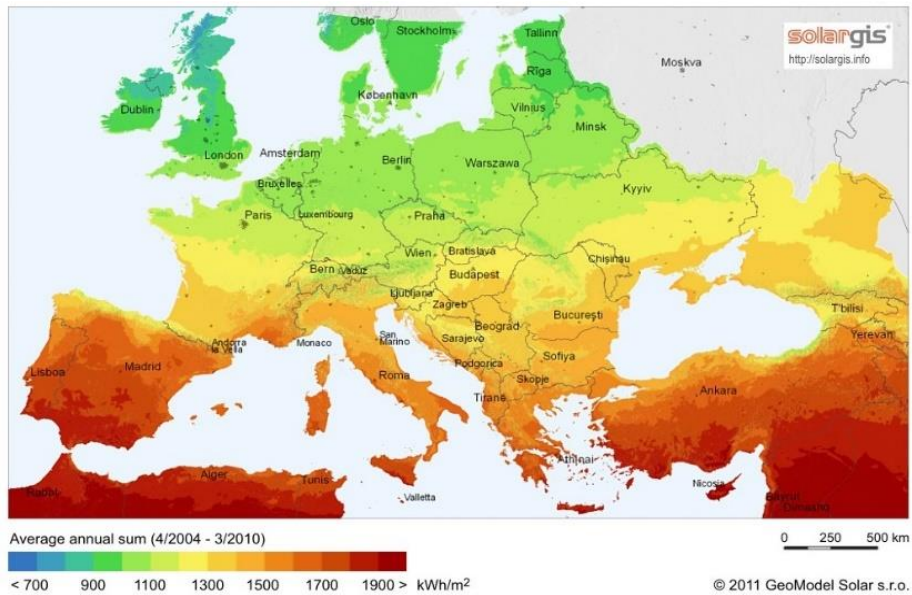
Figure 5: Global horizontal irradiation on Europe [13].
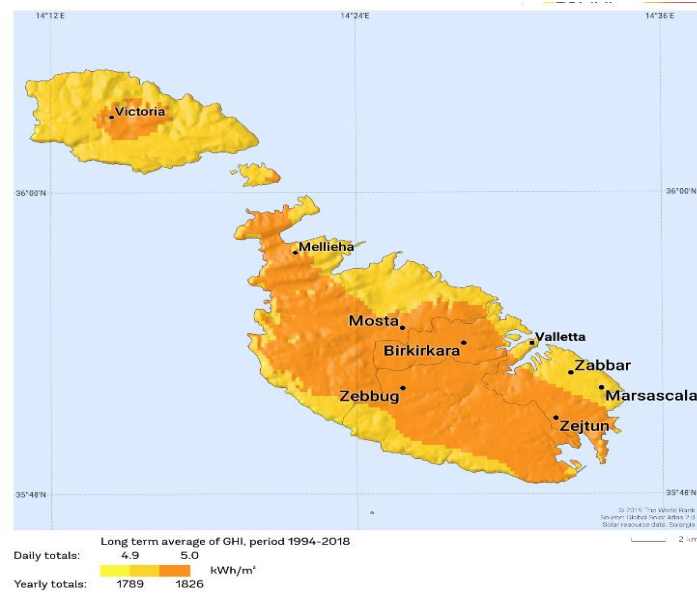
Figure 6: Global horizontal irradiation for Malta [13].

On the other hand, the widespread use of solar photovoltaics is jeopardized by the limited space available free of shading and scarce land area, while the regulations of the Planning Authority for rooftop photovoltaics as of 2015, severely limit the optimum installation of such system, given that no solar PV modules can be installed higher than 1 metre above roof level [14]. As a result, Malta will not be able to reach its 2020 RE target of 10% but may achieve 8.5%, according to a 2018 EU report, which shows Malta having the second lowest deployment of RE within the EU after Netherlands. The remaining 1.5% will have to be achieved through statistical transfer from other EU MS that have an excess of RE, such as Estonia [15].
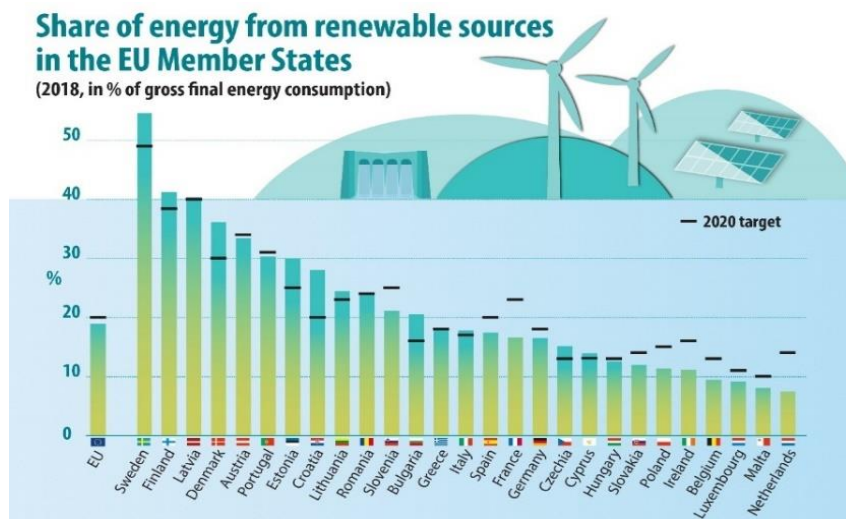
Figure 7: % of final energy consumption produced by renewable sources in the EU Member States in 2018 [16].

Given this deficiency in RE generation, the rationale of this dissertation is to identify any additional opportunities where solar concentrated systems can be exploited in Malta to supplement the renewable energy generation, improving the energy infrastructure as well as making it possible to contribute more to future targets set by EU. An overview of all possible concentrated solar options will be studied and analysed, while taking into consideration all limitations and space availability in Malta.

1.1   Aims, objectives and structure

1.1.1 Aims

The main aim of this dissertation is to:

> Study the viability of installing distributed solar concentrated systems in confined spaces such as roundabouts or car park corners.

1.1.2 Objectives

The objectives of the dissertation will consider:

- To analyse the spatial availability of potential areas suitable for the installation of solar concentrated systems in Malta, using appropriate GIS software.
- To identify feasible solar concentrated systems following a detailed research and analysis of the state of the art of such systems.
- To estimate the energy generation potential of each identified concentred solar technology, when operating in the Maltese weather climate.
- Identify the best-case scenarios for applying solar concentrated systems for Malta and estimate their potential contribution towards the RE target and CO_2 reduction.

1.1.2.1 Justification of objectives

The improvement in solar concentrated systems across the years has been dramatic both in the mega-scale systems as well as the modular systems, which can even fit on rooftops. Therefore, the consideration of concentrated solar power systems for energy generation could assist the widespread use of flat-plate solar collectors and collectively achieve a higher renewable energy target for Malta.

Given that space is valuable in Malta, one will need to think outside the box to try and maximize the use of available spaces. In so doing, one has to be sensitive to the needs of society and strive to make full use and to some extent double use of the available sites that can house concentrated solar power systems. In other words, when a site is considered as suitable for such installations, it should not limit the original use of the site for other purposes.

The achievement of the objectives will be carried out in a scientific manner using well-established spatial planning tools and modelling software. In so doing, one will take into

consideration the spatial aspects of the site such as the existence of trees, construction or other obstacles in order to realistically evaluate the potential. Moreover, modelling software that will calculate the expected output from such installations will accurately consider the effects of shading on the systems.

On the other hand, not every concentrated solar power system will be suitable for Malta. Therefore, it becomes apparent that the available systems need to be carefully scrutinised in order to make objective comparisons to choose the most preferable or the one with more benefits. The comparisons will be done in a way to ease the comprehension of technical issues and other parameters to highlight the suitability of each system in a user-friendly manner (e.g. by use of a range of colours to classify the features of each concentrated solar technology).

The final result obtained will answer the aim of this dissertation based on a scientific approach to provide a complementary solution for improving renewable energy generation in Malta.

1.1.3 Structure

The project has the following chapters:

- Chapter 1: Introduction. Brief overview on Malta's energy system and other different topics and general analysis of its current situation from an energetic side as well as background about EU targets and purposes. The main aim, objectives, justification of the study and structure of the dissertation is depicted.
- Chapter 2: Literature review and its relevance to this research work. Concentrated Solar Power (CSP) operation, types, available models and emerging technologies will be explained.
- Chapter 3: Methodology will delve into all the aspects and approaches to be used to achieve the objectives. This will include detailed explanation of the tools to be used as well.
- Chapter 4: Results and Discussion will cover all the relevant outcomes of this work and put them into perspective vis-à-vis the main aim of the project.
- Chapter 5: Conclusion and Recommendations will cover the main deliverables of this project and highlight any limitations, while recommending future developments in the research aspects of this topic.

CHAPTER 2: LITERATURE REVIEW

2.1   Concentrated Solar Power (CSP)

Concentrated Solar Power (CSP) or otherwise called Solar Thermal Electricity (STE) is a type of renewable energy, which consists in concentrating direct beam solar radiation into one point using concentrators. Solar thermal concentrators are systems based on mirrors or lenses which reflect or re-direct the sunlight concentrating all onto a small area called receiver. On the receiver a high-temperature heat source is thus created. This conversion is facilitated by the presence inside the receiver, of a heat transfer fluid (HTF) which heats up with the concentrated incident light.

The temperature can reach up around 3,250K, but so far technology can only use temperatures around 1,250K, because higher temperatures overcoming this amount, would fundamentally provoke the receiver to melt [17].

Electricity is then generated when the heat boils water to generate steam and drive an electrical generator, although it is also able to work powering a thermochemical reaction. The common thermodynamic cycles employed in this type of renewable energy are Rankine, Stirling and Brayton cycles.

The asset for CSP plants, devices and technology is the feasibility of incorporating thermal storage systems or fast action batteries to store the energy in the form of heat, either latent or as sensible, which allows the plant to continue generating electricity during hours when there is lack of solar radiation or at night. It is harder to store electricity than to store heat, so this gives CSP a huge competitive edge. Molten salt TES can be heated and cooled daily for at least 30 years, unlike batteries that can only be cycled limited times. After this period, the tanks may need to be repaired due to corrosion issues, so the molten salt would be removed and then turned back to the tanks to operate again during some more years.

However, the best option for storage seems to be a combination of both of them (thermal storage and batteries), in order to reduce the start-up time of the power plant during emergencies and power ages, thus increasing the plant's capacity factor. This fact makes CSP a flexible and dispatchable source of energy.

It is remarkable to mention too the possibility of setting up hybrid projects that include both solar PV and CSP technology for lower levelized costs of electricity (LCOE), by

handling inexpensive solar PV generation through daylight hours and CSP with TES during night or daylight hours with poor irradiance.

2.1.1 Global overview of CSP systems

Growth of CSP was hindered by a number of circumstances, although the technology has been in existence since the 1980s. Factors such as competition from other low-cost renewable technologies such as wind and solar PV, global economic slowdown resulting in lack of finance, high cost of capital, and lack of specific favourable policies providing government support.

However, in the last decade, CSP growth has been astonishing, with global CSP capacity growing by 11% in 2019 when 600 MW capacity was added online in one year. This brings the total installed capacity 6,200 MW in 2019 compared to 354 MW in 2005. Half of this total capacity is installed in Spain (2,300 MW), as shown in Figure 8 [18].
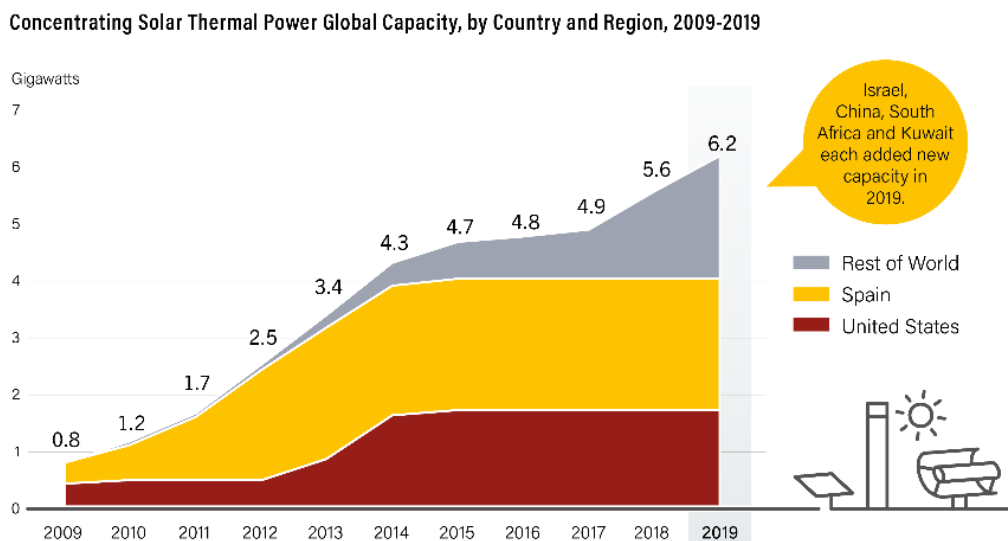
Figure 8: CSP global capacity upgrowth from 2009 to 2019 [18].

CSP has also made an impact on TES systems for electrical power generation. Figure 9 shows that interest in TES systems has been increasing with planned projects coming online in the next few years, thanks to EU subsidies favouring energy storage systems.
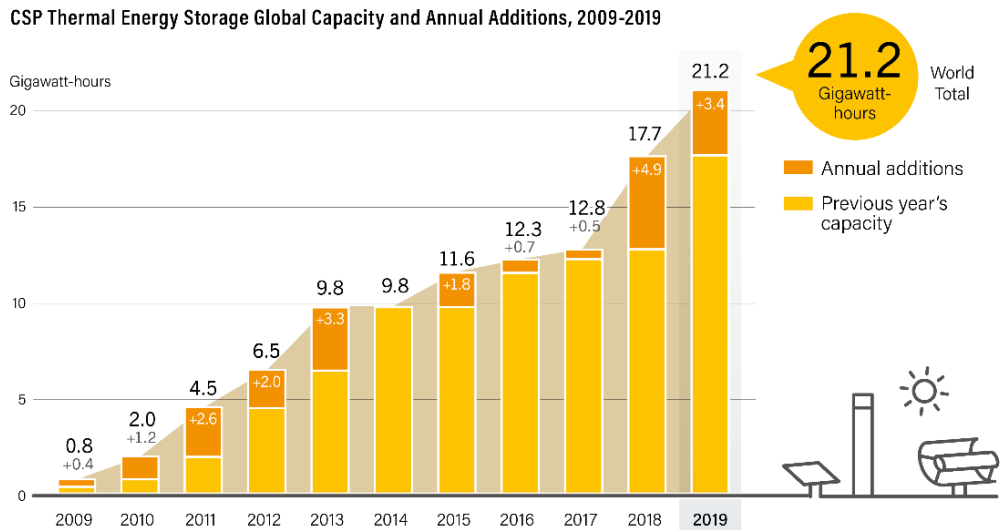
Figure 9: Global CSP storage capacity and annual additions2009 to 2019 [18].

In fact, considering data from 2018 [19] as can be seen in Figure 10, of the 5.6 GW active CSP capacity, around 3 GW is without storage and around 2.6 GW is with energy storage. In contrast, the CSP projects undergoing construction, only 4.2% are without storage, with a 95.8% of the upcoming capacity having storage.

As shown in Figure 10, the bulk of active CSP projects with storage have a TES capacity in the range of 6-10 hours. In the case of the newly developed CSP storage, a storage of 10-13 hours represents the 62.8% being 14% of over 13-hour storage. This shows how project developers and owners are given an increased importance to long hours of storage, to provide grid stability as well as reliable power during all day at reduced levelized cost of energy (LCOE), thanks to energy storage.
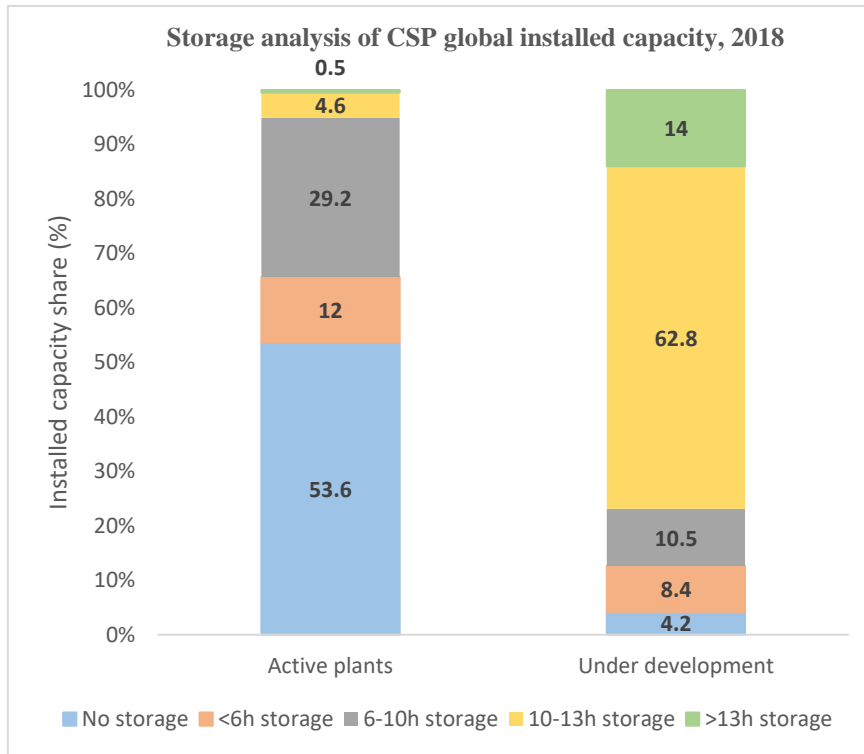
Figure 10: CSP global market, installed capacity with and without storage, 2018 [data from 19].

In terms of concentrator systems and technology, parabolic trough plants were initially dominating the market worldwide, being the oldest and most widespread CSP technology, accounting about 90% of CSP plants at one point. Beginning from 2010, the central tower receiver has been favoured in newest plants as result of its higher operation temperature up to 838K vs 673K, the trough's maximum, which ensures better efficiency [20]. In 2019, as much parabolic trough capacity as tower capacity were completed, an unprecedent situation [18]. The LCOE from CSP is declining, to get lower costs and raise capacity value CSP technology is being built increasingly alongside both wind power and solar PV. 18.5$/MWh, the CSP global weighted average LCOE in 2018, was 46% lower than in 2010, and 26% lower than it was in 2017 just as a 2019 study has estimated [18].

On the other hand, for CSP plants, compared to onshore wind energy and solar PV, the O&M costs that include insurance and other management costs are considerable. In the past, a major part of costs was spent on maintaining or replacing mirrors and receivers, but due to the advancements in technology, most of the O&M are used to cover insurance costs. For CSP plants in operation today, the typical O&M costs is in the range 0.02$/kWh to 0.04$/kWh. One IRENA analysis found that, in 2019, about 18% of the LCOE in CSP technology for G20 countries was averaged by Q&M costs. Data in the IRENA Auction

and PPA Database shows that for CSP projects to be commissioned in 2020 and 2021 electricity will have a weighted-average price of between 0.075$/kWh and 0.094$/kWh. Compared to the global weighted-average project LCOE in 2019, this price represents a reduction of 48% to 59%, thus increasing the competitiveness of CSP projects compared to fossil fuel alternatives [21]. In addition, when taking a look on Figure 11, it can be seen that the LCOE of CSP has the most significant reduction of all renewables, when comparing the year 2012 to that of 2020.
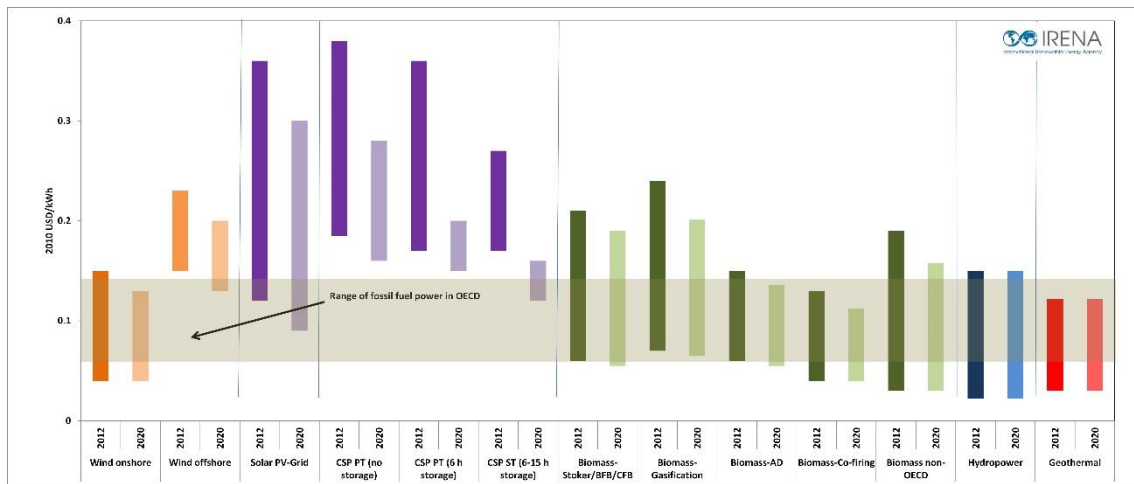
Figure 11: Evolution of typical LCOE costs ranges for renewable power [22].

An area equal to one km^2 of desert receives solar energy equivalent to 1.5 million barrels of oil, according to the 'Trans-Mediterranean Renewable Energy Corporation' (TREN). Through an estimation is known that, the total amount of electricity consumed worldwide in the year 2000 could be produced whether CSP plants were installed in a total dessert area about 1% of the Sahara Desert, ergo 65,000 km^2 [23]. European Union's current electricity consumption could be produced with just one fifth of this area.

2.1.2 Advantages and disadvantages of CSP

In general nowadays, CSP can be considered a clean and reliable energy with an important number of advantages and reasons to consider it as a huge renewable energy system for the future. The advantages are:

> ➢ Thermal storage allows quick sourcing of renewable power on demand, usually within half an hour from outage.

> ➢ Avoid fluctuations on the power grid.

> ➢ Dry, wet, and hybrid cooling techniques can be utilized in CSP systems to maximize efficiency in water conservation and electricity generation.

> ➢ In large-scale projects, the comparison between TES (CSP) and battery storage (PV) evidence a lower price for CSP than PV.

However, CSP presents some disadvantages that should be mentioned:

> ➢ Large projects need to be provided with financial support.

> ➢ Needs large spaces.

> ➢ CSP only operates in areas where beam direct solar radiation is high. To obtain the economic viability of CSP plants at today's rates, the direct normal irradiance should be at least 2000 kWh/m^2/y [17].

> ➢ Access to water resources for cooling and cleaning of mirrors/lenses is essential.

> ➢ Possibility of leakage of the high temperature fluid may contaminate the soil.

2.1.3 Heat transfer fluids (HTF)

As it has been aforementioned, in CSP a thermal energy carrier known as the heat transfer fluid (HTF) is the responsible of collecting the heat from the receiver. The HTF can transfer heat to another fluid known as the cycle fluid within a heat exchanger or can be used to directly drive a turbine for production of power. To generate higher thermal performance which results in higher solar to electrical efficiency, HTF plays a vital role.

Desired properties and characteristics of a HTF are: high boiling point, low vapour pressure (<1 bar) at high temperature, high energy storage heat capacity, , high thermal conductivity, low corrosion when the HTF is contained into metal alloys, low melting point and thermal stability, low viscosity, and low cost. Different types of materials can act as HTFs depending on the general purpose of the installation:

1. **Water or 'dry steam':**

Using water as a HTF is problematic as its pressure increases significantly with temperature and in high temperature or pressure situations can prove unstable and difficult to manage. In spite of this, its use is one of the most common which generally,

returns the greatest efficiency when a steam turbine is used, because it avoids efficiency losses and extra costs in the exchanger. On the other hand, when water is heated up to well above boiling point a super-heated form of steam is produced, the 'dry steam'. One disadvantage of using steam is that it does not perform well with thermal storage, so excess heat to heat a storage reservoir cannot be efficiently used by a steam installation.

2. Organics:

These fluids have higher thermal performances. Therminol VP1 is commonly used. It is a two very stable organic compounds eutectic mixture, Diphenyl-oxide ($C_{12}H_{10}O$) and Biphenyl ($C_{12}H_{10}$).

3. Molten salt:

It is widely used for reaching higher temperatures up to 725K because of its excellent properties:

- Good physical and thermal properties when working at high temperatures
- Low corrosive property and low vapour pressure
- High heat capacity

A mixture of 40% KNO_3 and 60% $NaNO_3$ is the composition of the most common molten salt used as HTF. A fairly low melting point (500K), as well as a high boiling point (around 873K) [17] characterize this compound.

The general advantage of the majority of molten salts is their high melting point. However, during winter salt usually crystallises or freezes and blocks the pipelines. To avoid these issues, auxiliary safety arrangement needs to be provided which increase operational and investment cost. Moreover, the use of molten salt as the initial heat transfer fluid is highly desirable because it is the medium commonly used to store any excess heat produced by a CSP plant within a storage reservoir.

4. Oil:

Oil is the most widespread together with water/dry steam. This can be synthetic oil or mineral oil. One disadvantage of using oil is that it disintegrates at temperatures above 673K thus limiting the efficiency of the CSP plant.

5. Liquid metal:

Some metal alloys are being studied as possible HTF's. Main features searched must include non-corrosive, remain stable above 1273K and a freezing point below 373K [17].

6. Inert gases:

Other alternatives for HTF are sCO_2, helium, air etc. because they eliminate the corrosion and thermal decomposition problems and enable the direct use of the gas in the turbines or thermal engines. The use of air provides the following advantages:

- ➢ Easy operation, maintenance and high dispatchability.
- ➢ Higher working temperatures.
- ➢ Environmentally-friendly characteristics.
- ➢ Availability from the ambient.
- ➢ Suitable in desert areas, where water availability is scare.
- ➢ No troublesome phase changes.

However, its low density complicates the integration of energy storage, while its low heat transfer rate poses challenges for receiver design.

On the other hand, Supercritical CO_2 is also being studied as HTF since it can be directly used as working fluid in sCO_2 turbines, provides suitable thermophysical properties related to the supercritical state and can operate at very high temperatures. Currently, a number of H2020 CSP projects working with sCO_2 are ongoing, such as SCARABEUS [24].

7. Solid particles:

Solid particles are currently being investigated as ceramics could work as HTF reaching temperatures up to 1273K [25]. Also ideal for storage applications, which can be easily implemented by simple hot particle bulk storage. Worst consequence is that particles conduct very high heat fluxes but large heat losses and difficulties to control the particle flux within the receiver may be encountered.

Within this approach, the classic heat transfer model (HTM) solid particle has an alternative in dense particle suspension (DPS), which combines the high temperature properties of solid particles with the ease of handling of gases and the good heat transfer properties of liquids. DPS basis are µm scale particles that can fluidize at low gas speeds and then be conveniently moved in gas phase.

2.2 Solar Collectors working parameters

Solar collectors are characterized by a variety of parameters which define its size, operation range, costs and suitability. These parameters are given below [26]:

Aperture area (A$_a$): the incident solar beam radiation falls all over this area on the front of the solar concentrator.

Receiver area (A$_r$): area in which falls upon the concentrated solar beam radiation. It has to deliver the valuable thermal energy to the generation engine.

Acceptance angle (2θ$_c$): when this angle is exceeded the incident solar beam radiation path deviates from normal to the aperture plane and reflects to reach the receiver. Smaller angles require to track the sun by moving continuously, whereas for larger acceptance angles is required to move the solar concentrator seasonally.

Geometric concentration ratio (GC): it is the result of dividing the aperture area to the receiver area.

$$GC = \frac{A_a}{A_r} \qquad\qquad (1)$$

Concentration ratio (C): considering the Sun of radius r and a solar collector with its receiver with areas A$_r$(receiver) and A$_a$ (aperture) separated a generical length, R, θ$_s$ is the half of the angle subtended by the Sun. Parameters are shown in Figure 12.
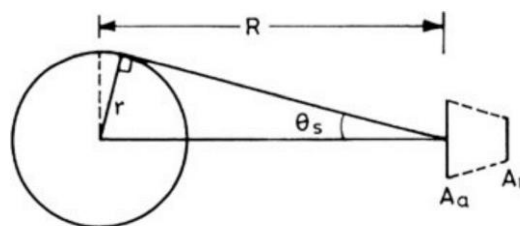
Figure 12: Parameters to explain concentration ratio [26].

In an ideal case, the sun's beam radiation on the aperture is the portion of the sun's solar radiation which is taken by the aperture area (Aa). So for circular solar concentrators, the maximum concentration ratio is:

$$\left(\frac{A_a}{A_r}\right)_{(max)} = \frac{R^2}{r^2} = \frac{1}{sin^2(\theta_s)} \qquad (2)$$

Intercept factor (γ): fraction of concentrated solar beam radiation captured by a receiver of a given size. Typically it is in the range between 0.9-1, although it depends on the size of the receiver.

Rate of solar radiance available at a receiver ($\dot{Q}_{AB}$): total amount of radiation the receiver is able to capture. Considering a receiver area A_r, with an η_o optical efficiency, incident over the concentrator (I_b), concentration ratio of C for beam radiation, absorptivity (α) and transmittivity (τ), it can be expressed as:

$$\dot{Q}_{(AB)} = \alpha\tau\eta_o C I_b A_r \qquad (3)$$

Rate of thermal energy lost by radiation ($\dot{Q}_L$): from a receiver operating at high temperature T_r, only radiative heat loss is considered, hence, it can be expressed as:

$$\dot{Q}_L = \varepsilon\sigma A_r T_r \qquad (4)$$

Where σ=Stefan-Boltzmann constant and ε=Emissivity of the receiver.

Net rate of useful thermal energy available ($\dot{Q}_u$): total amount of thermal energy which is used to heat the working fluid to generate power:

$$\dot{Q}_u = \dot{Q}_{(AB)} - \dot{Q}_L \qquad (5)$$

Rate of useful energy per m² in W/m² ($\dot{q}_u$):

$$\dot{q}_u = \frac{\dot{Q}_u}{A_a} \qquad (6)$$

Optical efficiency (η_o): ratio of the rate of useful energy to the incident beam radiation available at the receiver after transmission and absorption. It involves the solar beam incident angle, the shading by the receiver, different losses (absorption, transmission and reflection) and the effect of the shape of mirror surface.

$$\eta_o = \frac{\dot{q}_u}{\alpha\tau I_b} \qquad (7)$$

Instantaneous thermal efficiency (η_c): rate of useful energy to the beam energy incident on the aperture A_a.

18

$$\eta_c = \frac{\dot{q}_u}{I_b} \qquad (8)$$

Optical thermal efficiency ($\eta_{i,th}$): ratio of the net rate of useful thermal energy to rate of solar radiance available at a receiver.

$$\eta_{i,th} = \frac{\dot{Q}_{(AB)} - \dot{Q}_L}{\dot{Q}_{(AB)}} = 1 - \frac{\alpha \varepsilon T_r}{\alpha \tau \eta C I_b} \qquad (9)$$

With ideal conditions it is fulfilled $\quad \alpha = \tau = \eta_o = \varepsilon = 1$

Thus the optical thermal efficiency can be expressed now as:

$$\eta_{i,th} = 1 - \frac{\sigma T_r}{C I_b} \qquad (10)$$

$$\eta_i = \left[1 - \frac{\sigma T_r}{C I_b}\right]\left[1 - \frac{T_a}{T_r}\right] \qquad (11)$$

As can be seen in Figure 13, the overall solar-to-work instantaneous efficiency relies on operating receiver temperature, T_r and concentration ratio, C.
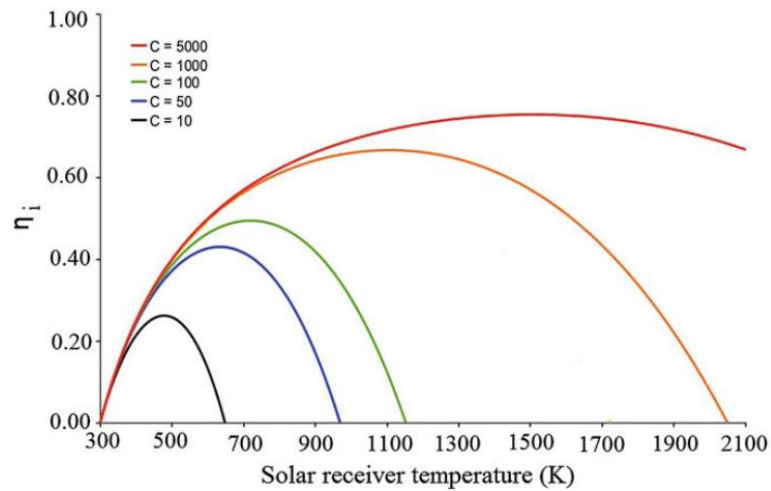
Figure 13: Concentrator solar-to-work efficiency depending on receiver temp. (K) and concentration ratio [26].

Few important conclusions can be extracted from this graph:

➢ The increment in the instantaneous efficiency is not proportionally with the increment suffered by the receiver temperature. Instead, it reaches a maximum

and from there, efficiency starts to decrease drawing a parable. This is explained by Stefan law (see Eq.12), the receiver is approximately a blackbody (to absorb light efficiently) and any blackbody loses energy by emitting blackbody radiation whatever its temperature is.

$$H = \varepsilon\sigma T^4 \qquad\qquad (\,12\,)$$

Where:

- H: energy losses
- T: temperature of the body
- σ: Stefan-Boltzmann constant (σ=5.67x10^{-8} W/m^{2}K^4)
- ε: Emissivity (ε=1 for blackbody)

Thus, at the beginning, an increment in temperature means better efficiency, but the amount of energy lost (H) due to blackbody radiation increases rapidly with temperature (T^4), so when a limit of temperature is reached, H is as high that heat losses are higher than captured energy by the absorber. It is in this moment when efficiency starts to decrease.

Hence, it can be affirmed that all concentrator has a peak of solar-to-work efficiency and this is why in order to improve the efficiency the operating temperature is limited.

➢ Instantaneous efficiency increases proportionally with the concentration ratio. By increasing the concentration, more light is focused onto the same collecting area, which causes more energy to be deposited in the same amount of time.

2.3 Classification of solar collectors

Solar concentrated technology can be classified according to different criteria, depending on the feature or parameter chosen. Based on design, work temperature, optical properties and even tracking applications [27,28]:

2.3.1 Classification based on temperature

Considering the operating temperature range concentrated systems can be grouped in three different categories:

➢ Low temperature: operation under the boiling point of water (373.2 K). They are used for water conditioning and domestic hot water.

➢ Medium temperature: they operate between 373K and 673K and their common use is steam supply in industrial processes. The most common devices in this range are concentration collectors.

➢ High temperature: they operate between 523K and 2273K producing direct electricity and steam. Proper systems in this range are thermoelectric centrals systems with distributed collectors (heliostats) and a central tower.

2.3.2 Classification based on optical principle

Considering the manner they proceed with the light:

➢ Reflector: Depending on the design, a focal point or line is the place where the incident beam radiation is concentrated after being reflected.

➢ Refractor: Operates equal as the reflector but also refracting the beam radiation.

➢ Hybrid: To concentrate beam radiation towards focal points, both refraction and reflection take place.

➢ Luminescent: First, a total internal reflection is experienced by the photons of visible wavelength of solar radiation for then being guided towards to solar cell.

2.3.3 Classification based on tracking

Depending on whether they track the sun during the whole day there are either tracking or non-tracking concentrators. Furthermore, the tracking concentrators can be separated in two groups:

➢ One-axis tracking concentrator: if it can rotate along one axis to receive across its aperture the maximum solar radiation.

➢ Two-axis tracking concentrators: when two axes track the sun to permit both daily and seasonal solar tracking. This is used by concentrators with double curvatures to achieve high concentrations for high temperature solar processes.

2.3.4 Classification based on design

Centring the point on the design, CSP technologies exist in four most common forms, namely Solar Power Tower, Fresnel Concentrator, Stirling Dish and Parabolic Trough, with the earliest in use being the trough, and the fastest growing as of 2017 being the tower. Although in past years some variants have developed from these originals, with improved features.

2.3.4.1   *Parabolic Trough Concentrator (PTC)*

As its name indicates it is a parabolic-shaped single-axis automatic tracking collector which can concentrate the sun up to 80 times, although the solar concentration ratio for this type of collector can vary between 5 and 30. It is made by curving sheet glass reflective aluminium (anodized or aluminized Mylar) mirror or silvered, into this particular shape. The modules reflect the incident solar radiation onto its focal line, along which the receiver is placed. In Figure 14 is shown how the single axis let all the solar radiation fall parallel to the axis maximizing in this way the efficiency.
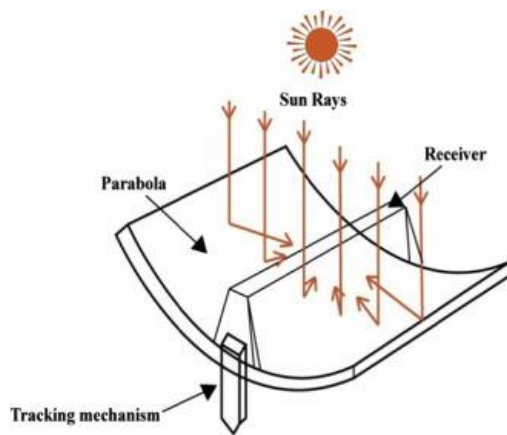
Figure 14: Parabolic-trough solar collector [28].

The receivers are composed of evacuated glass tubes with black interiors which minimise light absorption and thermal loses. Although it can also be manufactured of either copper, steel or mild (low carbon). Operating temperatures are around 425K- 700K [29] and common fluids used inside the receiver pipe are synthetic oil, molten salt and pressurised steam. It is the most extended and thoroughly proven CSP technology because of its long

operational history. It can be used for solar thermal energy for industry, solar thermal power generation and as heat source for efficient solar cooling.

The collector has three ways of performing, oriented in an east–west direction, tracking the sun from east to west, or otherwise, oriented in a north–south direction, tracking the sun from north to south. The choice of orientation often depends on when it is necessary more energy whether winter or summer and the application because over a whole year, a horizontal east–west trough field normally receives slightly less energy than a horizontal north–south one. Nevertheless, the north–south field receives a lot of energy in summer and much less in winter and the opposite for the east–west field, collecting less in summer and more in winter which provides a more regular annual output. However, these orientations have greater losses. There is only one more single-axis tracking configuration that gives less losses, known as polar East-West tracking. The best performance is achieved when more beam radiation per unit area is intercepted, for that reason the polar configuration is better than other modes. Thus, it gives the better performance. The word "Polar" implies that the axis is inclined at an angle equal to the latitude of the site and therefore, the panels would be parallel to the line joining the North and South poles, and hence the name Polar.

Parabolic trough full-scale systems are composed of numerous modules connected together in large linear parallel rows up to 100 metres long with 6 metres aperture, or even wider, above an extensive land surface as shown in Figure 15. It is remarkable to note too that heat storage is often included on those plants, forcing them to have larger fields, compared to the steam generator size, available. This is purposely oversized to provide storage and enable better utilisation of the steam turbine. With a total capacity of 350 MW, a collection of nine plants is the largest operational solar system in the world [30].

2.3.4.2 *Central Tower Receiver (CTR)*

Central tower receiver (CTR), solar power tower or heliostat field collector (HFC) consists of a tall central tower which acts as a receiver surrounded by heliostats which are stationary mirrors permanently fixed to the ground at specific distances from each other to minimise cross-shading. Mirrors are up to 120 m^2 in area [31] and they can continually track the whole sun's trajectory, reflecting sunlight to the top section of the tower because they can be tilt in two directions. CTR plants basis components are a generator unit and

a thermal storage, a central tower with a receiver at the upper part and a heliostat field, as shown in Figure 15. The heliostat field can reach up to 1500 times concentration, which does not allow the use of oil as HTF because of the high temperature reached between 1050K and 1300K [31].
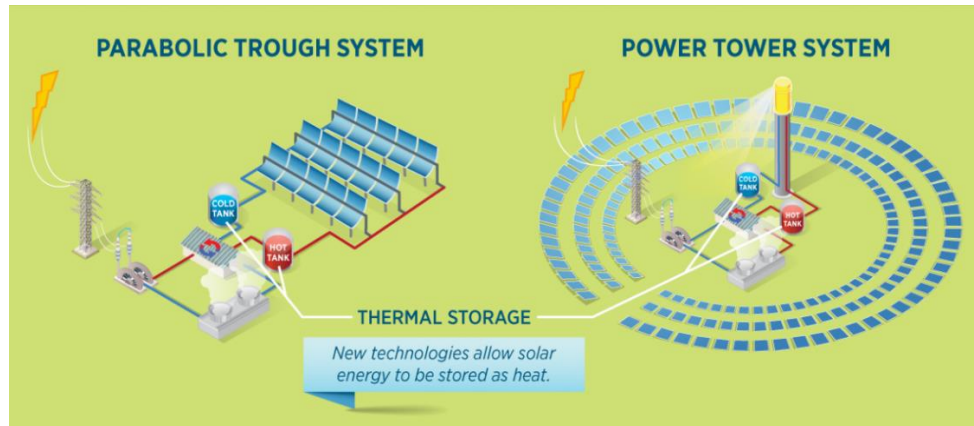
Figure 15: Parabolic trough plant and solar tower plant [32].

Quite often the HTF is water, and the resulting steam powers a turbine to generate electricity. However, newer models use a combination of molten salts with higher heat capacity than water, allowing to store some of that heat energy before using it to produce steam, which drives the turbines. This allows the possibility to realize highly critical operational modes such as supercritical or ultra-supercritical by cause of low pressures within the pipeline when it is operating at high-temperature, which results in greater efficiencies and the possibility of generating power even on cloudy days. Combined with an energy-storage device, this installation can produce reliable energy 24 hours a day.

Air can also be used as transfer fluid functioning with Bryton cycle in which air goes across the receiver to raise its temperature up to 973K before getting into the gas turbine [33]; power output is realized when the compressor is driven by the hot air. This notably decreases gas consumption, achieving operation efficiencies over 30%. Additionally, water-free operation can be realized and looking at the future it can also be used for developing solar tower thermal power plant with high operation efficiencies.

These plants may be erected in three general configurations.

1. If the receiver is a vertical plane with a north-facing heat transfer surface, the heliostats are located north of the central tower.

2. If the receiver is cylindrical with exterior heat transfer surface, the mirrors are situated completely surrounding the central tower.

3. If the receiver includes enclosed heat transfer surface, the mirrors are situated on the north of the central tower.

CTR system is the most economical provided that it is large enough up to 200 MW [33]. The advantage of this system over the parabolic trough is that it does not require any transfer of working fluid over long lines. Consequently, there is no need for insulation because the heat losses are minimal. However, a great disadvantage of this technology is the fact that it needs large land surfaces as shown in Figure 16, Smaller fields would imply that the tower will have to be much higher to receive the concentrated sun reflection from the mirrors, making it impractical and not rentable as multiple scientific studies had demonstrated. For this dissertation, this application of solar thermal concentration will be discarded because it is impossible to install it in Malta due to space constraints.

Figure 16: CTR 'Gemasolar plant' in Spain, owned by Torresol Energy [34].

2.3.4.3   Parabolic Dish and Stirling Dish

The collector consists of parabolic dish-shaped mirrors with an overall operating temperature over 1800K and a concentration ratio typically in the range between 1000 and 3000 [35] that concentrate the solar radiation toward the thermal receiver located on the focal point in front of the dish collector as shown in Figure 17.

It is a concentrator based on two axis solar tracking system so the sun's elevation that changes throughout the day and throughout the year can be tracked equally. This feature actually makes them reach efficiencies up to 40% [31], much more efficient than other CSP topologies. Moreover, this type of CSP offers quick installation, modular and siting flexibility, minimal water requirement and low maintenance.

Figure 17: Eurodish (Stirling dish) at Almeria solar platform (Ciemat) [36].

The size of the receiver needs to be optimized to minimize the shadow that can be created on the reflector by it and its support structure. That is why parabolic dishes look like a typical satellite dish with a diameter of about 10 m for a 25 kW dish-engine system at a direct normal solar insolation of 1000 W/m^2 [37]. The mass of the receiver needs to be optimized too. That is why commonly, each solar individual dish has its own heat engine placed at the receiver, which can be a Stirling engine (giving rise to its name) or a micro turbine, though steam turbines have also been tested powering the heat cycle with an array of solar dishes.

The solar-powered Stirling engine has greater efficiencies than steam engines and supress the usage of fossil fuels for power generation. When a Stirling engine operates on the receiver, the working fluid is hydrogen, and it heats up to 920K [37] even though helium is also employed. The dish working within a Stirling engine includes basically the following components:

- The generator attached to the engine to convert work into electricity.
- A waste-heat exhaust system to vent excess heat to the atmosphere.

26

- A control system to match the engine's operation to the available solar energy.

However, the cost and difficulty of producing Stirling dishes is also higher than other collectors and moreover, they lack storage capacity, which necessitates that the generated electricity is either consumed immediately or transmitted to the grid; so cloudy days can result in intermittent generation of electricity. Moreover, Stirling engines have shown reliability problems when working at high pressures (15-20MPa) and high temperatures (>873K) [38].

Stirling dish is more adapted to act as a distributed power source or to supplement other energy needs. It is most appropriate for small power-producing stand-alone systems. For this reason, for this research work, this type of technology and its multiple variants are going to be analysed deeply because they have a potential of being used in Malta.

2.3.4.4   *Fresnel Collectors*

There are two different variations of Fresnel collectors: linear Fresnel reflector (LFR) and Fresnel lens concentrator (FLC).

➢ Linear Fresnel reflector (LFR):

These systems present lower solar collector cost compared to other systems, but they also present the penalty of lower solar collection efficiency. The lower cost is explained by two facts, less structure is required to be mounted and elastically curved or flat reflectors are less expensive than parabolic ones.

Its performance consists in an approximation of the operation of a large lens by simply fractioning it into smaller curved portions spread out on a flat surface. An elevated long tower receiver which runs parallel to the reflector axis of rotation receives the collectively focus produced by these sections as shown in Figure 18.

With these systems the solar radiation can be concentrated about 30 times of the usual intensity. It is noted the less sharpness of the focal point, which reduces the maximum temperature that can be reached. Different HTF can be adopted, usually in several typologies of diathermal oil which can get heated up to 670K or molten salt mixture which may reach up to 800-900K. Additionally, other possible future HTF are the liquid sodium and the supercritical carbon dioxide because of their very high working temperatures, up to 1050-1300K [26].

A remarkable point on these devices is the avoidance of shading and blocking between adjacent reflectors leading to increased spacing between reflectors. Blocking can be reduced by increasing the height of the receivers, but this increases cost.

In certain systems, an additional secondary mirror behind the focal plane is used to direct the sunlight into the receiver as shown in Figure 19.

For the moment, these collectors are not reliable in the long-term, because cost data and long-term performance are lacking.

Figure 18: Linear Fresnel MAN collector from Almería Solar Platform (PSA) [36].
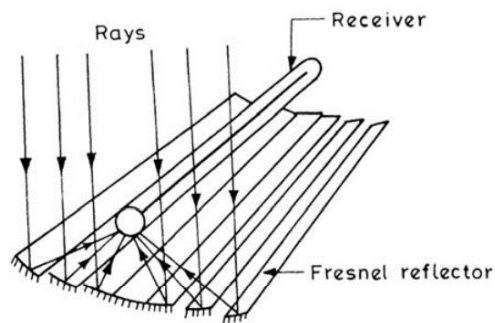
Figure 19: Scheme of parts and operation of a linear Fresnel system [26].

➢ Fresnel lens concentrator (FLC):

Fresnel lenses can be fabricated either with plastic or glass since both can be utilised as refracting materials. Due to its large surface tension and the difficult to mould, glass is seldom used. So the most preferable material for its construction is plastic because it is easy-manufactured and economical.

The Fresnel lens collector can be installed and mounted in any of the following configurations:

- Downward-facing grooves: This configuration exhibits a low concentration ratio given by large off-axis abnormalities and low thermal efficiency, both caused to the presence of a high surface reflection loss. In addition, the performance is affected by the fact the beam radiation does not fall perpendicularly.

- Sun-facing grooves: In this configuration, it can be given that not all the input beam light is transmitted to the focus. In accordance with Snell's law, when moving from a denser to a lighter medium, the refracted light is deviated away from the normal. Likewise, performance can be poor due to possible dust depositions in the grooves.

This FLC technology gives a solution for one particular problem of LFR. This allocation avoids shading issues by allowing adjacent linear elements to be interleaved. The groove angles are chosen with reference to a particular wavelength of incident beam radiation so that the lens acts as a converging one for the light, which is incident normally as shown in Figure 20.
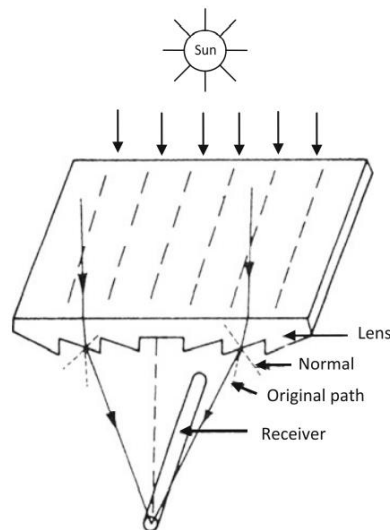
Figure 20: Operating scheme of a Fresnel lens collector (FLC) [26].

2.3.4.5 *Comparison data*

The following tables and plots show some comparisons between these big four mentioned technologies. Table 1 summarizes the main features on each technology, whereas Table

2 and Figure 21 should be interpreted together, giving a vision of the tested efficiency in different working environments for different technical options in each CSP family.

Table 1: Comparison of main features in each CSP technology treated [39].

Technology	Parabolic trough system	Central tower system	Linear Fresnel system	Parabolic dish system
Sketch				
Description	(i) Sun rays focused by parabolic through reflectors (ii) Pipes containing heat transfer fluid run through the reflector focal points	(i) Arrays of heliostats focus sunlight on a central receiver (ii) Heat transfer fluid runs through the receiver and generates steam	(i) Sun rays are focused by an array of linear mirror strips on a line receiver (ii) Linear fixed receiver is mounted on a tower	(i) An array of point-focus collectors tracks the sun in two axes (ii) Sun rays are focused on a receiver at the dish focal point
Maturity (2012)	Commercially proven (over 25 years), 3124 MWe installed as at 2013	Pilot commercial projects (medium to high maturity), 64 MWe installed as at 2013	Pilot projects (medium maturity), 288 MWe installed as at 2013	Demonstration projects (low maturity), 1.5 MWe as at 2013
Typical capacity (MW)	10–300	10–200	10–200	0.01–0.025
Operating range (°C)	150–550	250–1200	150–500	300–1500
Power cycles considered	Steam Rankine Organic Rankine	Steam Rankine Brayton cycle	Steam Rankine Organic Rankine	Stirling engine Steam Rankine
Plant peak efficiency (%)	14–20	23	18	30
Annual solar to kWh efficiency net (%)	11–16	7–20	13	12–25
Maximum slope of solar field	Up to 2%	Up to 4%	Up to 4%	10% or more
Water requirement (m³/MWh)	3 (wet cooling) 0.3 (dry)	2-3 (wet) 0.25 (dry)	3 (wet) 0.2 (dry)	0.05–0.1 (mirror washing)
Land occupancy	Large	Medium	Medium	Small
Typical surface area (m²)	300–900	100–200	30–300	50–100
Heat transfer fluid	Water/steam and synthetic oil	Water/steam, air, and molten salt	Water/steam	N/A (Stirling engine or microturbine)
Storage system demonstrated	Molten salt	Molten salt	Pressurized steam	Only indirect storage
Other storage options	Molten salt, concrete, and phase change materials	Concrete, ceramics, and phase change materials	Molten salt, concrete, and phase change materials	Concentrated heat to catalytically break NH_3 into N_2 and H_2 for storage to recombine for release of heat

Table 2: Technical options (HTF and storage) for each CSP technology family [40].

CSP technology	Technical options
Parabolic troughs (PT)	PT-oil: oil as HTF and molten salt storage PT-SHS: superheated steam as HTF PT-MS: molten salt as HTF and storage
Linear Fresnel systems (F)	Fresnel SaS: saturated steam as HTF Fresnel SHS: superheated steam as HTF
Towers (T)	T-SaS: saturated steam as HTF T-SHS: superheated steam as HTF T-MS: molten salt as HTF and storage T-AR: ambient pressure air as HTF and Rankine cycle T-GT: pressurised air as HTF and Brayton cycle T-SC: supercritical cycle T-CC: pressurised air as HTF and combined cycle
Parabolic dishes (DS)	DS: helium Stirling cycle
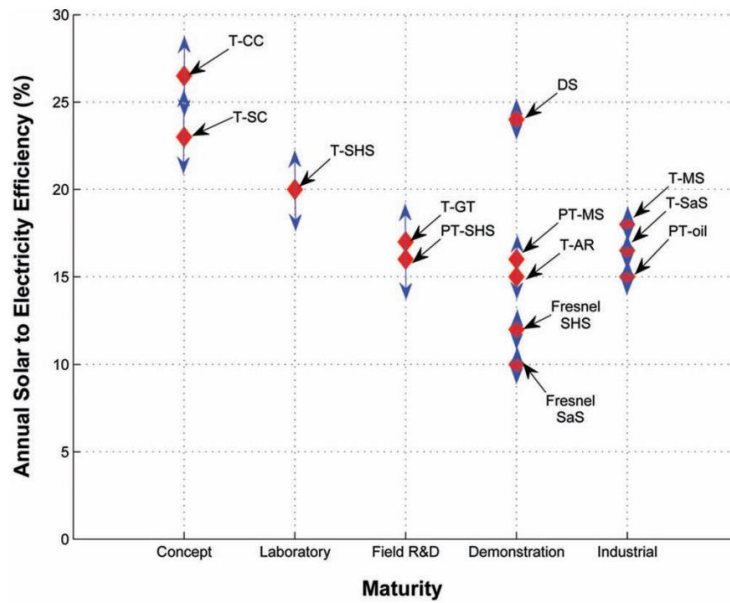
Figure 21: Annual solar-to-electricity efficiency as a function of development level [40].

2.3.4.6   Other collectors

The aforementioned are the main types of concentrated systems based on design, but in recent years there has been new developments emerging with new designs or a mix of the various existing technologies commented above. This dissertation is not centring on the analysis of all these systems and therefore only an overview is given.

1.1 Hyperboloid solar concentrator (HSC): as shown in Figure 22 it is a concentrator whose shape is produced by rotating two hyperbolic designs along its symmetrical axis. The inner surface is reflective. It is generally employed as a secondary concentrator and sometimes, lenses are used at the ØAA1 entrance for getting effective applications.
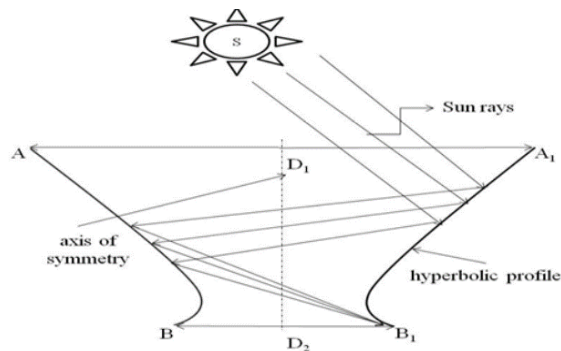
Figure 22: Hyperboloid solar concentrator (HSC) [26].

2.1 Compound parabolic concentrator (CPC): constituted by two rotated parabolic sections oriented reciprocal, as shown in Figure 23, in the way that each one receives on its bottom end point the beam radiation reflected from the another, and then both reflect the total to the receiver. The concentration ratio is the highest possible on it $(1/\sin(\theta a)$. It should be alternatively rotated towards the sun.

Its easy design and modelling makes it appropriate for many different applications. A lower cost may be achieved by reducing the CPC's height without changing the concentration ratio.

When beam radiation hits near the edges undergoes one or more reflections, whereas when is hit the central region of the aperture there is no reflection. The total of reflections depends on the collector depth, the incident angle and last but not least the concentration ratio.
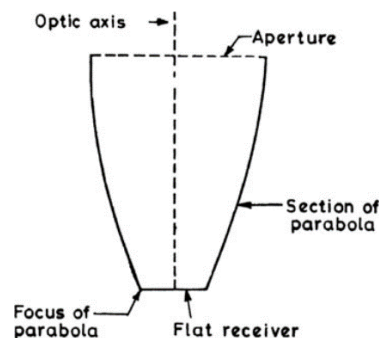
Figure 23: Compound parabolic concentrator (CPC) [26].

3.1 Dielectric totally internally reflecting concentrator (DTIRC): It has three basic parts: the front curved surface, the exit aperture and the profile which is an internal sidewall with total reflection. Each beam radiation is refracted through the front curved surface as shown in Figure 24. After a single total internal reflection (TIR), all beam radiation between S1-S2 is directed to S4. The refractive index would need to be higher to totally reflect the rays to S3. Beam ray hitting S2 exits from S4-S2-S3 and just satisfies the TIR.
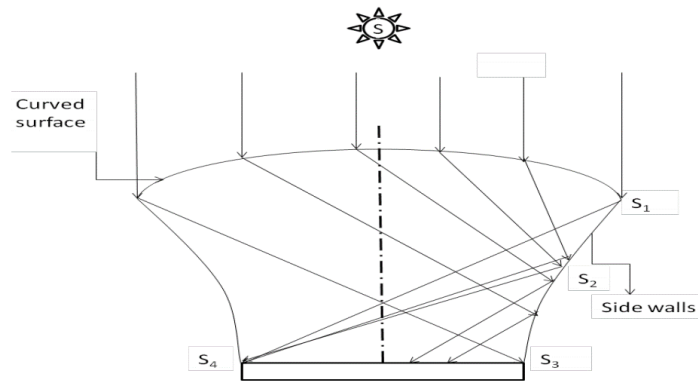
Figure 24: Dielectric totally internally reflecting concentrator (DTIRC) [26].

4.1 Fixed mirror solar concentrator (FMSC): as shown in Figure 25 it consists of group static mirrors with tracking receiver systems. Its construction only uses plane mirrors, so compared to other solar concentrators the electricity is generated at a much lower cost rate. An appropriate orientation increases total energy but not peak energy collection rate.
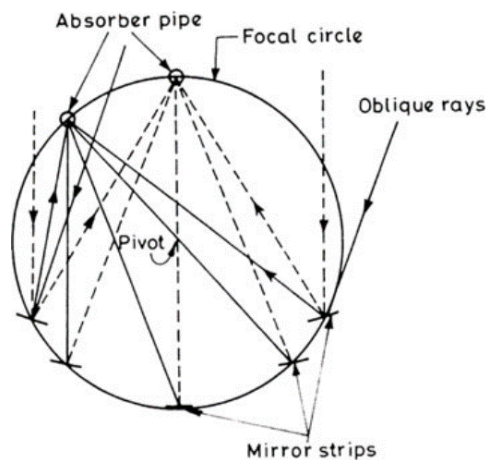
Figure 25: Fixed mirror solar concentrator (FMSC) [26].

5.1 Tabor-Zeymer circular cylinder: it is basically a triangular pipe receiver inside of an inflated plastic cylinder. To allow beam radiation to enter, the upper part is clear, whereas the bottom part is aluminized and acts like mirror, reflecting the beam radiation and focusing it on the receiver as shown in Figure 26. It requires only seasonal tracking and is able to be installed along an east–west axis. With this system, temperatures and collecting efficiencies are higher than in conventional flat plate collector (FPC).
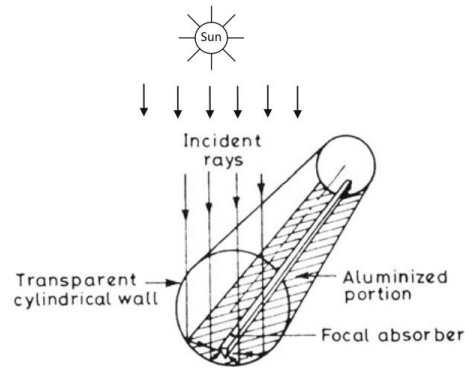
Figure 26: Tabor-Zeymer circular cylinder [26].

6.1 Hemispherical bowl mirror: This system consists of a moveable receiver-type concentrator and a fixed hemispherical mirror. Its operation is based on the symmetrical behaviour of light, all rays entering into the hemisphere after reflection cross the paraxial line at some point between the focus and the mirror surface as shown in Figure 27. To intercept all the rays, an absorber is placed in the centre of curvature of the dish.

It is a two axis tracking system, which enable this way of functioning. It may be noted that due to the spherical eccentricity in this concentrators lesser concentration than in paraboloids are given.
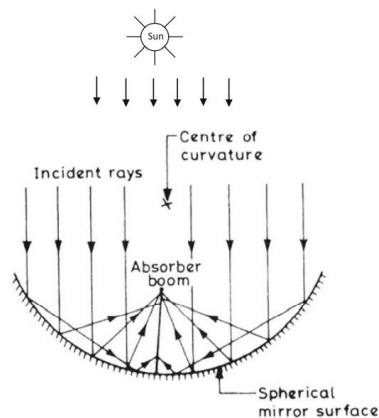
Figure 27: Hemispherical bowl mirror [26].

2.4   Concentrated Photovoltaics (CPV)

This dissertation focuses on CSP technology, but it is not the only concentrated technology that could help Malta in its transformation to a clean energy system. Light energy can also be converted into electrical energy following the same technique used by conventional PV technology but adding an optical system which concentrates the sunlight onto the cells. This technology is known as Concentrating Photovoltaic (CPV). After being the newest renewable field to appear it is now reaching commercial viability [41] after several years of development to reduce its costs, when compared to flat-plate PV as can be seen in the comparison made by Fraunhofer Institute in Figure 28.
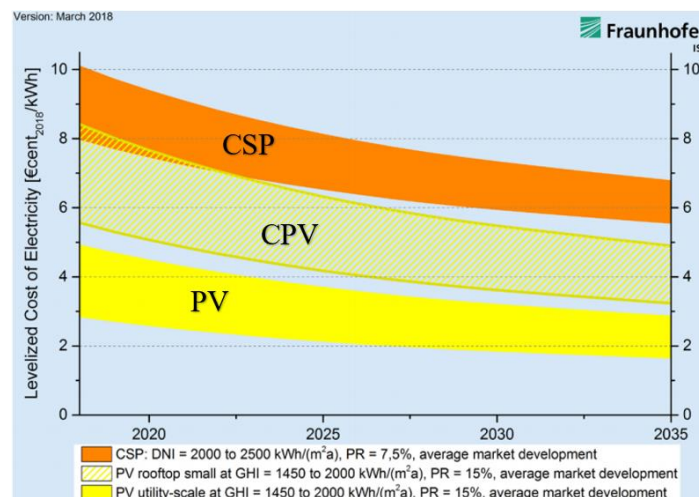
Figure 28: Development of LCOE for PV, CPV and CSP at locations with high solar irradiance kWh//m²[42].

CPV cannot use diffuse radiation being only able to use direct beam radiation, which implies that accurate two-axis tracking is paramount for these systems. There are three different classes of systems depending on the magnification ratio used [41], as shown in Table 3. The magnification or concentration ratio is expressed in number of "suns", hence in 10x the number which accompanies the x represent how many times major is the light intensity that hits the PV material compared to the same conditions but without the concentration.

- High concentration (HCPV), between 150X and 1000x.
- Medium concentration (MCPV), between 10x and 150x.
- Low concentration (LCPV), concentration ratio lower than 10x.

	LCPV	**MCPV**	**HCPV**
Concentration ratio	2x-10x	10x-150x	150x-1000x
PV materials	Silicon	Silicon, CdTe, etc	Multijunction cells
Cooling	Not required	Passive cooling	Active cooling
Tracking	Not required	One or two axis tracking	Two axis tracking

There are two different optic types; reflective, using mirrors as shown in Figure 29; and transmissive, in which Fresnel lenses are used, as shown in Figure 30.

Figure 29: SolFocus HCPV devices and reflective formers modules [43].
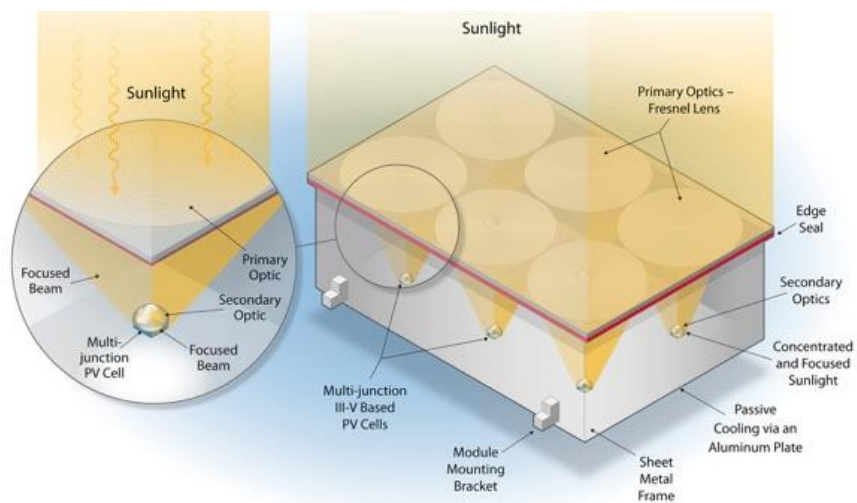
Figure 30: Schematic of a HCPV transmissive module [44].

Typically the majority of these systems require cooling which can be provided in two different ways [45]:

➢ Active cooling: normally liquid metal because of its capacity of cooling from almost 2000K to 400K.

➢ Passive cooling: the cell is placed on a cladded ceramic substrate with high thermal conductivity. The ceramic also provides electrical isolation.

The main advantages of this technology compared to flat-plate PV are:

➢ The photovoltaic material required to capture the same amount of irradiation as in non-concentrating PV is lower.

➢ Easily recyclable: the constitutive elements of CPV modules are made of inorganic compounds that can be fully recycled and easily separable, therefore the dismantling of a CPV module is easier.

➢ As result of the smaller space requirements the employment of expensive high-efficiency multi-junction cells becomes economically viable. The efficiency of multiple junction cells utilised for CPV can reach 46% with a more than probable improvement in next years as can be seen in Figure 31, whereas the best commercial silicon solar cells top only at 21% [46].
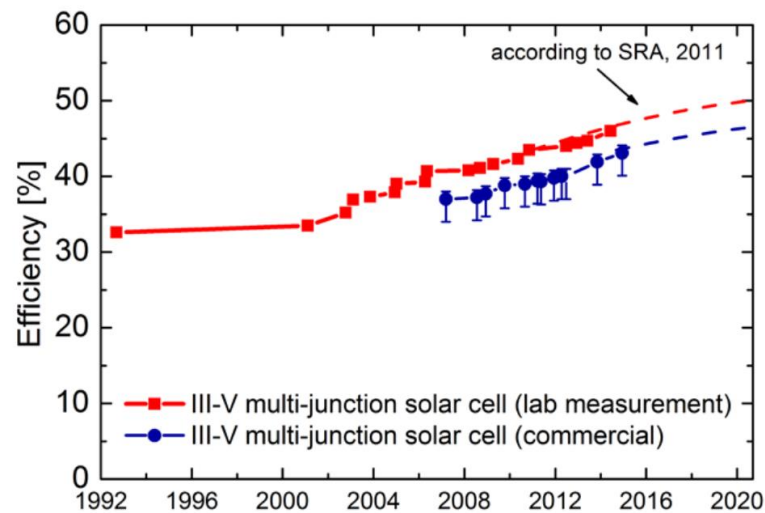
Figure 31: Development of record efficiencies of III-V multi-junction solar cells under concentrated light [46]. The trend lines show expected efficiencies provided by the European Photovoltaics Technology Platform in 2011.

➢ The optical system comprises standard materials, manufactured in proven processes. Moreover, optics are less expensive than cells.

- ➢ Potential multiple land use: devices are able to be high enough to enable the use of land underneath it.

- ➢ Very stable performance under high temperature: the materials from which CPV solar cells are made of have a very low power loss coefficient of about -0.05%/°C being able to even reach -0.01%/°C in the best cases, which compared to normal PV silicon solar cells is nearly 10-50 times better. Due to this feature, CPV can operate at quite high temperatures, above 373K [45].

- ➢ Great durability: CPV technology derives from military and space applications and has been tested immune to the majority of radiation or thermal damages, offering a very reliable performance even after 20 years since its commission.

2.5 CSP-PV hybrid systems

To date CSP and CPV technologies have been studied independently, but PV-CSP hybrid power generation systems can also be formed by combining together both technologies, given that to their features are complementary to each other. Currently, there are several different approaches for the hybridization:

- ❖ The power for a CSP plant can be provided by PV systems in the form of station-service power.

- ❖ These hybrid systems are intended to get the most out of solar energy to produce a regular stable power output throughout a whole day. Using the spectral beam splitting (SBS) technology thermal dissipation from PV cells can be retrieved as CSP system thermal energy source. A CSP system can work at the same time with the undesired energy from PV and a PV system can operate at relatively high efficiencies. Hybrid systems can be provided with stability from the CSP systems taking advantage of its power output characteristics, which decreases the impact of PV on the grid as well as benefits the power quality.

The PV-CSP hybrid system has numerous advantages over the CSP-alone or PV-alone system, the summary of benefits:

- ➢ Appropriate for the construction of large-scale solar power plants reducing the costs because of the scale effect: but also by employing compact PV-CSP hybrid

technology in remote districts, micro-scale solar power generation system might be built too.

➢ Lower cost: Because of its high capacity factor (CF) and its high generating efficiency, the hybrid systems present potential on cost-cutting the solar power generation. The CF would be pretty higher than the CF of other intermittent renewable power generation methods and close to that of conventional coal-fired plants, but to get it, proper conditions are needed.

➢ Higher generating efficiency: Proper energy allocation and energy cascade utilization can be achieved with SBS technologies and PV-topping, which leads to an improvement on generating efficiency, being possible to reach overall generating efficiencies over 42% based on the current technologies [47].

➢ Better power quality: as mentioned before, during cloudy days or night the electricity is produced by the thermal energy storage of CSP system, while during the day it is the PV system which satisfies the load demand of the power grid. As result of this complementation between CSP and PV operation modes, base or mid-merit load demand can be satisfied by the hybrid system supplying dispatchable power throughout all the time.

➢ Broad market and convenient final product: Electricity, which can be used and transported conveniently, is the only final product.

2.5.1 Types of CSP-PV hybrid systems

As shown in Figure 32, according to the essential characteristics of the optical system, the operating temperature and the system integration, the PV-CSP hybrid technology is classified into two types: the non-compact and the compact PV-CSP hybrid technology.
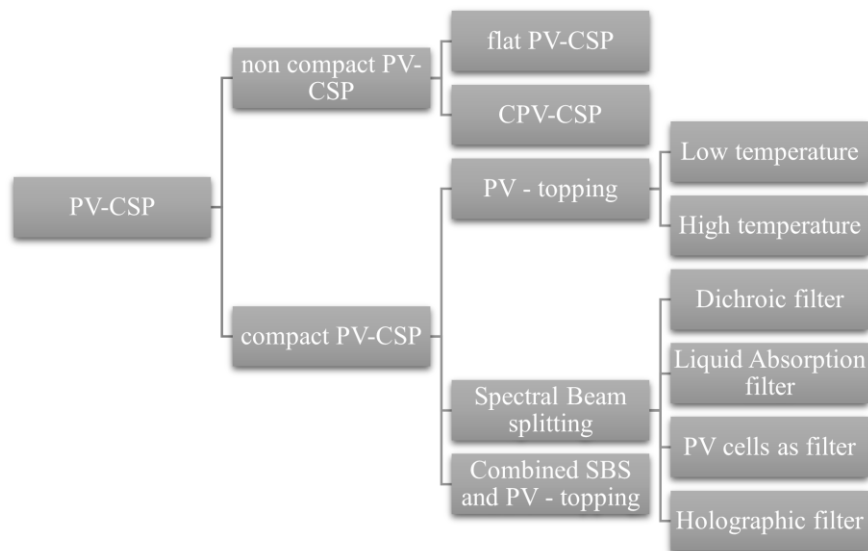
Figure 32: Classification of CSP-PV hybrid systems [47].

2.5.1.1   *Non compact*

For this type, both systems (PV and CSP) can operate independently, but also part of the CSP system station-service power can be provided by the PV system, reducing the overall electricity production cost. Furthermore, an extremely high CF and stable power output can be achieved by this approach [47], which makes this system capable of providing the grid with base load power.

This type of solar technology is not further analysed at this dissertation because as it was seen before with CSP large projects, they cannot overcome the space boundary limitations in Malta.

2.5.1.2   *Compact*

In accordance with the diverse hybridization approaches it can be grouped into three different parts:

➤ PV-topping technology:

This system generates power through using the CSP system as the bottoming cycle and PV system as the topping one, as shown in Figure 33. Moreover the CSP system can generate power by recovering the dissipated heat of PV cells. Solar cells are used at the same time as PV converter and thermal receiver. Besides, to achieve a higher hot end temperature and reduce the use of expensive solar cells, the solar radiation is frequently concentrated, leading to a significant improvement on the overall generating efficiency.

Many challenges are being faced by this technology, primarily the operating temperature limits imposed by photovoltaics. The photoelectric performance is degraded as consequence of the reduction of the bandgap of solar cells with the temperature. In fact, the limit temperatures at which Si and GaAs solar cells can operate are not normally higher than 350K for Si and 390K for GaAs. Under this restrictive temperatures, the power generation efficiencies became limited as consequence of the low hot end temperature of the bottoming cycle. That is the reason why this technology can be divided in two subtypes, depending on: the low temperature power generation technology and the high temperature PV cells.
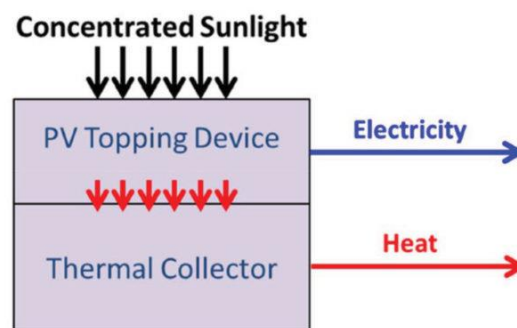
Figure 33: PV-topping system [48].

➤ SBS technology:

In these systems by means of splitting the solar radiation spectral beam as shown in Figure 34, the near-infrared or ultra-violet light is converted into heat at high temperatures for power generation in CSP systems and the visible light is directly converted into electricity in PV cells. Compared to cells under full-spectrum radiation, the efficiency of silicon cells is much higher, being able to reach 40% to 50% when using SBS technology [48]. Furthermore, solar cells will no longer limit the working fluid temperature of the CSP system, and the CSP system thermal receiver receives the below bandgap redirected radiation, which allows common CSP technology to be utilised.
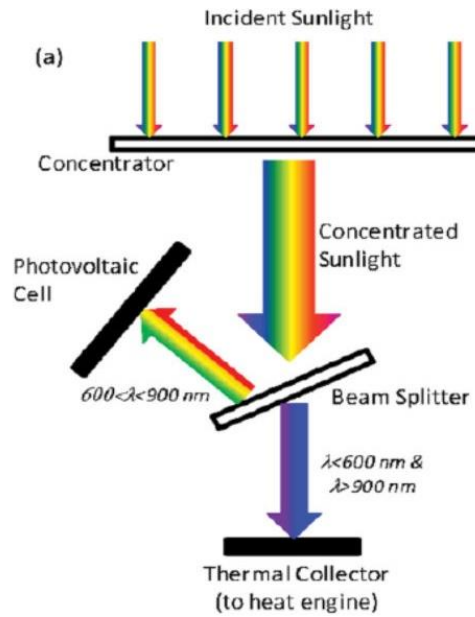
Figure 34: SBS system [48].

Holographic filters, PV cells as filters, liquid filters and dichroic filters are some of the variety of systems that have been considered for SBS technology. These kinds of filters can easily work within different CSP systems including the point-focusing (heliostat fields and parabolic dishes) and linear-focusing (linear Fresnel systems and parabolic troughs).

➢ Combined SBS and PV-topping technology:

Here, both the PV cells unwanted solar radiation and the dissipated heat are absorbed and then used to power generation through driving a heat engine. This combination is proposed to overcome the weaknesses of both technologies. In PV-topping systems, it is actually hard to operate the solar cells at high temperatures, which moreover turns down its conversion efficiency. The conversion efficiency might be certainly increased by SBS technology through reducing the solar cell temperature, although PV cells still receive a large part of radiation which is dissipated as heat without further use.

A dichroic mirror integrated in a PV module splits the concentrated sunlight and the HTF flows into the thermal receiver where reflected near-infrared (NIR) illumination heats it to a high temperature for power generation, after being preheated in the heat sink of the PV module, as shown in Figure 35. The combined technology conversion efficiency

should improve, in as much as it is possible to achieve a relatively high working fluid temperature without discarding the low temperature heat generated in the PV cells nor sacrificing on the PV efficiency.
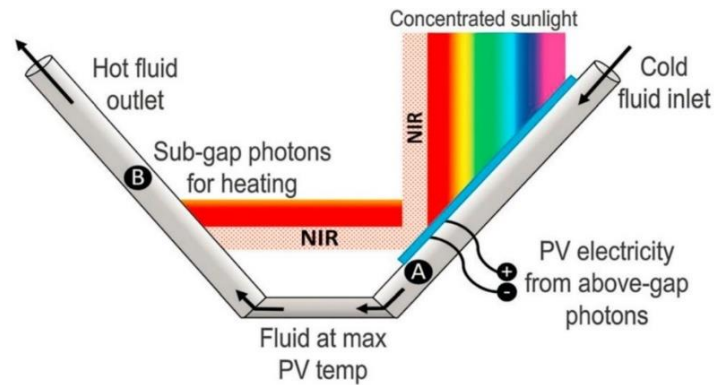
Figure 35: Combined PV-topping and dichroic filter (SBS) [47].

The PV-CSP hybrid systems mentioned above are at different stages of development with research gradually increasing in recent years. The compact systems are suffering a fairly restricted development due to several critical issues, whereas the non-compact systems, benefitting from both CSP and PV technologies maturity, are now entering the stage of commercialization. Due to this reason and taking into consideration all the key features of CSP and PV systems such as efficiency, costs, energy storage, power quality, and stability, it seems logical to consider the PV-CSP hybrid systems as promising candidates to provide dispatchable power with renewable energy in Malta. But for the moment and given the lack of available products, systems and devices it is still not a realistic technology, and hence it should be studied in further projects in the coming years.

2.6   Collectors in the market

This section includes all the products, systems or technologies that have been identified from thoroughly combing the current market. Systems capable of approaching or matching all the properties sought after, as well as manage all the requirements and/or overcome limitations already explained before are considered, with the scope of identifying the best options of solar concentration systems for Malta.

The product research for this dissertation has been centred mainly on the CSP technology maintaining the overall tone of the entire project.

2.6.1 CSP systems

Inside the CSP field, the main protagonists are the parabolic dishes (Stirling dishes) since as it was mentioned beforehand through the literature review chapter, they are the most suitable systems for the dissertation's boundary conditions.

2.6.1.1 *Solar Powered Stirling Engine Generator (25kW)*

This Stirling Dish (25kW) shown in Figure 36, from the Chinese company "Oriental Great Ocean New Energy Technology Development Co. Ltd" (GOE), is a parabolic dish constituting of several parabolic reflectors, provided with a horizontally coordinated system dual-axis tracker and a solar Stirling engine attached to produce power.

It is characterized by an easy deployment and very simple structure with flexibility in arrangement and a strong versatility to landscapes. Solar energy is converted directly to power during its operation, so there is no need for water as the working fluid, which makes it suitable in several conditions.
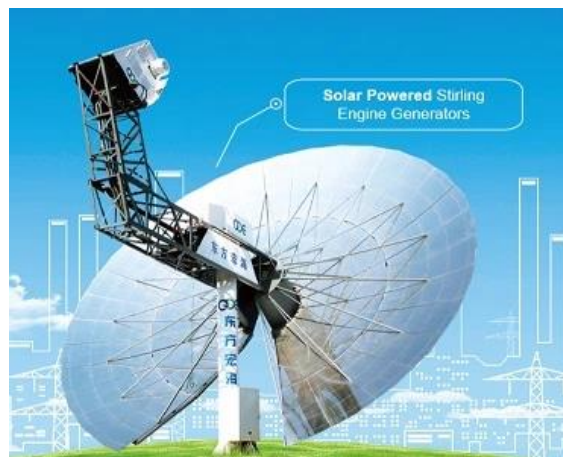
Figure 36: GOE Solar Powered Stirling Engine Generator [49].

It is considered an environmentally-friendly product, with energy savings and zero noise during operation as well as a small footprint. In addition its manufacturing process does not produce any pollution. An easy maintenance programme and absence of power

44

degradation during its service life, makes this system highly reliable systems [49]. The product is ISO and CE certified.

Given its big development potential as well as low operational cost, its applications include stand-alone power plants for remote places such as pasturing areas, small villages and islands. It can also be applied to build distributed power stations, to centralized grid connection, apartments and office buildings, independent household, and as off-grid and on-grid power supply. This product is a good CSP candidate for Malta.

In Table 4, the technical features related to the power conversion unit (Stirling engine) and the solar dish collector are shown.

Table 4: Technical data of GOE Dish Solar Collector - 25 kW [data from 49].

GOE Dish Solar Collector	
Dish Diameter	12.56 m
Mirror Reflectivity	93%
Projected Area	92 m^2
Required Annual Average DNI	$\geq$ 2000 kWh/m^2
Concentration ratio	1500
Efficiency	26% ~ 30%
Operating Temperature	-25ºC ~ 40ºC
Tracking Mode/Accuracy	Dual-axis tracking of elevation and azimuth
Tracking Accuracy	1 mrad
Tracking Range	Azimuth Angle: 0°~360°; Elevation Angle: -10°~90°
Power Conversion Unit	
Rated Output Power	25 kW
Engine Speed	1500 rpm
Working Media Gas	Helium or Hydrogen
Input Energy	$\geq$ 90 kW
Length × Width × Height (m)	1.3 × 1.1 × 1.8
Weight of Equipment	925 kg
Cooling System/Coolant	Closed-cycle Coolant

2.6.1.2   *Solar Invictus*

The Solar Invictus dish developed by the Pakistani based "ZED Solar Company" can absorb about 92% of the sunlight falling on the receiver. The company AEDesign combined this dish with a Stirling engine, as shown in Figure 37, reaching net solar to electric conversion rates of over 30%. This AEDesign design is very efficient, removing the necessity of vast structures, by using stiff and strong mirrors mounted on spokes. All

45

of them are held up on standard pipes base structure. This composition makes the entire device easy to assemble, economical, transportable, modular and lighter. The dish architecture is developed to operate suitably with wind speeds of 16 m/s and up to 45 m/s.

The dish uses dual axis tracking, with a linear actuator for elevation and a rotary actuator for azimuth rotation, and a sophisticated system controls and monitors both actuators movements, tracking the sun with an accuracy of 0.01° in both axes. Its RS-485 Modbus protocol enables it to communicate with other devices and it disposes from a self-diagnostic system, which checks the operation status daily before the start of the day. Relevant operational and technical parameters are shown in Table 5.

Table 5: Technical features of Solar Invictus [data from 50].

Solar Invictus 53E			
Dish diameter	9 m	*Reflectivity*	96%
Focal length	5 m	*Total weight*	3000 kg
Reflecting area	53 m^2	*Operating temperature*	298K-348K
Concentration ratio	2500x	*Efficiency*	30%

Figure 37: Solar Invictus dish [50].

Unfortunately, the current status of both companies in charge are unknown, and therefore the most probable hypothesis that can be considered is that this dish is no longer available on the market.

2.6.1.3   Ripasso Dish

It is considered one of the most efficient systems of recent years. It is a Stirling dish, as shown in Figure 38, with an aperture area of 100m^2 [51]. It uses an adaptation of an 1816 Scottish engine (Stirling) based on a Kockums' license and merges it with Swedish military technology that was used for many years on submarines for the Swedish Navy.

Figure 38: Ripasso dishes [51].

There is no water involved in its operation, neither central turbines nor AC/DC converters because the system is modular. Through a heat engine, the solar energy is converted directly to three phase electricity, which works via a closed-cycle regenerative heat engine. Hence, the engine is powered by alternately heating and cooling an enclosed gas, which drives the pistons to create the electricity. Its huge advantage is that it dispenses the necessity to convert the power produced into grid-ready electricity. It captures around 32% of the incident sun rays and converts it to useable electricity with minimal record energy losses [52]. IT Power (UK) carried out a few tests which confirm that 24 typical UK homes can be powered with a single dis, equivalent to a total of 75-85 MWh [51] per year.

This technology is particularly suited for deserts and locations with hot and arid climates; hence it is perfect for Malta's climate conditions. Operating at the best solar conditions, in places such as Chile, South Africa or MENA, the LCOE result was found to be less than 0.1 €/kWh [52].

As Gunnar Larsson, Managing Director for Ripasso Energy said, Ripasso technology features such as very accurate solar tracking and large engine size of 30 MW makes it a robust and cost efficient CSP technology.

The Ripasso dish is a modular and cost efficient system capable of tracking the sun automatically and operate individually with a generation of 2×30 kW three phase AC power for each module, as a result of the further development and commercialization that Ripasso has carried out. Relevant technical features are provided in Table 6.

Table 6: Technical features of the Ripasso energy dish-Stirling unit [data from 53].

Ripasso Dish Concentrator		Power Conversion Unit	
Dish Diameter	12 m	*Type of Stirling engine*	4 cylinders double acting
Focal Length	7.45 m	*Displaced volume*	4 x 95 cm^3
Reflecting area	101 m^2	*Typical output at DNI = 960 W/m^2*	31.5@2300 rpm kWe
Concentration Ratio	3217x	*Weight*	700 kg
Reflectivity	95%	*Receiver temperature*	993 K
Total height	14 m	*Working gas*	Hydrogen
Total weight	8000 kg	*Power control*	Pressure – Speed control
Soil area occupation	500 m^2	*Max gas pressure*	200 bar

The company Swedish Stirling, creator of this device has closed down the energy project in 2019, so at this moment Ripasso Dish cannot be bought but its technical conditions made it a very appropriate system for this dissertation's aim.

2.6.1.4   Infinia Dish, PowerDish

The PowerDish [54], shown in Figure 39, is a dual axis tracking 17 m^2 parabolic dish made of a curved sheet-melding compound bonded to uncoated high-reflectivity mirrors which concentrate sunlight up to 800 times. The generated heat drives a free-piston Stirling power generator, raising the concentrator's temperature to 2,273K. This is reduced to 923 K when the Stirling generator converts this heat to electricity.

The high-pressure Helium (HTF) present inside the generator quickly heats up and expands and it is pressurized to about 34.5 bar to densify it making it able to dispatch

even more heat. At the beginning, single-phase AC power is generated, then through a rectifier it is converted from AC to DC, and lastly is converted it back to grid-quality, three-phase AC electricity by an inverter.

Infinia cools the backside of the Stirling generator to get consistent power output, no matter what the local climate conditions are, maintaining it at about 333K or even less, by utilising a closed-loop, liquid-based system [55]. To circulate about four litres of a half-glycol half-water mix around the Stirling generator's cool side the dish uses a fan-cooled radiator and an electric pump. In terms of noise pollution, the device creates 65dBA in a 10 metres distance around the dish, which is similar to noise generated by a home air-conditioning unit [55]. The systems hardly requires maintenance except for replacing components, replenishing the Helium and water or lubrication.
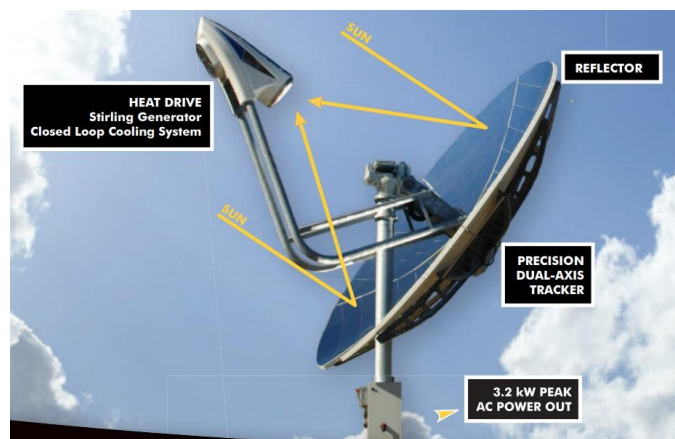
Figure 39: PowerDish [55].

One important asset of the PowerDish is that shade cast on the dish only degrades the output by the fraction of the dish that it covers. Hence, when a 5% of the dish mirrors is shaded, power output only drops by 5%. Conversely, when 5% surface of a traditional flat plate PV solar system is shaded, power output might drop by 40% or more.

Otherwise, a serious drawback of the PowerDish is the necessity of direct normal irradiation (DNI). Stored heat allows it to function on for a while, but will not work at all on rainy, foggy or overcast days. Wind can degrade power output by about 4% for every 24 km/h of wind due to the increased convection losses from the heater head and the

decreasing of heat input. But on the positive side, the system is suitable for deployment on sloped terrain and has a faster deployment rate than other CSP technologies because of its five components; heat drive, chassis, reflector, dual-axis tracker and power electronics/control system; which are easily transported and assembled on site. It is easily recyclable due to the lack of by-products and rapid return of inversion.

One 860 kg PowerDish generates 3.2 kW grid quality AC power and it costs 8,200€ [55]. In addition, for each year, one can avoid up to: 6.05 tonnes of CO_2, 31 kg of NOx and 15 kg of SO_2 [55]. Relevant technical features are shown in Table 7.

Table 7:Technical features of PowerDish [data from 55].

Power Conversion Unit		Infinia PowerDish	
Type of Stirling engine	Free-piston	*Dish diameter*	4.7 m
Typical output at DNI = 1000 W/m²	3.2 kW AC = 3.83 kW DC	*Mirror surface*	17 m²
Receiver temperature	923 K	*Total weight*	860 kg
Working gas	Helium	*Total height during operation*	6.4 m
Power control	Pressure – Speed control	*Efficiency*	24%
Max gas pressure	34.5 bar		

Unfortunately, similar to Ripasso Dish, the developing enterprise has declared bankruptcy.

2.6.1.5 HelioBooster

The HelioBooster [56] from an Israeli company Heliofocus is a large dish solar concentrator with 219 mirror facets, 1.5mx1.5m each, in a Fresnel-like arrangement, which acts in the same way as smaller mirrors would for a conventional Central Tower Receiver (CTR). The surrounding air can be heated up to 1273K by reflecting and capturing sunlight. Then, to produce the steam that spins a turbine in a Combined Cycle, that air is channelled through a heat exchanger system. The mirror consists of bent glass

with five point supports and its structure is made of steel and includes a stiff torque box with seven extended cantilever arms. It uses a two-axis tracking system where the azimuth and the elevation are driven by hydraulics. The receiver was made by 'HelioFocus' whereas the concrete and steel structure including the drive technology was built by 'Schlaich Bergermann und partner'. The dish is shown in Figure 40 with its technical data in Table 8 and the parts and components broken down in Figure 41 and Table 9.

Compared to traditional CSP, this technology uses less land space, and it is more efficient according to company officials. The unit can produce up to 120-130 kW of electricity reaching a solar-to-electric overall efficiency greater than 30% [57], although it only requires 500 m^2 of land for its base. It can be concluded it provides a higher production than most PV systems with this land occupancy.

Figure 40: HelioBooster dish prototype [56].

Table 8: Technical features of Heliofocus prototype [56].

HelioBooster Prototype	
Dish size	25.7 m x 27.5 m
Focal length	14 m
Mirror surface	493 m^2
Weight	130 t
Typical output at DNI = 1000 W/m²	120-130 kW
Efficiency	> 30%

Concentrator
220 mirror facets (1.5 m x 1.5 m each)
15 purlins from circular hollow sections, carrying the mirrors
Six cantilever arms from rectangular hollow sections, 18 m long
A welded rigid rectangular torque box of circular hollow sections, 22.5 m long
Four-leg receiver support mainly made of circular hollow sections

Table 9: HelioBooster prototype concentrator's components [58].
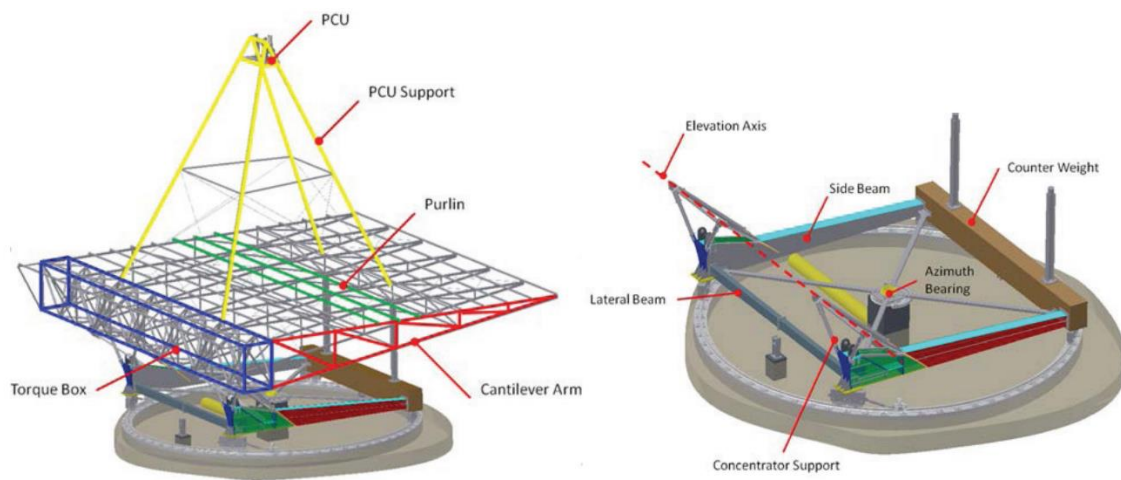
Figure 41: HelioBooster system components on concentrator and turn table [58].

It is remarkable to mention that there exists a second version of Heliofocus dish, known as Orion dish [59], which was developed to be installed in the Orion project in China. This dish, including the drive system, is an optimized version of the previous HelioBooster prototype, improving the surface and reducing mass and cost. The operation is identical as well as the electricity production of a stand-alone unit.

Both devices were really known in the market a few years ago till HelioFocus company formally shut down in early 2017. Therefore, nowadays it is impossible to acquire this product.

2.6.2 Concentrated Photovoltaic (CPV) systems

2.6.2.1   *120X MCPV - Zytech CPV*

120X MCPV from the Spanish company "Zytech CPV" is a Medium Concentration Photovoltaic (MCPV) concentrator system, whose module does not require neither critical nor individual on site alignment. With a very uniform energy distribution pattern, the Sun's radiation is refracted onto the cell through the innovative prismatic lens.

The module can generate lower heat density profiles than other similar technologies due to the lower concentration ratio. Also, excellent passive heat dissipation is provided by the innovative design by removing the necessity of individual cell heat sinks. This largely, ensures each cell to work throughout their lifetime at their optimum efficiency.

A single junction mono crystalline silicon cell with a conversion efficiency of 18% is the key element of the system [60]. Single junction silicon technology is proven to be long lasting, easy to manufacture and inherently reliable. The entire module, shown in Figure 42, present some great properties such as durable, extremely robust and structurally very strong, which makes it an excellent product. Relevant technical properties are shown in Table 10.

Figure 42: 120x MCPV Zytech solar module [60].

Table 10: Zytech 120x MCPV technical properties [data from 60].

Electrical specifications		Temperature Coefficient	
Maximum Power (Pmax)	150 W	Current Temperature Coefficient	+4.4 mA/K
Open Circuit Voltage (Voc)	29.39 V	Power Temperature Coefficient	-0.46 %/K
Max Power Point Voltage (Vmpp)	23.22 V	NOCT Normal Operating Cell Temperature	70ºC ± 2ºC
Max Power Point Current (Imp)	6.62 A	Other data	
Short Circuit current (Isc)	7.18 A	Concentration ratio	120x
Dimension data		Conversion efficiency	18%
Cell (W) x (L) (cm)	2.4 x 2.0	Limits	
Module (L)x(W)x(D)	134x102x21 cm	Operating Temperature Limits	-25ºC to +85ºC
Cells per Module	48	Power Tolerance	± 3%
Module weight (kg)	27	Maximum System Voltage	1000 V DC

2.6.2.2 uModule by Arzon Solar

Arzon Solar company has a full range of developed CPV systems that are based on its patented universal CPV module "uModule" (uM). This is an easy to install, fully integrated, CPV module designed for reliable and robust solar power electricity generation for ground mount, industrial, commercial and parking lot applications. This versatility is due to the existence of different options depending on the dimensions desired as well as the installation site. Options such as the uM, uM2, uM6. Compared to other PV systems on the market, uMx products can produce more power per surface area with an easy installation methodology.

Due to the fact that all solar power generators systems are composed of the same basic module, the uModule, all the systems have some features in common, in terms of overall efficiency (30%), multi-junction cells efficiency (40%) and land energy density (2,800 kWh/kW). Basically as their names indicate, the uM2 generator is composed of two basic

uMs. Some of its highlights is that the voltage remains constant, with the current varying proportional to solar radiation. Similar, the uM6 shown in Figure 43, but in this case, it is composed of six basis uM. uM is logistically easy to transport being able to be shipped anywhere in the world.

uM relevant features, and technical and operational parameters are shown in Table 11 whereas uM IV and PV curves are shown in Figure 44, while Table 12 shows the specifications of two different uM systems. [61].

Table 11: uModule's relevant technical and operational parameters [data from 61].

Electrical specifications		Physical specifications	
Rated Power (CSTC[1])	2.7 kW	*Weight*	285 kg
Rated Power (CSOC[2])	2.3 kW	*Frontal Area*	11.2 m^2
Module Efficiency[3]	30%	*Outer Dimensions*	2.16x5.11x0.31 m
Rated Voltage (Vmp CSOC)	475 V DC	*Ground Interface*	Buried or flanged pedestal
Open Circuit Voltage (Voc CSOC)	540 V DC	*Geom. Concentration ratio*	1000x 900x (actual)
Rated Current (Imp CSOC)	4.9 A	Other specifications	
Short Circuit Current (Isc CSOC)	5.4 A	*Temperature range*	-40 ºC to 60 ºC
Temp Coefficient of Power	-0.14%/ºC	*Max survival wind speed*	40 m/s stowed

1: CSTC is 25 ºC cell temperature, 1000 W/m^2.
2: CSOC is 2 m/s wind, 20 ºC ambient temperature and 900 W/m^2.
3: Aperture efficiency in CSOC conditions.

Figure 43: uM6 solar power generator composed by 6 x uM modules [61].
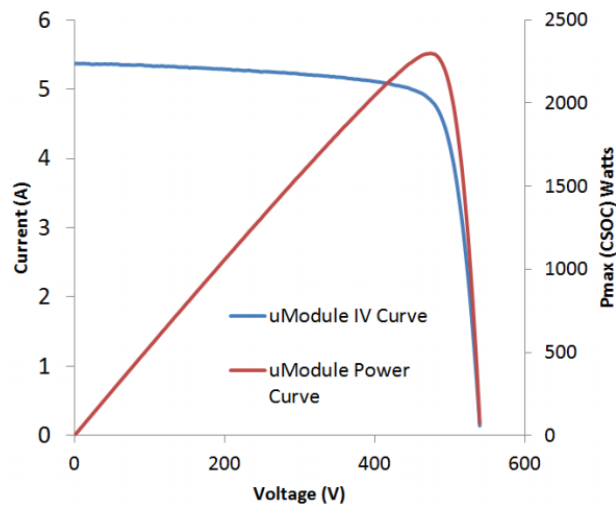
Figure 44: uM IV curve [61].

Table 12: Relevant specifications of uM2 and uM6 [data from 61].

Electrical specifications	uM2	uM6
Rated Power (CSTC[1])	5.4 kW	16 kW
Rated Power (CSOC[2])	4.6 kW	14 kW
Short Circuit Current (Isc CSOC)	10.8A	29 A
Rated Current (Imp CSOC)	9.7 A	32 A
Physical specifications	uM2	uM6
Weight	998 kg	3323 kg
Frontal Area	22.4 m^2	66 m^2
Outer Dimensions	5.1x5.1x1.6 m	7.5x10.2x1.7 m

2.6.2.3   BSQ-D280 HCPV Module by BSQ Solar

Similar to the previous technology, BSQ has created many different CPV systems but all are integrated with the same basis component, the BSQ solar basis module "BSQ-D280 HCPV Module". The module stands out for its simple and rugged module design, a wide acceptance angle non-imaging optics, a very high concentration factor, and high efficiency, which enables it to provide high-density and sustained solar energy output. Relevant data is shown in Table 13. Its performance is based on:

- Triple junction cells with high average efficiency.
- A uniform light flux over the cell created by secondary optical based on kaleidoscope.
- Singular concentrating Fresnel lens, with top dimple and domed-shaped, which maximizes pointing tolerance of the acceptance angle up to 0.9°.

Table 13: Relevant data of BSQ-D280 HCPV Module [data from 62].

Module features		Electric features	
Dimensions (L)x(W)x(D)	1005×1005×238 mm	**Module Efficiency**	28%
Solar aperture	1 m^2	**Voc**	78 V
Weight	23.6 kg	**Isc**	4.3 A
Maximum static load	2400 Pa (back panel) 5400 Pa (else)	**Vmpp**	70 V
Cells per module	25	**Impp**	4.0 A
Geometrical concentration ratio	820x	**Power**	280 W
Acceptance Angle (90% output)	±0.92 °	**Max. System Voltage**	900 V
Lens Material	PMMA	**Temp. Coefficient**	-0.21 %/K
Cell Material	InGaAs/GaAs/Ge	**Connector model**	Amphenol® Helios4

BSQ Solar can provide CPV systems custom made designs especially devised for installation in urban areas including parks, pedestrian sidewalks, parking lots, or even in domestic gardens, which is very interesting for the main purpose of this project. The

transit of people and vehicles underneath the HCPV array is possible due to the tracker's larger poles. Also customized HCPV designs with reduced height and enhanced landscape type aspect ratios can be produced to be installed in places where the visual impact has to be reduced. In Figure 45, the different possible BSQ-CPV systems [62] can be appreciated with the number of basic modules for each one of them placed between parentheses.
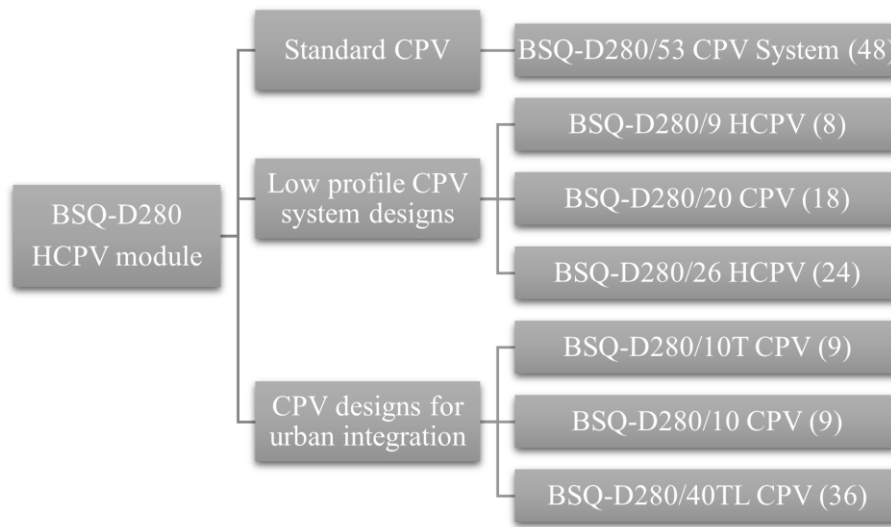
Figure 45: BSQ available CPV systems.

As can be appreciated, the BSQ-D280/53 CPV system contains the highest number of modules with a total of 48, returning the highest electricity generation compared to other BSQ systems. This model will be further analysed in the next chapters. Relevant specifications are shown in Figure 45.

2.6.3 CSP-CPV hybrid systems

2.6.3.1   *Z10 Combined heat and power*

Z10 systems manufactured by the company "Suncore Energy" are collectors capable of providing hot water and electricity, with an overall system efficiency >67% and making use of multijunction cells which reach an efficiency greater than 39%. It includes an accurate 2-axis tracking which tracks the sun producing stable output during the whole day and can be managed by a user-friendly web-based monitoring system. Another

remarkable property is the optimized land usage because of its installation trough penetration or ballasted foundations. It is a cost effective technology characterized by its easy installation and quick payback. A collector is shown in Figure 46, meanwhile its properties are shown in Table 14.

Table 14: Z10 CHP technical and operational parameters [data from 63].

General		Electricity	
Total aperture area	12 m^2	*Nominal electrical power**	1.5 kWDC
Tracking technology	2-axis	*Short-circuit current* (Isc)*	13 A
Azimuth range	0-360º	*Open-circuit voltage* (Voc)*	218 V
Elevation range	10-95º	*Operating current* (Imp)*	10.2 A
Tracking control	Closed or open loop	*Operating voltage* (Vmp)*	146.5 V
Thermal		Physical	
Working fluid	RODI water or coolant	*Weight*	540 kg
Nominal thermal power*	6.5 kW$_{th}$	*System height*	3.5 m
Nominal fluid flow	6-9 L/min	*System width*	6 m
Max fluid supply temperature	70 °C	*Max operating wind speed*	40 km/h

* Rated at 40 ºC Input Temp, 8 LPM Flow Rate and 1 kW/m^2 direct normal irradiance.

Figure 46: Z10 CHP solar collector [63].

59

2.7   Other related research projects in Malta

Previous projects carried out at the University of Malta had pointed out to the importance of developing sustainable energy in Malta, mainly due to its favourable and promising climatic conditions.

In a project entitled "Assessing the potential of installing photovoltaic panels in car parks to reach 2020 EU targets" [64], R. Tanti made an analysis of the possibilities of installing PV technologies in car parks and disused quarries, pointing some advantages such as the added benefit of providing shelter for the cars, government financial support and implementation of vehicle charging stations. Nonetheless, the methodology employed differs greatly from the one carried out in this dissertation.

In terms of concentrated technology F. Magro in "Design and testing of a low-level concentrator" [65] builds up and tests a prototype system in Malta. Essentially, this was a concentrator module which holds up to four Fresnel Lenses that concentrate the sunlight onto the receiver.

Lastly and more concretely in CSP, R. Mangion et' al. have worked with a local enterprise "Sirius Systems Ltd" to develop a low-priced system consisting of a solar parabolic trough coupled to a Stirling engine, making it suitable for small spaces such as rooftops. The M.Sc. dissertation was entitled "Development of a Stirling engine powered by parabolic trough collectors" [66].

2.8   Summary

From the extensive literature review carried out in this chapter, one can conclude that although the potential of CSP technology is huge, only modular CSP system may be applicable in Malta due to space restrictions. Within that category of CSP technologies, the actual commercially available and operating systems are still rare. The only Stirling Dish available on the market is the one developed by GEO company. Other technologies developed by Ripasso, Infinia or HelioBooster, among many others, which were developed and installed in some parts of the world can no longer be supplied, either because the respective companies have declared their bankruptcy or they have decided to stop production, such as "Zenith Solar", "SES", "SouthWest Solar" or "Solar Systems".

As part of the literature review, the opinion of some experts in the field has been obtained through personal contacts by e-mail and telephone. These experts were researchers from CIESOL and the European CSP Platform (PSA) in Almeria, such as Eduardo Zarza Moya, as well as CEOs of some of the aforementioned enterprises such as Manos Ioannidis from Maximus Solar.

The conclusion reached is that nowadays there is a huge lack of these systems in the market due to several financial and technical reasons. For example, the low competitive prices of other energy sources and systems and the fact that till now, the Stirling dishes have been incapable of overcoming certain technical problems that have been identified such as:

- The connection between the tank where thermal energy is stored and the Stirling engine itself.
- The low power output limitations of the Stirling engine itself.
- The need to store the generated energy during the day to provide it during the night to the head of the engine, where electricity generation takes place.

On the other hand, CPV technology, also developed throughout this extensive literature review chapter, has emerged as a cutting edge technology, with a huge upgrowth and appearance of new prototypes during last years, reaching commercial viability to compete against flat-plate PV after years of deployment. Like CSP, CPV is a renewable energy based on the production of electricity by using solar concentration. However, the carried process to achieve this purpose is totally different to CSP, resembling more to conventional PV technology but concentrating the sunlight by several tens of folds.

Unlike CSP, a number of available CPV products have been identified to exist in the market.

Lastly, CSP-CPV hybrid systems have also been mentioned. Systems where both technologies (CSP and CPV) are combined together provide greater advantages over PV/CPV-alone or CSP-alone, as long as there is the need for the generated thermal energy output.

CHAPTER 3: METHODOLOGY

3.1 Determining the most appropriate locations for installing modular solar concentrators

In order to evaluate the feasibility of installing solar concentrated projects in Malta, the first goal that needs to be overcome is to survey and find the suitable areas which fulfil the boundary conditions, as amply discussed in Chapter 1: Introduction above. By using multiple computer software, mainly ArcGIS 10.6.1 [67], Google Earth [68] and Google Maps with its function satellite view [69], a systematic methodology has been developed as explained below. The results of these studies are shown in Chapter 4. It is to be noted that the use of ArcGIS was completely learned and applied within the course of this dissertation and this required the dedication of many hours of studying and the support of the co-supervisor.

3.1.1 Analysis of Malta's territory to select the available spaces

The determination of the potential sites for installing the technology has been developed working simultaneously with the renowned software on Geographical Information System, the program ArcGIS Desktop 10.6.1 along with its extension "Spatial Analyst", as well as the use of satellite images of Malta's territory taken from Google Maps, to visualize the spatial limitations and opportunities.

Spaces sought included portions of free land property of Maltese Government or public entities with secondary uses. This included large roundabouts on arterial roads, large car parks and wide curbs and disused spaces surrounding industrial estates.

Some of the basic constraints that were introduced when looking for potential sites on Google Maps Satellite and Street View [67] were to ensure that the locations do not have other uses such as embellishments with large mature trees and availability of ample space when considering road safety. The ArcGIS software was then used to analyse the sites in terms of dimensions, total available area, cross-shading by adjacent obstacles as well as the quantification of incident solar radiation, all contributing to achieve the purpose of identifying the potential sites for placing modular concentrated solar power systems. The method followed included the use of an Open Street Map (OSM) file for Malta [70], as shown in Figure 48, with the World Geodetic System 'WGS 1984' centred to Malta. An

OSM is a typical map that represents all the urban structure (all the roads, city limits, names, quarries, interesting places etc…) for any place in the world [70]. The OSM served as a base map for the software ArcGIS. Then "heads up" editing was used to create the spaces that were eventually used for analysis. The feature class was a polygon and the vectorisation exercise involved heads up digitising of all the spaces that were selected beforehand. Simultaneously, the software created a layer's attribute table with the fields FID (long integer type) and Shape (string type). Another one called ID_1 (long integer type) should be created, with identical values as FID whose function is to ensure the initial numerical order is not changing when modifications as remove rows are made in the table. Once this procedure was completed the software had the necessary information to compute the modelling exercise as shown in examples Figures 49, 50, 51. The polygons are in black as indicated in the legend on the maps. All the maps shown below were taken when working with the "Layout View", adding their respective legends, scale bars and orientations (compass).

Figure 47: An OpenStreetMap view of Malta [70].

Figure 48: Portion of Malta with some potential spots such as roundabouts selected on main roads.
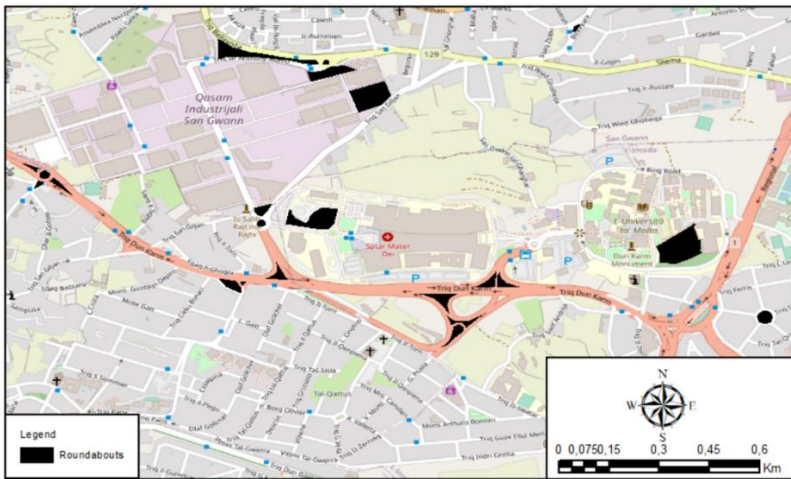
Figure 49: Example of spots in car parks and other locations.

Figure 50: Example of some spots selected inside industrial estates.

64

3.1.2 Solar radiation simulation

Analytical, visual and numerical results were obtained through the ArcGIS software, Arc Map [67] and its extension "Spatial Analyst".

To carry out this exercise, a Digital Surface Model (DSM) from Malta was needed. A DSM is a numerical data structure which symbolizes the Earth´s surface including all bodies on it as the reflective surfaces of buildings, trees, and other features elevated above the "Base level of Earth" and storing the elevation information of each pixel. Once included in ArcMap, the DSM provides a map with a scale range of colours, which represent the different heights in each pixel [71]. It is a powerful resource, often used for radio frequency (RF) planning, landscape modelling, city modelling, visualization applications and more. In this case, the DSM from Malta used, shown in Figures 52 and 53, has been obtained from Malta Information Technology Agency (MITA) [72] through an official request.
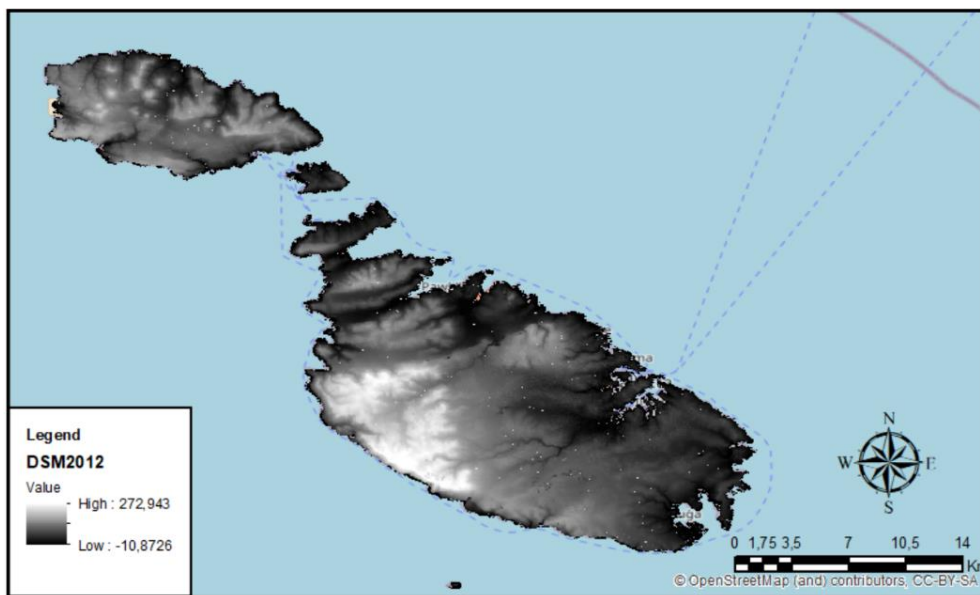
Figure 51: DSM of Malta represented in ArcMap 10.6.1 [67,72].
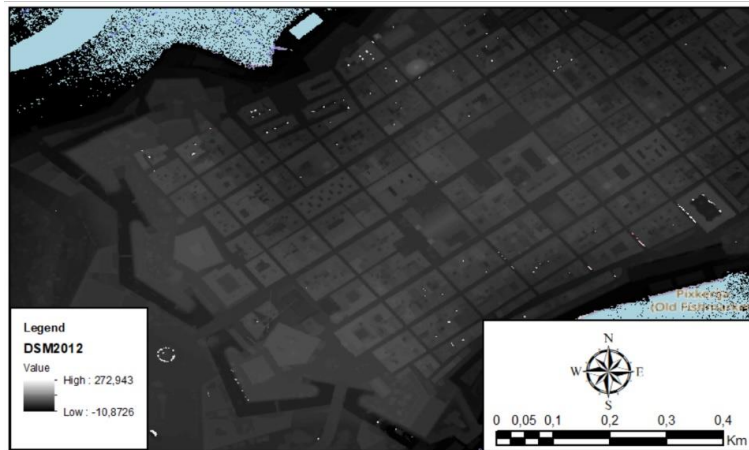
Figure 52: Zoomed in view of DSM to appreciate details.

By adding DSM as a layer in ArcGIS and imposing a 40% transparency layer parameter and a Hillshade raster feature (a tool from Spatial Analyst extension), the outcome gives a perfect visualisation of the ground surface where buildings, trees, and obstacles are seen in three dimensions, as shown in Figure 54.
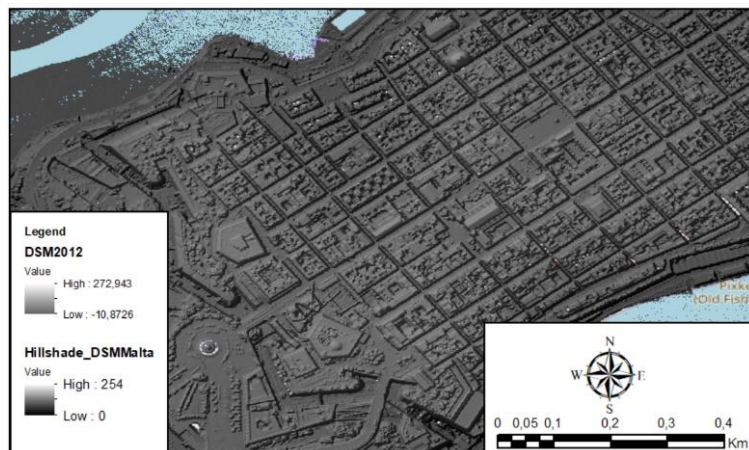
Figure 53: Aspect of Hillshade raster layer along with DSM.

Hence, now that any element of Malta's map can be perfectly distinguished, it is necessary to introduce a new layer which is going to represent the solar radiation by means of ArcMap [67] extension Spatial Analyst tool named "Area Solar Radiation".

Following this, a new layer that diagnosed the availability of solar radiation on this 3D map was superimposed, by means of ArcGIS extension Spatial Analyst tool named "Area

Solar Radiation". The tools from the solar radiation analysis extension allow to analyse and map the effects of the sun automatically. The software calculates the solar radiation over a geographic area for precise time period based on viewshed algorithm methods developed by 'Rich' (1990, 1994) and lately extended by 'Fu and Rich' (2000, 2002). Topography is a major aspect when talking about determining the spatial variability of insolation, factors as orientation, shadows cast by topography, and elevation affect the total insolation at a determined location. This variability depends on the time of day and season or period of the year too and, likewise, contributes to variability of climate conditions including factors such as snow melt patterns, ground and air temperature, ground moisture, and light availability.

This model considers daily and sun angle's seasonal shifts, compass direction (aspect) and steepness (slope), atmospheric conditions, and shadows cast effects generated by surrounding topography, elevation and site latitude, as well as obstacles such as nearby trees or buildings that could block sunlight. The obtained outputs are able to be effortlessly combined with other GIS data.

Solar global radiation on the horizontal is the sum of direct, reflected and diffused radiation on that plane horizontal. The direct radiation component accounts for solar radiation reaching the Earth without attenuation by the atmosphere and is the strongest component on clear days, followed by diffuse radiation. Diffuse radiation can be described as solar radiation that has been dispersed by particles and molecules in the atmosphere but has still reached the surface of the Earth, as well as that radiation that has been emitted from surrounding topologies. Diffuse radiation is much lower in intensity than direct radiation. Reflected radiation is that component of solar radiation that has been reflected from shiny bodies such as white surfaces, the sea or snow. Hence, it is only significant when a location is surrounded by high reflective surfaces. Considering these definitions, ArcMap [67] calculates the global solar radiation on the horizontal considering only the direct and diffuse radiation [73], as shown below (13).

The model developed through ArcGIS [67] used to simulate the radiation includes [74]:

1. Based on topography, the estimation of an upward-looking hemispheric viewshed.

   A viewshed can be defined as a raster rendering of the entire sky viewed from a particular location that can be obstructed or clear. It is calculated by determining the horizon angle (maximum angle of sky obstruction) and searching in several

directions around the location of interest. To calculate the rest of unknown directions, two nearby or adjacent known points are taken as basis from which horizon angles are interpolated. Then, to represent a two-dimensional raster image these angles are turned into a hemispheric coordinate system (CS). An only value which depends on whether the sky directions are viewable or not is assigned to every raster cell of the viewshed. Output cell locations correspond to azimuth angle (α) and zenith angle (θ) on the hemisphere of directions. The resultant viewshed characterizes both visible sky directions (white), and obstructed (grey) as shown in Figure 55.
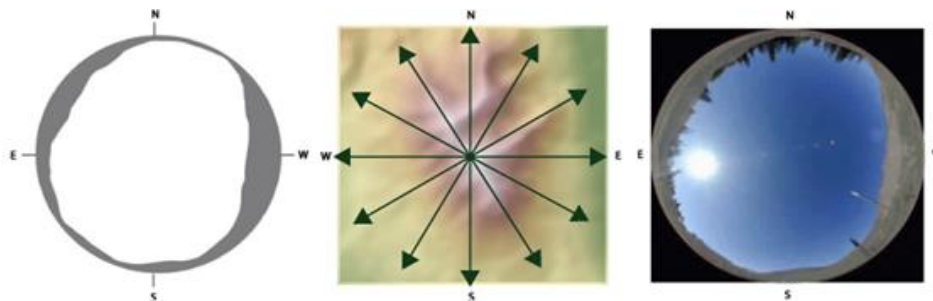
Figure 54: Resultant viewshed, horizontal angles, and viewshed painted over sky view [74].

2. Direct radiation is estimated by overlaying the viewshed on a direct sun map.

   A sun map can be defined as a raster representation that exhibits the sun's relative position or its track, as it changes throughout time (hours, days and years). A sun map in the same hemispherical projection as the viewshed is used to calculate the direct solar radiation arising from every sky direction. The sun track is determined via the latitude of Malta and the time configuration is set according to interest. A particular identification value along with its azimuth (α) and zenith (θ) angles are specified for each sun map sector. To calculate the direct radiation, viewshed is superposed over the sun map, therefore solar radiation arising from any of the sectors is computed independently.

3. Diffuse radiation is estimated by overlaying the viewshed on a diffuse sky map.

   As result of the scattering by atmospheric elements, the diffuse radiation is originated into all sky directions. Diffuse radiation is calculated through creating

a sky map which represents a hemispheric view of all the sky fractioned into groups of sky sectors characterized by a unique identifier value, θ and α angles.

4. To produce the insolation map, the procedure is repeated for every location of concern by overlaying the viewshed with sky and sun maps as shown in Figure 56.

During the insolation calculation, the sky and sun maps rasters are superimposed with the viewshed raster. Dividing the total clear cells by the overall cells per sector, the total amount of visible sky area is computed for every sector. Then, by summing both, diffuse and direct insolation proceeding from the clear sky directions, the global solar radiation is calculated, as shown in the equations below.
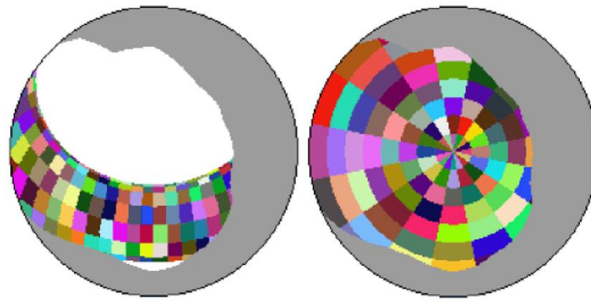
Figure 55: Viewshed superimposed with sun map and with sky map [74].

The information related to obstacles, orientation and pendant is offered by the DSM as well as geographical data like latitude and longitude. The software analyses data taking in account only the time during daily solar hours. The obtained map result shows the quantity of solar radiation in kWh/m^2 in each cell. The calculation of total solar radiation is as follows [73]:

$$Global_{total} = Direct_{total} + Diffuse_{total} \qquad (13)$$

Direct total is the sum of all sun map sectors direct insolation on the horizontal ($Dir_{\theta,\alpha}$). This direct insolation ($Dir_{\theta,\alpha}$) with a centroid at azimuth (α) and zenith (θ) angles is calculated using the equation below:

$$Dir_{\theta,\alpha} = S_{const} * \beta^{m(\theta)} * SunDur_{\theta,\alpha} * SunGap_{\theta,\alpha} * cos(AngIn_{\theta,\alpha}) \qquad (14)$$

where:

- β: atmosphere's average transmissivity for the zenith direction shortest path taken.
- S_{Const}: solar constant. It is defined as the solar flux external to the atmosphere at the average Sun-Earth distance. In the analysis, $S_{Const} = 1.367$ kW/m^2, proportioned by World Radiation Centre (WRC).
- m(θ): relative length of the optical path. It is determined by the altitude above sea level and the solar zenith angle (θ). For θ < 80°, it can be calculated as:

$$m(\theta) = \frac{e^{-0.000118 * h - 1.638 * 10^{-9} * h^2}}{cos\theta} \qquad (15)$$

   where:

   - h: height above sea level (m).
- $SunGap_{\theta,\alpha}$: sun map sector gap fraction.
- $SunDur_{\theta,\alpha}$: time duration represented by each sky sector. The way to calculate it is by multiplying the hour intervals by the day intervals.
- $AngIn_{\theta,\alpha}$: incidence angle between the centroid of the sky sector and the normal-to-surface axis. It is calculated as:

$$AngIn_{\theta,\alpha} = acos(cos(G_\theta) * cos(G_z) + sin(G_\theta) * sin(G_z) * cos(\alpha - G_a)) \qquad (16)$$

   where:

   - G_a: surface azimuth angle.
   - G_z: surface zenith angle. Refraction acquires importance when this angle is greater than 80°.

Similarity, diffuse total is the sum of all sky map sectors diffuse insolation ($Dif_{\theta,\alpha}$). $Dif_{\theta,\alpha}$ is calculated at its centroid for each sky sector, integrated over the time intervals, and then should be rectified with the incidence angle and the gap fraction through the equation below:

$$Dif_{\theta,a} = R_{glb} * P_{dif} * Dur * SkyGap_{\theta,a} * Weight\theta, a * cos(AngIn_{\theta,\alpha}) \qquad (17)$$

where:

➢ R_{glb}: value of global normal radiation, resulted from:

$$R_{glb} = \frac{S_{const} * \Sigma(\beta^{m(\theta)})}{1 - P_{dif}} \qquad (18)$$

➢ $SkyGap_{\theta,\alpha}$: gap fraction which express the proportion of visible sky sector.

➢ Dur: time interval for analysis.

➢ P_{dif}: diffused fraction of the total global normal radiation flux. It is usually set depending on the sky conditions, being possible to take values from 0.2 (very clear) to 0.7 (very obstructed).

➢ $Weight_{\theta,\alpha}$: fraction of diffuse radiation from a particular sky sector, relative to the total sectors. For the uniform sky diffuse model used to carry the analysis in this dissertation it is calculated as:

$$Weight_{\theta,\alpha} = \frac{(cos(\theta_2) - cos(\theta_1))}{Div_{azi}} \qquad (19)$$

where:

- Div_{azi}: on the sky map, number of azimuthal divisions.
- θ_1, θ_2: zenith angles responsible of bounding the different sky sectors.

The simulation was run using the year 2019 as reference to be as recent as possible and simulating hourly data for the whole year. Moreover, 32 different directions in each DSM cell for the analysis to find possible obstacles interfering with light. During the characterization there is a parameter "Z-factor" that needs to be specified. The Z-factor is essential for correcting calculations related to surface units. In this case, equal units have been used, so to get accurate results, Z-factor=1. The obtained result is shown in Figures 57, 58, 59 with different zooms to appreciate details.
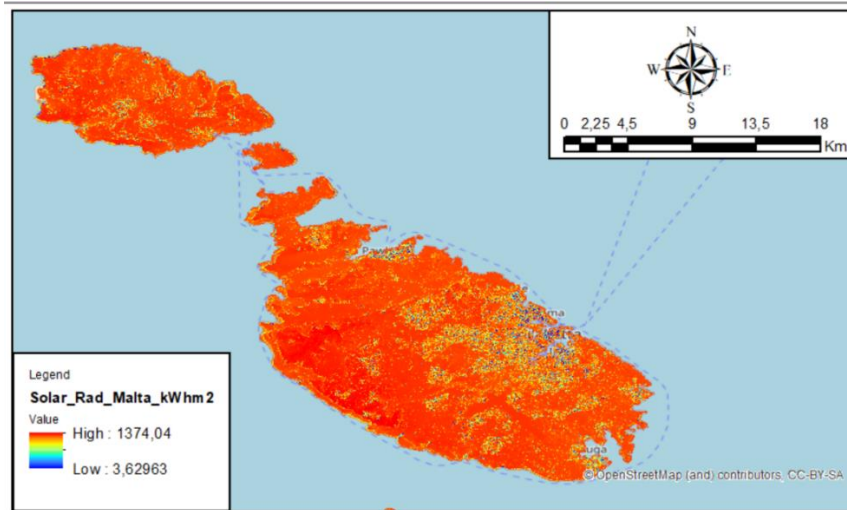
Figure 56: Malta's average solar radiation during the whole 2019.

.
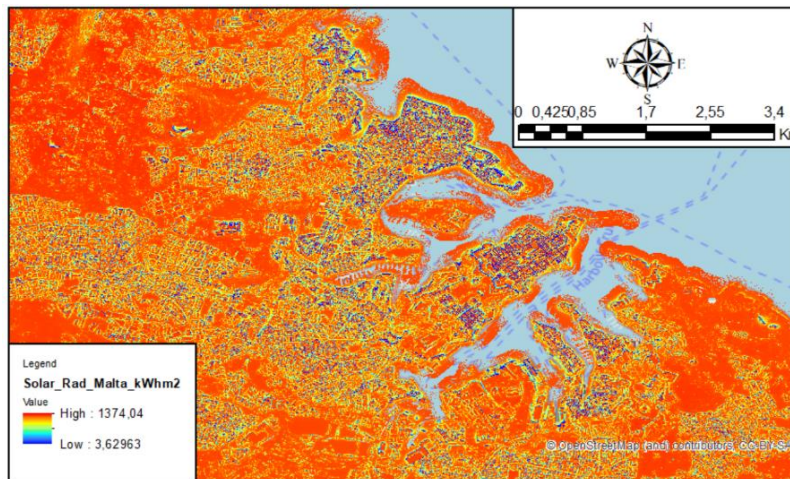
Figure 57: Zoomed-in view of Malta´s solar radiation map.
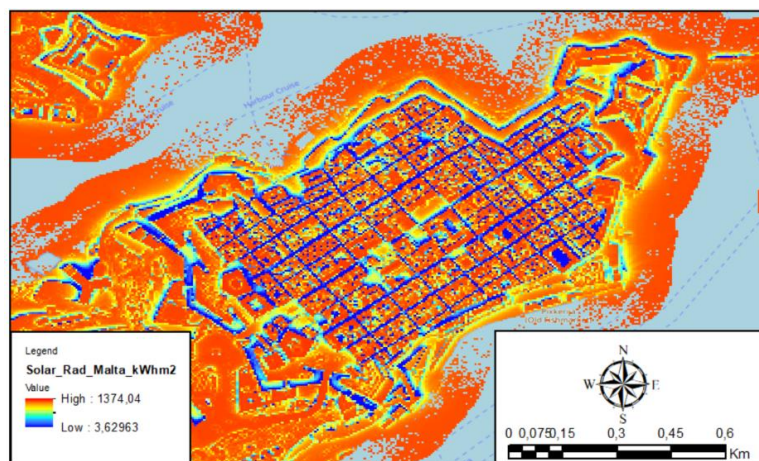
Figure 58: Valletta's solar radiation view.

This solar analysis facilitates the choice of potential locations based on their solar availability for installing concentrated solar technology.

Furthermore, a number of constraints have been additionally imposed to arrive to the final outcome of the suitable sites. These constraints included:

➢ Orientation layer: best possible orientation for solar collection is south direction. The basic principle of the orientation layer is to represent all the map with different colours according to different degrees ranges for each cardinal point as shown in Figure 60. After selecting the most suitable locations basing the choice on solar radiation field, this layer would be useful to narrow down the options by checking and removing the area if it is oriented to the north.
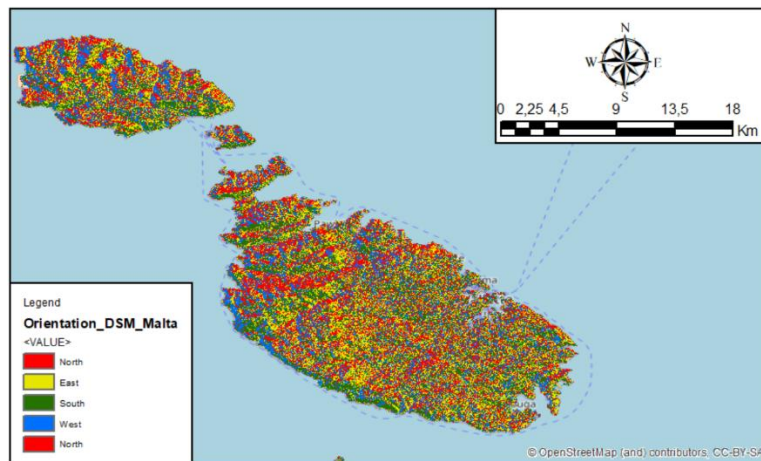
Figure 59: Orientation layer for Malta with the fourth cardinal points.

➢ Pendant layer: the same theory as the orientation layer applies. Pendant layers represent in the map four different colours depending on ground's inclination degrees as shown in Figure 61. After selecting the most suitable locations basing the choice on solar radiation field, high pendant locations are going to be discarded due to interference with optimum operation of tracking systems and complications in installation structures.
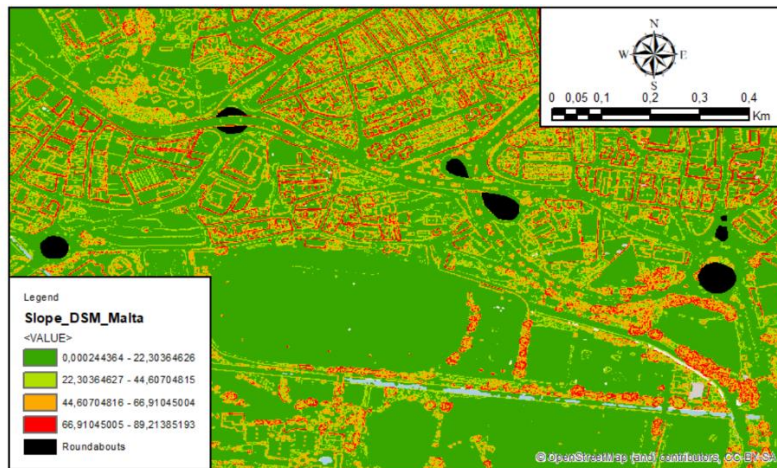
Figure 60: Pendant layer for Malta's map.

➢ Areas with low solar radiation: in order to be cost effective, areas in locations with lower amounts of solar radiation would need to be filtered off. This filter is being applied in two different ways.

For the analytical part, the table with potential sites will be filtered by removing all sites that have less than 1000 kWh/m^2 per year. It is to be noted that for Malta, a sunny horizontal surface collects a total global solar radiation of up to 1875 W/m² per year. This can be visually made by using the conditional evaluating tool applied as input to the solar radiation layer and setting a minimum of 1000 kWh/m² limit to it. By reducing the range in this way, the colour rendering is enhanced, which allows a better visual interpretation of the map and an easier way to compare the locations and make choices. Figures 62 and 63 show the new solar radiation layer obtained. As it can be seen, the colour distribution in this layer is so different from the one shown previously in Figures 57, 58 and 59.
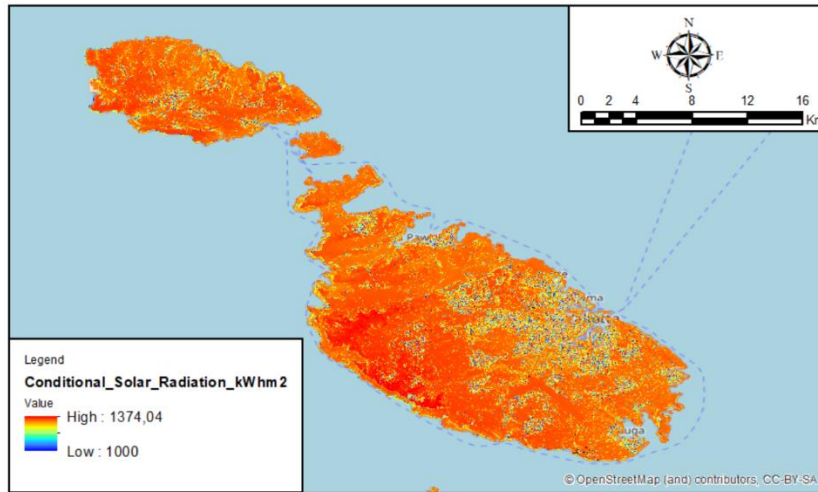
Figure 61: Conditional solar radiation layer.
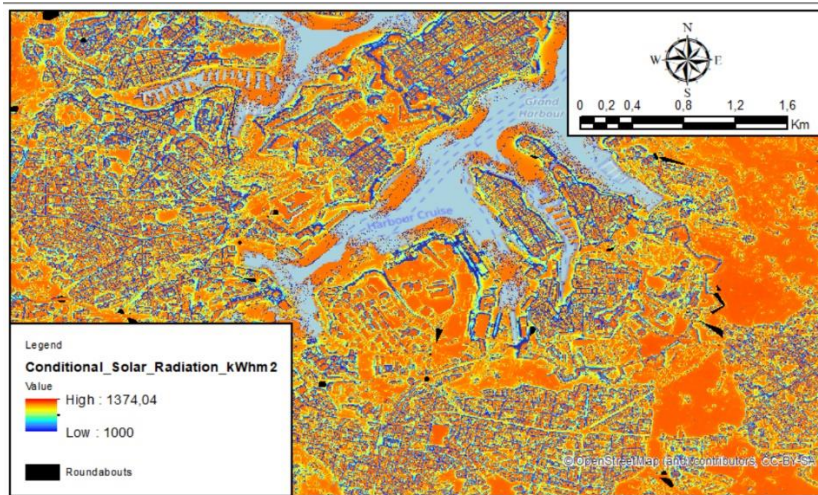
Figure 62: Conditional solar radiation layer zoomed in to appreciate the difference.

➢ Minimum area attribute: as it can be read in literature review (Chapter 2), solar concentrators especially Stirling dishes need a minimum area for installation and operation due mainly to their big dish size. Thus, taking as reference the area parameter from the polygons, and following a similar procedure as before, a minimum area of 150 m^2 was set and this helps to eliminate small locations from the list of potential sites. This filter is applied later in the final table by using 'selection by attribute' tool. The set limit of 150 m² includes space around the site, which is necessary for road safety in case of car accidents.

Hence all these raster layers and conditions are fundamental to provide evidence to discard spots that for example, aim to the north range, do not receive enough solar radiation or do not have a minimum area to install the different devices.

3.1.3 Quantifying solar radiation in every location

Finally, the current map obtained shows the total amount of solar radiation each raster cell receives. In the raster layers, the cells cover a relatively small area (0.5 m^2), thus this information is not that significant alone, and one needs to integrate all these points for the entire earmarked site to obtain the overall solar radiation received for each location in a year, which will eventually be utilised by the concentrated solar power system to convert to electricity.

Working with 'Zonal Statistics as Table' tool, and selecting statistic type mean, ArcMap [67] would develop a table containing fields for the average solar radiation in kWh/m^2 (MEAN), identification of polygon (ID), area in square meters (AREA), and number of cells (COUNT) for each polygon. Also, it includes other fields which represent the minimum (MIN) and maximum (MAX) solar radiation on site, the difference between these two parameters (RANGE), the standard deviation for solar radiation attribute (STD) and the total sum of all cell solar radiation values in each polygon (SUM). This table is created separately from the spatial data on the map, so it has to be linked to it using the "Add Join" tool. The Add Join tool links a table to a layer's attribute table or another table and matches the fields from both table and spatial map to each other. In this case, the matching field used was the FID parameter. So a new table with all fields of information is now created as can be seen in Table 15.

Therefore, it is possible to obtain the total usable radiation in each location, and for that a new field called "Usable Solar Radiation" should be created in the attribute table. Choosing a double data type and multiplying both fields AREA and MEAN and dividing the result by 1,000 to convert it from kWh to MWh, all Usable Solar Radiation column is obtained.

For this dissertation, only the irradiation in kWh/m^2 is needed, so the MEAN parameter is the field of interest for later calculation of the electricity generated by the concentrated solar power system.

Table 15: Portion of the table resulted from running 'Zonal Statistics as Table' tool with different fields as AREA, COUNT and MEAN (average solar radiation in kWh/m^2) for each polygon.

OBJECTID*	FID*	COUNT	AREA	MIN	MAX	RANGE	MEAN	STD	SUM
1	0	13	325	1267,957275	1327,08313	59,125854	1311,90456	19,692541	17054,759277
2	1	41	1025	1313,101685	1338,764648	25,662964	1332,892477	5,727333	54648,591553
3	2	84	2100	1251,036499	1339,755981	88,719482	1328,376126	14,188709	111583,594604
4	3	65	1625	1324,082031	1336,48645	12,404419	1333,77564	2,336056	86695,416626
5	4	78	1950	1084,739746	1340,688721	255,948975	1313,379933	44,826348	102443,634766
6	5	15	375	775,959351	1340,773071	564,813721	1166,541056	163,24006	17498,115845
7	6	7	175	1336,737183	1337,907471	1,170288	1337,264038	0,416197	9360,848267
8	7	14	350	1291,891602	1323,346069	31,454468	1312,689802	9,348355	18377,657227
9	8	72	1800	1110,883057	1330,665405	219,782349	1291,801059	45,196342	93009,67627
10	9	73	1825	1189,671021	1327,086304	137,415283	1308,066165	21,485576	95488,830078
11	10	24	600	1107,619263	1330,368408	222,749146	1282,538086	53,634096	30780,914063
12	11	27	675	786,256104	1332,119751	545,863647	1181,8644	151,119325	31910,338806
13	12	94	2350	1160,703369	1328,290161	167,586792	1309,711997	28,134733	123112,927734
14	13	39	975	901,928101	1326,559692	424,631592	1259,165934	80,878906	49107,471436
15	14	122	3050	718,755127	1329,899536	611,144409	1238,878051	109,695878	151143,122253
16	15	46	1150	911,332825	1339,682983	428,350159	1264,958799	93,536614	58188,104736
17	16	70	1750	1091,933838	1336,378662	244,444824	1311,431942	44,100151	91800,235962
18	17	21	525	1329,396606	1334,89209	5,495483	1332,635452	1,156259	27985,344482
19	18	29	725	1086,272949	1340,530762	254,257813	1268,908039	73,211177	36798,33313
20	19	45	1125	1335,74939	1339,42749	3,678101	1338,08007	0,820241	60213,603149

(0 out of 169 Selected)

Rad_Solar_Table_Ex

It must be highlighted that the software can mix the data of the table if any modification is made like deleting a row or filtering some values. Thus, the last stage involves including a new field called ID_1 in the feature class in which each polygon has the same value as the FID to always keep an invariant field. Also, to ensure the program does not make any undesired modifications when the data of the table is sorted or edited, a copy of the table has been exported to an Excel sheet [75], which acts as master copy in case of need to compare or check any data.

The Excel file is further analysed using advanced sorting, filtering the different fields from highest to lowest values and selecting 'zoom to selected' in each row to identify the polygon. By setting appropriate limits to different parameters as shown in Table 16, [75] the best possible spots are chosen for further analysis and discussion in the next chapter (Chapter 4: Results and Discussion) reducing the total options from 154 to the best 40.

Table 16: Limit values settled to reduce the sample of locations.

Field / Parameter	Limit condition
Mean	> 1325 kWh/m^2
Standard Deviation (STD)	< 5 (95% confidence)
Area	> 200 m^2
Range	< 50 kWh/m^2

The limits shown above have been established taking into account different facts, the accuracy and dispersion of values, minimum space requirements, higher efficiency, etc… and in case of Mean and STD, analysing the scattering of values too, as shown in Figures 64 and 65.
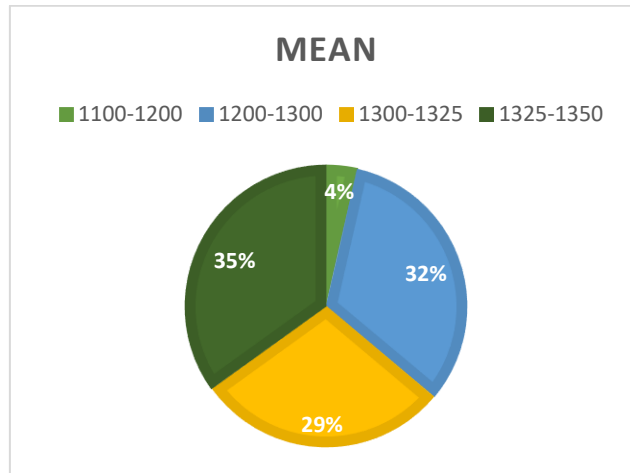
Figure 63: Percentages dispersion of mean values.
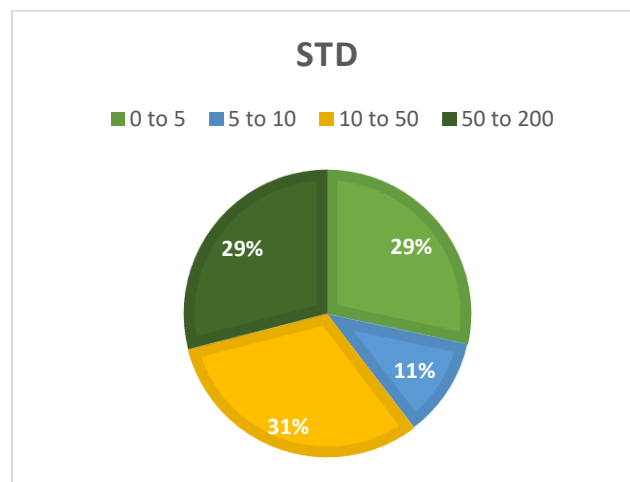
Figure 64: Percentage dispersion of standard deviation STD values.

As can be seen in both figures, the limits chosen represent a significant huge percentage out of the total which means that there is a great concentration of values there. Some percentage ranges are higher, but it has to be noted looking at the graph's legends that not all the options have the same range and amplitude, because they have been done trying to clarify the visual comparison.

3.1.4 Solutions implemented to arising issues in the methodology

The DSM layer has been obtained from an external source, so the GCS was not the same as that being used in this project, with the result that there was a mismatch between the two layers, namely, the vector layer (developed by the author) and the DSM. The best way to solve this problem was to add the DSM layer again but making an automatic GCS transformation with ArcGIS with what is known as 'an on the fly projection', as shown in Figure 66.
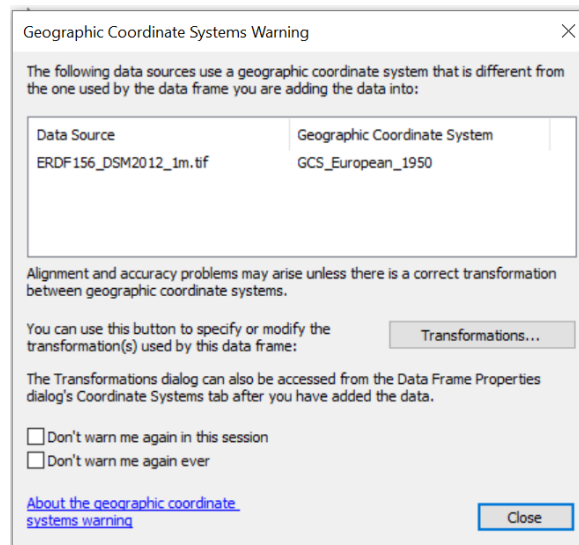
Figure 65: Menu with the transformation "an on the fly projection".

Another issue was found when layers such as orientation and slope were created. The software automatically generates an extensive number of different colours and ranges, which makes it impossible to differentiate between them. For example, in the case of orientation, ArcMap [67] generates different intervals for cardinal points as shown in Figure 67.
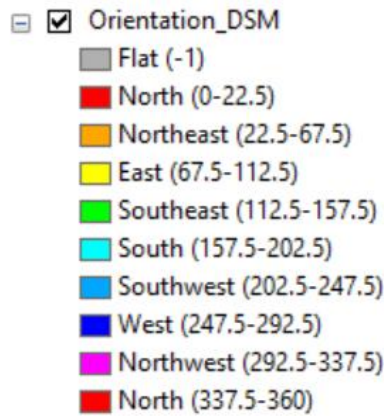
Figure 66: Different intervals initially created by ArcMap in an orientation layer.

The solution employed consisted of editing the legend menu within the properties window, to establish the ranges of values and colours that suits our needs, as shown in Figure 68.
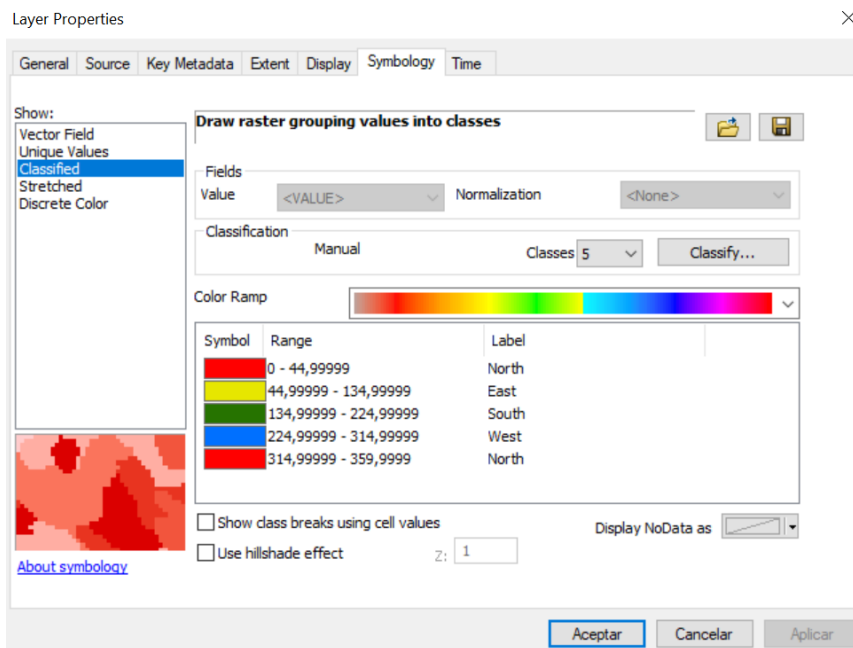
Figure 67: Symbology menu with desired intervals.

3.2 Energy generated by each system

This section explains how to calculate the annual output of using the selected systems available on the market under weather conditions of Malta. The process to calculate the

energy generated by each available system considered as an option to be installed in Malta depends on the type of technology.

In the case of CSP systems, issues such as the lack of appropriate software to carry out the calculations or the lack of some parameters in various technical data sheets offered by the manufacturers make the process to obtain an approximation or simulation of the operation in Malta, really complex (impossible in the cases of data deficiency). For these reasons, and due to the absence of defined and reliable systems in the market, the solutions considered are:

- To take as reference the value of generation rated at 1 kW/m^2 given by the seller.
- Ask the manufacturer company to check if they use any software capable of obtaining the output production.

On the other hand, in the case of CPV, through the use of PV F-Chart [76] software, an analysis of the electricity power generated by the cells can be carried out. By introducing several operational and technical parameters the software simulates the operation of the CPV technology in Malta obtaining as output the electricity generated over one year. The process to make the calculations involve a few steps.

Primarily, considering that this dissertation operates with CPV, the PV F-Chart allows the choice of a 2-axis tracking array option, because CPV technologies track the sun on two-axis as the primary condition for proper operation.

Secondly, inside the Weather tab of PV F-Chart, one needs to select the weather data of Malta for the project.

Last but not least, in the Load tab, Change/View load button, it is very important to set all the load values to 0, because the scope is to feed all the generated energy to the grid and to supply local loads.

Once all these settings are changed, one display, as shown in Figure 69, pops up on the screen. It is in this display named "Utility Interface System" where all the device parameters have to be introduced.
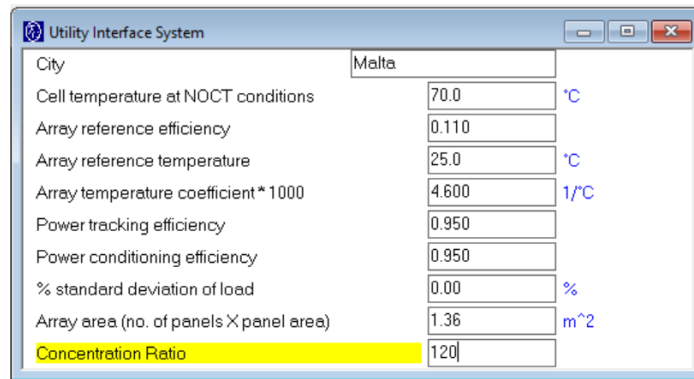
Figure 68: "Utility Interface System" window in PV F-Chart [76].

Once all the fields are filled, one can press the Calculate button in PV F-Chart, which will return another window called "System Performance Results", as shown in Figure 70, in which all the results of the simulation are displayed. The column "Sell" provides the results of interest, the production of electricity in kWh for each month. These results will be represented in graphs through transferring them to an Excel spreadsheet [75].

Figure 69: "System Performance Results" window with the results in PV F-Chart [76].

CHAPTER 4: RESULTS AND DISCUSSION

This chapter presents the findings of the study beginning with the exposure of all the highlighted best possible spots as reported by ArcMap [67] and continuing with the estimated generation of energy through the analysis of the obtained results from PV F-Chart [76], which present the energy production if a commercial product (from section 2.6) is implemented.

4.1 Exposure of the best possible spots

The best locations and their data returned from ArcMap are shown in Table 17. Looking at the radiation values returned from ArcGIS and grouped in the mean parameter at the table, it can be easily noticed that the values are comparatively low to what is to be expected in the region of 1825 kWh/m².year on the horizontal. Apparently, ArcGIS does not return the total global radiation on the horizontal but only the beam horizontal component of that radiation. The missing part is an average of about 35% diffuse radiation Therefore, given limitations, the calculations were manually carried out by adding a constant percentage of 35% to the beam radiation that ArcGIS has returned for each site, as shown in table 18.

Table 19 shows the characteristics of each location by its coordinates and a key parameter related to its dimensions, moreover than being presented one by one through images obtained from Google Earth [68].

Table 17: Numerical analysis of each location, obtained with ArcMap [67].

Fid	Shape	Count	Area (m²)	Min-Max beam rad (kWh)	Range	Mean beam rad (kWh/m² /year)	Std	Beam total radiation (MWh/year)
37	Polygon	37	925	1342.64-1350.06	7.43	1348.31	1.59	1247.18
21	Polygon	13	325	1342.62-1343.62	0.99	1343.16	0.26	436.53
137	Polygon	33	825	1338.49-1340.95	2.46	1339.76	0.53	1105.3
54	Polygon	18	450	1323.73-1344.55	20.83	1338.87	5.32	602.49
19	Polygon	45	1125	1335.75-1339.43	3.68	1338.08	0.82	1505.34
154	Polygon	81	2025	1331.80-1339.70	7.90	1337.69	2.05	2708.82
73	Polygon	53	1325	1334.40-1337.65	3.26	1336.94	0.60	1771.45
72	Polygon	27	675	1336.27-1337.41	1.14	1336.71	0.27	902.28
74	Polygon	42	1050	1334.22-1337.39	3.17	1336.08	0.72	1402.89
75	Polygon	106	2650	1319.05-1337.91	18.86	1335.89	2.43	3540.1
67	Polygon	91	2275	1323.93-1336.99	13.07	1335.18	1.60	3037.54
49	Polygon	25	625	1332.12-1335.88	3.76	1334.72	1.00	834.2
42	Polygon	33	825	1330.00-1336.71	6.71	1334.52	1.52	1100.97
144	Polygon	18	450	1325.52-1336.75	11.22	1334.43	2.71	600.49
167	Polygon	24	600	1331.12-1336.09	4.97	1334.26	1.32	800.56
3	Polygon	65	1625	1324.08-1336.49	12.40	1333.78	2.34	2167.39
68	Polygon	146	3650	1311.40-1336.48	25.08	1333.49	2.87	4867.24
1	Polygon	41	1025	1313.10-1338.76	25.66	1332.89	5.73	1366.21
69	Polygon	70	1750	1308.69-1335.93	27.23	1332.80	4.30	2332.4
85	Polygon	27	675	1331.36-1333.30	1.94	1332.68	0.48	899.56
122	Polygon	8	200	1328.61-1335.89	7.28	1332.64	2.77	266.53
17	Polygon	21	525	1329.40-1334.89	5.50	1332.64	1.16	699.63
78	Polygon	42	1050	1309.15-1335.17	26.02	1331.68	4.73	1398.26
70	Polygon	30	750	1321.98-1334.11	12.13	1331.48	2.68	998.61
121	Polygon	41	1025	1318.59-1336.72	18.13	1331.42	3.89	1364.71
22	Polygon	8	200	1328.04-1334.80	6.77	1331.35	1.90	266.27
32	Polygon	22	550	1327.27-1332.52	5.25	1330.19	1.41	731.6
89	Polygon	44	1100	1317.69-1331.16	13.47	1328.01	2.46	1460.81
87	Polygon	8	200	1320.69-1331.07	10.38	1327.34	2.97	265.47
47	Polygon	20	500	1324.21-1328.99	4.78	1327.30	1.43	663.65
48	Polygon	60	1500	1310.91-1330.49	19.58	1327.05	4.68	1990.57
46	Polygon	9	225	1321.71-1328.40	6.69	1327.02	2.33	298.58
81	Polygon	14	350	1324.88-1328.47	3.60	1326.99	1.24	464.45
34	Polygon	12	300	1317.50-1331.50	14.00	1326.64	3.65	397.99
52	Polygon	18	450	1325.60-1326.53	0.93	1326.32	0.22	596.84
82	Polygon	8	200	1323.21-1327.77	4.55	1326.15	1.45	265.23
50	Polygon	20	500	1325.15-1326.36	1.21	1325.81	0.33	662.91
51	Polygon	24	600	1316.48-1326.88	10.40	1325.53	2.32	795.32
88	Polygon	19	475	1310.82-1331.35	20.53	1324.61	5.19	629.19

Table 18: Radiation returned from ArcGIS and total global radiation on the horizontal for every location.

Fid	Mean (kWh/m²/year)	Total rad (kWh/m²/year)	Fid	Mean (kWh/m²/year)	Total rad (kWh/m²/year)
37	1348.31	1820.2185	122	1332.64	1799.064
21	1343.16	1813.266	17	1332.64	1799.064
137	1339.76	1808.676	78	1331.68	1797.768
54	1338.87	1807.4745	70	1331.48	1797.498
19	1338.08	1806.408	121	1331.42	1797.417
154	1337.69	1805.8815	22	1331.35	1797.3225
73	1336.94	1804.869	32	1330.19	1795.7565
72	1336.71	1804.5585	89	1328.01	1792.8135
74	1336.08	1803.708	87	1327.34	1791.909
75	1335.89	1803.4515	47	1327.3	1791.855
67	1335.18	1802.493	48	1327.05	1791.5175
49	1334.72	1801.872	46	1327.02	1791.477
42	1334.52	1801.602	81	1326.99	1791.4365
144	1334.43	1801.4805	34	1326.64	1790.964
167	1334.26	1801.251	52	1326.32	1790.532
3	1333.78	1800.603	82	1326.15	1790.3025
68	1333.49	1800.2115	50	1325.81	1789.8435
1	1332.89	1799.4015	51	1325.53	1789.4655
69	1332.8	1799.28	88	1324.61	1788.2235
85	1332.68	1799.118			

:

The global solar radiation values shown above are now in line with the long-term solar radiation in Malta of 1825 kWh/m²/year.

FID	Figure number	Location	Coordinates		Characteristic parameter
37	71	Roundabout	35º53'30" N	14º24'17" E	R = 17.16 m
21	72	Roundabout	35º50'20" N	14º27'49" E	R = 10.17 m
137	73	Roundabout	35º53'30" N	14º25'32" E	R = 16.21 m
54	74	Roundabout	35º57'20" N	14º21'28" E	R = 11.97 m
19	75	Roundabout	35º50'54" N	14º28'55" E	R = 18.92 m
154	76	Land portion	35º51'41" N	14º28'21" E	A = 2025 m²
73	77	Land portion	35º48'55" N	14º30'33" E	A = 1325 m²
72	77	Roundabout	35º48'55" N	14º30'34" E	R = 14.66 m
74	77	Land portion	35º48'54" N	14º30'34" E	A = 1050 m²
75	77	Land portion	35º48'55" N	14º30'35" E	A = 2650 m²
67	78	Car park	35º48'49" N	14º30'15" E	A = 2275 m²
49	79	Roundabout	35º58'35" N	14º20'47" E	R = 14.1 m
42	80	Roundabout	35º55'00" N	14º25'03" E	R = 16.21 m
144	81	Roundabout	35º54'22" N	14º26'19" E	R = 11.97 m
167	82	Roundabout	35º55'05" N	14º25'32" E	R = 13.82 m
3	83	Roundabout	35º51'21" N	14º29'20" E	R = 22.74 m
68	84	Land portion	35º48'48" N	14º30'42" E	A = 3650 m²
1	85	Roundabout	35º49'23" N	14º30'08" E	R = 18.06 m
69	84	Land portion	35º48'48" N	14º30'42" E	A = 1750 m²
85	86	Roundabout	35º53'29" N	14º32'19" E	R = 8.46 m
122	87	Roundabout	35º54'23" N	14º28'29" E	R = 7.98 m
17	88	Roundabout	35º50'55" N	14º31'31" E	R = 12.93 m
78	89	Car park	35º48'25" N	14º31'04" E	A = 1050 m²
70	90	Roundabout	35º48'47" N	14º30'49" E	R = 15.45 m
121	87	Land portion	35º54'23" N	14º28'28" E	A = 1025 m²
22	91	Roundabout	35º50'31" N	14º27'54" E	R = 7.98 m
32	92	Roundabout	35º53'03" N	14º32'33" E	R = 13.23 m
89	93	Roundabout	35º53'40" N	14º31'49" E	R = 18.71 m
47	94	Roundabout	35º59'10" N	14º20'31" E	R = 12.62 m
48	95	Car park	35º58'51" N	14º19'58" E	A = 1500 m²
46	96	Land portion	35º59'13" N	14º19'41" E	A = 225 m²
81	97	Car park	35º52'03" N	14º34'24" E	A = 350 m²
52	98	Roundabout	35º58'09" N	14º20'59" E	R = 11.97 m
50	98	Land portion	35º58'10" N	14º20'59" E	A = 500 m²
51	98	Land portion	35º58'09" N	14º21'00" E	A = 600 m²
88	93	Land portion	35º53'39" N	14º31'50" E	A = 475 m²

Figure 70: Location FID 37.

Figure 71: Location FID 21.

Figure 72: Location FID 137.

Figure 73: Location FID 54.

Figure 74: Location FID 19.

Figure 75: Location FID 154.

Figure 76: Locations FID 72, 73, 74 and 75.

Figure 77: Location FID 67.

Figure 78: Location FID 49.

Figure 82: Location FID 3.

Figure 79: Location FID 42.

Figure 83: Location FID 68 and 69.

Figure 80: Location FID 144.

Figure 84: Location FID 1.

Figure 81: Location FID 167.

Figure 85: Location FID 85.

Figure 86: Location FID 121 and 122.

Figure 90: Location FID 22.

Figure 87: Location FID 17.

Figure 91: Location FID 32.

Figure 88: Location FID 78.

Figure 92: Location FID 88 and 89.

Figure 89: Location FID 70.

Figure 93: Location FID 47.

89

Figure 94: Location FID 48.

Figure 96: Location FID 81.

Figure 95: Location FID 46.

Figure 97: Location FIDs 50, 51 and 52.

As can be seen in all the figures above, all the possible places chosen overcome all the conditioning factors, fulfilling the main requirement of free space or non-interference with the main purpose of the place. The spots are placed in descending order according to the availability of solar radiation on the site (MEAN), which is the most interesting parameter that is going to be used for all the calculations related to electricity production by the different systems.

It is important to mention that, as shown in Figure 79, the study carried out in this dissertation has considered the whole of Malta territory. That is the main reason why the resultant spots are scattered all over the island, although a small concentration can be noted in the southern part of the island due to its favourable plain level compared to other parts of the island, as returned by the DSM, Hillshade and scope layers created in ArcMap. Another advantage of having such systems distributed around the island is to reduce visual impact given that the systems will be modular and also serve as an awareness-raising initiative to encourage citizens to embrace more renewable energy systems in their own households or properties.

Figure 98: A map of Malta with all the locations previously exposed [68].

4.2   Estimation of energy generation

As far as electricity generation is concerned, as it was well explained in Chapter 3: Methodology, only CPV is analytically analysed here. The lack of available CSP systems on the market as well as the mandatory fulfilment of the restrictive conditions set by various factors makes it too difficult a task of finding Stirling Dish systems that are

already tested and reliable. The only available Stirling Dish option from the company "Oriental Great Ocean New Energy Technology Development" after a deep research on the global market does not specify and makes it hard to obtain results. Moreover, after getting in touch with the manufacturer of the system to try to obtain a possible estimation, it was confirmed that there is no specific software that can be used to estimate the output of this system.

On the other hand, the calculation of energy output from CPV systems were carried out using PV F-Chart software [76]. The systems that were evaluated included:

- Zytech 120x MCPV
- uM, uM2 and uM6
- BSQ-D280/53 HCPV

Table 20 shows all the input parameters for the different systems as introduced in the appropriate "Utility Interface System" menu of PV F-Chart.

Table 20: Characterization parameters introduced in the "Utility Interface System" PV F-Chart menu for each collector.

	Zytech 120x MCPV	uM	uM2	uM6	BSQ-D280/53 HCPV
Cell temperature at NOCT conditions (ºC)	70	70	70	70	70
Array reference efficiency	0.18	0.3	0.3	0.3	0.28
Array reference temperature (ºC)	25	25	25	25	25
Array temperature coefficient*1000 (1/°C)	4.6	1.4	1.4	1.4	2.1
Power tracking efficiency	0.95	0.95	0.95	0.95	0.95
Power conditioning efficiency	0.95	0.95	0.95	0.95	0.95
(%) standard deviation of load	0	0	0	0	0
PV active cells area / module (m^2)	0.02304	0.01089	0.02178	0.06534	0.059112
Concentration Ratio (x)	120	180	180	180	180

As can be noticed, there are some coincident values through all systems for a few specifications such as the cell temperature at NOCT conditions, the array reference temperature, the power tracking efficiency, the power conditioning efficiency, the standard deviation of load or the concentration ratio. These similarities are correct.

The only parameter that is not fully correct is the concentration ratio of 180, because the PVF-Chart has a limitation of accepting greater values.

Nevertheless, a test was carried out for different concentration ratios and it was found that the calculated energy output is practically proportional to concentration , with very little drop due to higher temperatures at higher concentration ratios.

Therefore, the solution taken to achieve the total energy output of a 900x solar concentration system, was to first determine the outcome results from PV F-Chart for a concentration ratio of 180, import the results to an Excel Spreadsheet [75], and upscale the results by multiplying them by 5 to reach a concentration ratio of 900.

As a result, Table 21 shows the estimated monthly and annual energy generation in kWh for each system throughout a year.

Table 21: Electrical energy generation for each system by month and yearly total.

	Output energy to the grid [kWh]				
Month	Zytech 120x MCPV	uM	uM2	uM6	BSQ-D280 HCPV
Jan	57.10	326.50	653.00	1959.50	1518.37
Feb	57.70	330.00	660.50	1981.50	1534.77
Mar	83.60	480.00	959.50	2879.00	2228.58
Apr	83.40	482.00	963.50	2891.00	2234.96
May	106.50	621.50	1243.00	3729.50	2876.38
Jun	110.40	653.00	1306.00	3917.50	3012.59
Jul	117.80	703.00	1406.50	4219.00	3238.09
Aug	109.70	656.00	1311.50	3935.00	3018.97
Sep	85.10	505.50	1011.00	3032.50	2330.17
Oct	77.80	457.00	913.50	2741.00	2111.50
Nov	61.70	358.00	716.50	2149.50	1659.59
Dec	54.20	311.00	622.50	1867.50	1445.48
Year	1004.90	5883.50	11767.50	35302.50	27208.97

However, it is important to calculate the energy generation of each system per m² of total module area because the whole module would need to be placed in the earmarked sites and not only the active solar cell area. This would be detrimental in choosing the best option for the earmarked sites. Results are shown in Table 22 and are expressed in kWh/m² of total concentrator module area.

Table 22: Energy generation for each system per square metre of cell surface.

	Power generation per total solar module area [kWh/m^2]				
Month	Zytech MCPV (120x)	uM (900x)	uM2 (900x)	uM6 (900x)	BSQ-D280/53 HCPV (820x)
Jan	41.99	29.15	29.15	29.16	28.24
Feb	42.43	29.46	29.49	29.49	28.55
Mar	61.47	42.86	42.83	42.84	41.45
Apr	61.32	43.04	43.01	43.02	41.57
May	78.31	55.49	55.49	55.50	53.50
Jun	81.18	58.30	58.30	58.30	56.04
Jul	86.62	62.77	62.79	62.78	60.23
Aug	80.66	58.57	58.55	58.56	56.16
Sep	62.57	45.13	45.13	45.13	43.34
Oct	57.21	40.80	40.78	40.79	39.28
Nov	45.37	31.96	31.99	31.99	30.87
Dec	39.85	27.77	27.79	27.79	26.89
Year	738.90	525.31	525.33	525.33	506.12

The visual comparison shown in Table 23, also includes as an option, the expected output of a conventional flat-plate PV, whose generation in Malta is 1600 kWh/5.5 m^2. As can be seen, the systems with the best production of electricity per surface unit area are the CPV. Effectively, this is the direct result of using concentration ratios for these systems. It is remarkable the high generation output returned from Zytech per m² of module area, which has lower concentration ratios than the other CPV. This is probably achieved because lower concentration ratios would not require large module area to allow for cooling, and therefore an optimum module area to concentration ratio is achieved by Zytech.

Table 23: Annual generation of power, comparative table.

System	m^2	kWh/m^2 per year
Zytech 120x MCPV	1.36	738.897
uM	11.2	525.313
uM2	22.4	525.335
uM6	66	525.335
BSQ-D280 HCPV	25.25	506.119
Conventional Flat Plate PV	5.5	290.909

On the other hand, the lowest production is returned from the conventional flat plate PV because its concentration ratio is equal to 1.

Figure 99 shows the monthly output for each of the analysed CPV systems in MWh/m²/year. Clearly, more energy is generated in summer when the direct solar irradiance is higher.
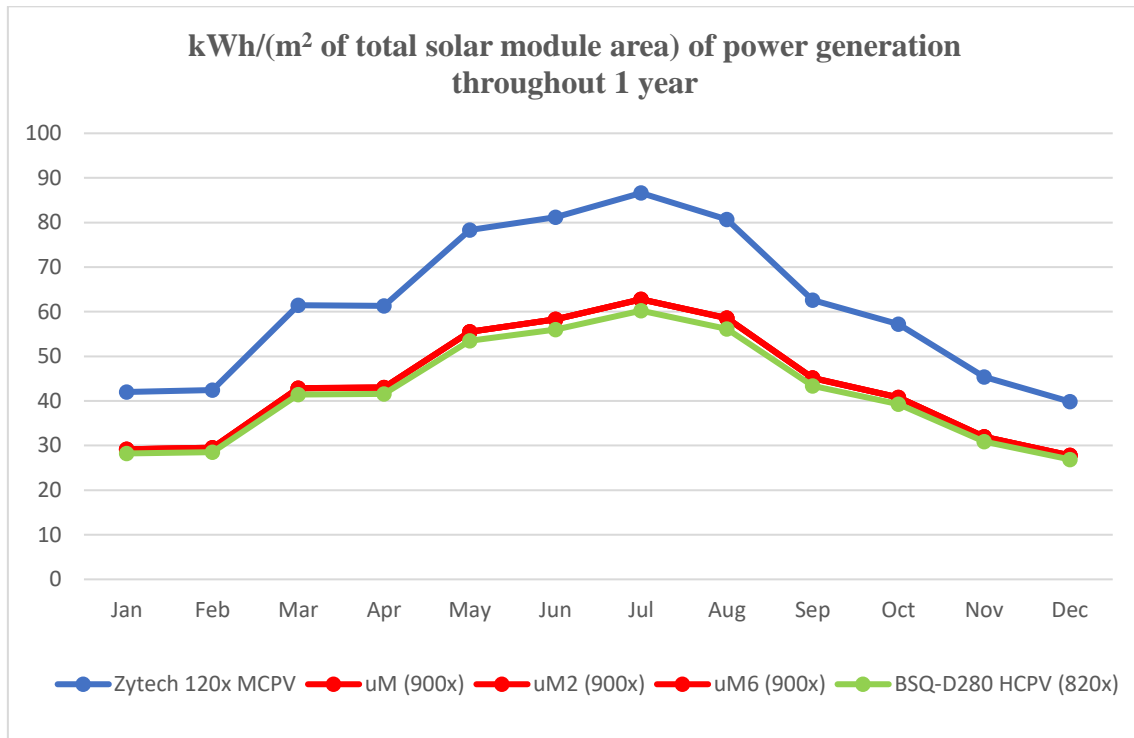
Figure 99: Modelled monthly outputs per total solar module area throughout a year.

In the graph, all technologies based on the uM cell technology achieve the same output per m² of module area and therefore the three lines are superimposed on top of each other.

Another comparative study is shown in Tables 24, 25 and Figure 100 below, whereby the energy generated is calculated per unit of concentration ratio of each system.

Table 24: Power generation of each system per concentration unit.

Power generation per concentration unit [kWh/x]				
Month	Zytech MCPV 120x	uM (900x)	uM2 (900x)	uM6 (900x)	BSQ-D280/53 HCPV (820x)
Jan	0.4758	0.363	0.726	2.177	1.852
Feb	0.4808	0.367	0.734	2.202	1.872
Mar	0.6967	0.533	1.066	3.199	2.718
Apr	0.6950	0.536	1.071	3.212	2.726
May	0.8875	0.691	1.381	4.144	3.508
Jun	0.9200	0.726	1.451	4.353	3.674
Jul	0.9817	0.781	1.563	4.688	3.949
Aug	0.9142	0.729	1.457	4.372	3.682
Sep	0.7092	0.562	1.123	3.369	2.842
Oct	0.6483	0.508	1.015	3.046	2.575
Nov	0.5142	0.398	0.796	2.388	2.024
Dec	0.4517	0.346	0.692	2.075	1.763
Year	8.3742	6.537	13.075	39.225	33.182

Table 25: Annual generation of power, comparative table

System	x	kWh/year per concentration unit (1x)
Zytech 120x MCPV	120	8.374
uM	900	6.537
uM2	900	13.075
uM6	900	39.225
BSQ-D280 HCPV	820	33.182
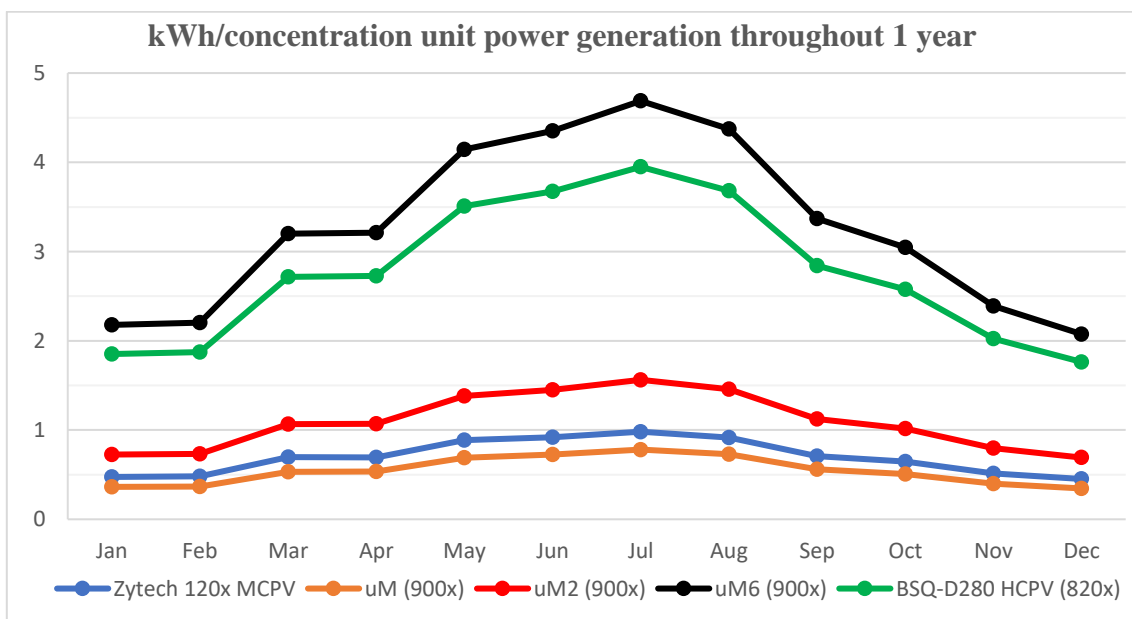
Figure 100: Energy generation per concentration ratio for different CPV modules.

Here, it is seen that the uM6 stands out as one of the best possible systems to be installed, but this is misleading, because this module occupies much larger space. Therefore, for cases where available area is limited, it is best to install the medium concentration ratio of Zytech, rather than the high concentration ratio of uM6 modules.

4.3 Contribution of CPV to the overall energy generation

In 2018, the total electricity consumption in Malta reached 2532 GWh of which solar photovoltaic systems generated 189.576 GWh [7].

If one were to install the Zytech 120x, uM6 or BSQ-D280/53 in the potential sites and considering that only 30% of the area will be occupied by these systems, in order to avoid cross-shading, then the total number of systems that can be installed can be calculated as represented in Tables 26, 27 and 28, respectively.

Table 26: Total number of Zytech 120x systems that can be installed.

Fid	Area	Theorical total panels	Real total panels	Fid	Area	Theorical total panels	Real total panels
37	925	204.0	204	122	200	44.1	44
21	325	71.7	72	17	525	115.8	116
137	825	182.0	182	78	1050	231.6	232
54	450	99.3	99	70	750	165.4	165
19	1125	248.2	248	121	1025	226.1	226
154	2025	446.7	447	22	200	44.1	44
73	1325	292.3	292	32	550	121.3	121
72	675	148.9	149	89	1100	242.6	243
74	1050	231.6	232	87	200	44.1	44
75	2650	584.6	585	47	500	110.3	110
67	2275	501.8	502	48	1500	330.9	331
49	625	137.9	138	46	225	49.6	50
42	825	182.0	182	81	350	77.2	77
144	450	99.3	99	34	300	66.2	66
167	600	132.4	132	52	450	99.3	99
3	1625	358.5	359	82	200	44.1	44
68	3650	805.1	805	50	500	110.3	110
1	1025	226.1	226	51	600	132.4	132
69	1750	386.0	386	88	475	104.8	105
85	225	49.6	50	Total number of systems			7748

Fid	Area	Theorical total panels	Real total panels	Fid	Area	Theorical total panels	Real total panels
37	925	3.6	4	122	200	0.8	1
21	325	1.3	1	17	525	2.1	2
137	825	3.2	3	78	1050	4.1	4
54	450	1.8	2	70	750	2.9	3
19	1125	4.4	4	121	1025	4.0	4
154	2025	7.9	8	22	200	0.8	1
73	1325	5.2	5	32	550	2.2	2
72	675	2.6	3	89	1100	4.3	4
74	1050	4.1	4	87	200	0.8	1
75	2650	10.4	10	47	500	2.0	2
67	2275	8.9	9	48	1500	5.9	6
49	625	2.5	3	46	225	0.9	1
42	825	3.2	3	81	350	1.4	1
144	450	1.8	2	34	300	1.2	1
167	600	2.4	2	52	450	1.8	2
3	1625	6.4	6	82	200	0.8	1
68	3650	14.3	14	50	500	2.0	2
1	1025	4.0	4	51	600	2.4	2
69	1750	6.9	7	88	475	1.9	2
85	225	0.9	1	Total number of systems			137

Table 28: Total number of BSQ-D280/53 systems that can be installed.

Fid	Area	Theorical total panels	Real total panels	Fid	Area	Theorical total panels	Real total panels
37	925	4.7	5	122	200	1.0	1
21	325	1.6	2	17	525	2.6	3
137	825	4.2	4	78	1050	5.3	5
54	450	2.3	2	70	750	3.8	4
19	1125	5.7	6	121	1025	5.2	5
154	2025	10.2	10	22	200	1.0	1
73	1325	6.7	7	32	550	2.8	3
72	675	3.4	3	89	1100	5.5	6
74	1050	5.3	5	87	200	1.0	1
75	2650	13.3	13	47	500	2.5	3
67	2275	11.4	11	48	1500	7.5	8
49	625	3.1	3	46	225	1.1	1
42	825	4.2	4	81	350	1.8	2
144	450	2.3	2	34	300	1.5	2
167	600	3.0	3	52	450	2.3	2
3	1625	8.2	8	82	200	1.0	1
68	3650	18.4	18	50	500	2.5	3
1	1025	5.2	5	51	600	3.0	3
69	1750	8.8	9	88	475	2.4	2
85	225	1.1	1	Total number of systems			177

Table 29 shows the summary of all the calculations for the overall total potential of generating CPV from the earmarked sites. The "% over the total energy consumption" indicates the percentage energy generation share of installing CPV in the earmarked sites compared to the total 2018 electrical energy consumption in Malta. While the "% over PV total generation" is the comparison of the CPV output to that generated by all installed flat PV systems in Malta, basis year 2018.

Table 29: Potential total production.

	Zytech 120x	uM6	BSQ-D280/53
Total production (GWh/year)	7.786	4.836	4.816
% over total consumption	0.31	0.19	0.19
% over PV total generation	4.11	2.55	2.54

Results reflect how Zytech stands out as the best option of CPV for Malta.

While the percentage share of CPV seems to be low, one needs to appreciate that the earmarked sites are currently under-utilised when it comes to renewable energy generation. Moreover, with the increase of electric cars on the Island, the production of renewable energy during the day will further contribute to greening the transport sector.

4.3.1 Contribution of CPV to households

In Malta, the average annual electricity consumption stands at 5,000 kWh per person, according to recent statistics [77]. Considering an average of three people living per household, then the different CPV systems installed in the earmarked areas would offset the equivalent of hundreds of households, as shown in Table 30.

Table 30: Households fed with the energy generation

	Zytech 120x	uM6	BSQ-D280/53
Total houses	519	322	321

4.4 CO$_2$ reduction potential analysis

Considering data issued in 2017 [78] the estimated amount of CO$_2$ per kWh generated in Malta stands at about 441.77 tCO$_2$/GWh per year. Hence, if one were to install the systems in the potential sites and considering each system production, the potential CO$_2$ reduction is shown in table 31.

Table 31: Potential CO$_2$ reduction

	Zytech 120x	uM6	BSQ-D280/53
Total CO2 reduction (tCO2/year)	3439.60	2136.59	2127.55

CHAPTER 5: CONCLUSIONS AND RECOMMENDATIONS

5.1 Conclusions

This results achieved have successfully provided answers to the prime aims of this dissertation, namely, to evaluate the potential of installing concentrated solar systems in under-utilised public land on arterial roads, such as roundabouts.

Numerous challenges in using the relevant software were encountered but were overcome with the support of the supervisor and co-supervisor.

Among the challenges encountered, one may highlight first, the challenge to inspect the Maltese territory looking out for some spaces in such a densely populated country. To achieve this, an extensive spatial analysis was carried out as well as a quantification of the solar insolation to determine the best possible sites to place the concentrator systems. This study was realized using ArcGIS, a geographical information software, which returned both, analytical results with numerical quantities and visual results through mapping all of Malta's territory with several layers such as solar radiation or topographical features as slopes or heights. The study has found about 170 potential sites but these were reduced to about 40, after applying certain constraints such as the minimum size of a site of 200 m².

Moreover, this dissertation has carried out an extensive search for all possible small-scale concentrator technology that can be applied. One important conclusion was that Stirling Engine concentrator systems that were very popular a few years back have virtually disappeared from the market, making way for concentrated photovoltaic systems. To this end, a number of commercial products have been studied and analysed in terms of their output under Maltese climatic conditions and solar irradiation availability. This was achieved by the use of the PVF-Chart sizing software.

Finally, the objective of calculating the potential contribution of these CPV systems in the earmarked sites was calculated and it was found that a conservative 7786 MWh/year can be generated from the Zytech, which had the best output per m² of concentrator area, which is equivalent to 0.31 % of the total electrical energy consumption in 2018. This is equivalent to supplying electricity for 519 dwellings per year and saving 3440 tonnes of carbon dioxide per year. This will contribute towards achieving Malta's commitment to further its renewable energy portfolio.

Solar concentrator systems can bring an element of diversification of renewable energy systems to Malta and contribute towards increasing the renewable energy share, while bringing more awareness to the general public who will be seeing these systems working in practice.

5.2   Recommendations for further work

A number of recommendations are hereby presented for future studies:

1. This project only evaluate the best 40 locations out of a potential of 170 sites. In evaluating the other remaining sites, attention should be given to the standard deviation parameter of solar radiation as calculated by the software ArcGIS, as it provides the expected dispersion of the average solar radiation measure.

2. This dissertation has documented in detail all the steps that are needed to carry out a spatial analysis of potential sites. Based on this, analysis of the Gozo Island can be carried out to identify similar potential sites for the installation of solar concentrator systems, thus contributing to the sustainability of the island.

3. The identified CPV systems can also be installed on potential rooftops. Therefore, a study can be carried out to evaluate spaces on large industrial rooftops, storage warehouses and other potential non-residential roofs.

4. Carry out a detailed economic analysis, taking into consideration not only the capital cost of the system but also other expenses such as construction of base for the CPV systems, cabling, connection to the grid and maintenance costs.

REFERENCES

[1]   European Comission, *Initiative for Global Leadership in CSP Implementation Plan,* p.3. [Online]. Available: https://setis.ec.europa.eu/system/files/set_plan_-_csp_initiative_implementation_plan.pdf. [Accessed: Oct. 16, 2020].

[2]   European Commission official website, "2050 long-term strategy," November 28, 2018. [Online]. Available: https://ec.europa.eu/clima/policies/strategies/2050_en. [Accessed: Oct. 16, 2020].

[3]   European Commission official website, "2030 climate and energy framework," November 28, 2018. [Online]. Available: https://ec.europa.eu/strategies/2030. [Accessed: Oct 16, 2020].

[4]   European Commission, *European Union Strategic Energy Technology Plan*, Publications Office of the European Union, Luxembourg, 2018. [Online]. doi:10.2777/04888.

[5]   European Commission official website, "2020 climate and energy package," November 28, 2018. [Online]. Available: https://ec.europa.eu/strategies/2020. [Accessed: Oct 16, 2020].

[6]   The European Parliament and the Council of the EU, "*DIRECTIVE 2009/28/EC on the promotion of the use of energy from renewable sources*," EU Publications Office, Luxembourg, April, *ANNEX1 National Overall targets,* 2009.

[7]   National Statistics Office (NSO), *News Release 163/2019*. Valletta, Malta, Oct 8, 2019. [Online]. Available: https://nso.gov.mt/en/News_Releases/View_by_Unit/Unit_02/Regional_and_Geospatial_Statistics/Documents/2019/News2019_163.pdf.

[8]   Enemalta pc, "Delimara Power Station," February 27, 2018. [Online]. Available: https://www.enemalta.com.mt/delimara-power-station/. [Accessed: Oct 18, 2020]

[9]   *Total finally energy consumption by sector in Malta*, International Energy Agency (IEA), 2018. [Online]. Available: https://www.iea.org/countries/malta.

[10]   European Statistical Office (Eurostat), *News Release 26/2019,* p 2. Luxembourg, Feb 7, 2019.

[11] World Energy Council, "*2020 World Energy Trilemma Index.*" [Online]. Available: https://trilemma.worldenergy.org/.

[12] National Statistics Office (NSO), *News Release 099/2020,* pp. 5-8. Valletta, Malta, June 18, 2018. [Online]. Available: https://nso.gov.mt/en/News_Releases/Documents/2020/06/News2020_099.pdf.

[13] *Global Horizontal Irradiation for Malta and Europe*, Solargis, 2019. [Online]. Available: https://solargis.com/maps-and-gis-data/download/malta.

[14] The Malta Environment and Planning Authority, *Development Control Design Policy, Guidance and Standards 2015,* Marsa, Malta. Nov 3, p. 168, 2015.

[15] "Malta must pay Estonia €2 million to reach renewable energy targets," Times of Malta, Jan. 25, 2020.

[16] European Statistical Office (Eurostat), "Renewable energy statistics," Jan 2020. [Online]. Available: https://ec.europa.eu/eurostat/statistics-explained.

[17] K. Lovegrove, J. Zapata and G. Nathan, "Concentrating Solar Thermal," Australian Academy of Science, Jun 21, 2016. [Online]. Available: https://www.science.org.au/curious/technology-future/concentrating-solar-thermal.

[18] "Renewables 2020 Global Status Report," REN21, Paris REN21 Secretariat, 2020, ISBN 978-3-948393-00-7.

[19] Global Data Power Database. [Online]. Available: https://www.globaldata.com/.

[20] JL. Sawin and E. Martinot, "Renewables Bounced Back in 2010, Finds REN21 Global Report," *Renewable Energy World*, Sept 29, 2011. [Online]. Available: http://www.renewableenergyworld.com. [Accessed Nov 4, 2020].

[21] PROTERMOSOLAR, "The cost of Concentrated Solar Power fell by 47% between 2010 and 2019," *Helioscsp* Jul 29, 2020. [Online]. Available: http://helioscsp.com/the-cost-of-concentrated-solar-power-fell-by-47-between-2010-and-2019/. [Accessed Nov 19, 2020].

[22] IRENA-International Renewable Energy Agency Database. [Online]. Available: https://www.irena.org/Statistics/.

[23]   SA. Kalogirou, *Solar Energy Engineering (Second Edition)*, Academic Press, Nov 14, 2013, ISBN: 9780123972705.

[24]   Scarabeus Project. [Online]. Available: https://www.scarabeusproject.eu/.

[25]   P. Falcone, J. Noring and J. Hruby, "Assessment of a Solid Particle receiver for a High Temperature Solar Central Receiver System," SANDIA National Laboratories, Livermore, California, United States, Tech. Report AC04-76DR00789, Feb 1, 1985.

[26]   G.N. Tiwari, A.Tiwari and Shyam, "Handbook of solar energy: Theory, Analysis and Applications," Springer, 2016, ISBN: 978-981-10-0807-8, pp. 247-275, 605-608.

[27]   D. Lebrón, *Replanteo de instalaciones solares térmicas.* Sevilla: MAD, 2012, p 80, ISBN: 978-84-676-7542-9.

[28]   G.N. Tiwari, D. Atheaya and A. Tiwari, "Review on solar thermal power concentrators," MedCrave, Volume 1 Issue 3, Sept 25, 2017, doi: 10.15406/mojsp.2017.01.00016.

[29]   M.G. Rasul, A.K. Azad and S.C. Sharma, *Clean Energy for Sustainable Development*, Academic Press, 2016, pp. 213-235, ISBN: 978-0-12-805423-9.

[30]   S.C. Bhatia, *Advanced Renewable Energy Systems*. Woodhead Publishing India, 2014, pp. 94-143, ISBN: 978-1-78242-269-3.

[31]   P. Breeze, *Power Generation Technologies.* Oxford: Elsevier Ltd., 3rd edition 2019, pp. 293-321, ISBN: 9780081026311.

[32]   Office of Energy Efficiency & Renewable Energy, *Concentrating Solar Power Could Provide the Flexibility and Reliability the U.S. Electric Grid Needs*, Washington DC, Nov 3, 2017. [Online]. Available: https://www.energy.gov/eere/articles/concentrating-solar-power-could-provide-flexibility-and-reliability-us-electric-grid. [Accessed: Nov 28, 2020].

[33]   Z. Wang, *Design of Solar Thermal Power Plants.* Cambridge, MA: Agence Press, 2019, pp. 1-46, ISBN: 9780128162194.

[34]   Torresol Energy. [Online]. Available: https://torresolenergy.com/en/.

[35]   K. Lovegrove and W. Stein, *Concentrating Solar Power Technology - Principles, Developments and Applications*, Woodhead Publishing, 2012, ISBN: 978-1-84569-769-3.

[36]   Almería Solar Platform PSA. [Online]. Available: http://www.psa.es/es/index.php

[37]   S. Qazi, *Standalone Photovoltaic (PV) Systems for Disaster Relief and Remote Areas*, Elsevier, 2016, pp. 217-237, doi: 10.1016/C2014-0-03107-3.

[38]   Eduardo Zarza-Moya, "Concentrating Solar Thermal Power - Parabolic Dishes" in *A Comprehensive Guide to Solar Energy Systems*, T. Letcher and V. Fthenakis, Academic Press, 2018, pp. 127-148, doi: 10.1016/C2016-0-01527-9.

[39]   M. H. Baig, D. Surovtseva and E.Halawa, "The Potential of Concentrated Solar Power for remote mine sites in the Northern Territory, Australia," *Journal of Solar Engineering*, vol.2005, p 3, 2015, doi: 10.1155/2015/617356.

[40]   "Concentrating solar power: its potential contribution to a sustainable energy future," European Academies Science Advisory Council, EASAC policy report 16, Nov 2011, pp. 9-10, ISBN: 978-3-8047-2944-5.

[41]   "Concentrated Photovoltaics," Zytech Solar. [Online]. Available: https://zytechsolar.com/concentrated-photovoltaics/. [Accessed: Dec 17, 2020].

[42]   Fraunhofer Institute for Solar Energy Systems ISE , *Levelized cost of electricity renewable energy technologies*, March 2018. [Online]. Available: https://www.ise.fraunhofer.de/content/dam/ise/en/documents/publications/studies/EN2018_Fraunhofer-ISE_LCOE_Renewable_Energy_Technologies.pdf.

[43]   P. Metz, "SolFocus Concentrator Photovoltaics," *ISETC*, Oct 2010, p. 1. [Online]. Available: http://www.isetc.org/English/Archives/201010/Presentations.html

[44]   K. Horowitz, M. Woodhouse, H. Lee & G. Smestad, "A bottom-up cost analysis of a high concentration PV module," *11th Intern. Conf. On CPV Systems: CPV-11*, 2015, p. 3, doi: 1679. 100001. 10.1063/1.4931548.

[45]   O. Loidi, "The Future of Solar Energy: High Concentrated Photovoltaic (CPV) Cells," *ennomotive.com*. May 20, 2019. [Online]. Available: https://www.ennomotive.com/future-of-solar-energy/. [Accessed: Dec 17, 2020].

[46]   Fraunhofer Institute for Solar Energy Systems ISE and National Renewable Energy Laboratory NREL, *Current status of concentrator photovoltaic (CPV) technology.   Version   1.3,*   April   2017.   [Online].   Available: https://www.ise.fraunhofer.de/content/dam/ise/de/documents/publications/studies/cpv-report-ise-nrel.pdf.

[47]   X. Ju, C. Xu, Y. Hu, X. Han, G. Wei and X. Du, "*A review on the development of photovoltaic/concentrated solar power (PV-CSP) hybrid systems,*" in Solar Energy Materials and Solar Cells, vol. 161, 2017, pp. 305-327, ISSN 0927-0248.

[48]   M. Rycroft, "CSP-PV hybrid power systems: An attractive future option," *EE Publishers*, May 27, 2019. [Online]. Available: https://www.ee.co.za/article/csp-pv-hybrid-power-systems-an-attractive-future-option.html. [Accessed: Dec 26, 2020].

[49]   Made-In-China, "Solar Powered Stirling Engine Generator (25kW)," *Made-In-China.com.*   [Online].   Available: https://www.made-in-china.com/showroom/susandgo/product-detailXBCmExYcgQVZ/China-Solar-Powered-Stirling-Engine-Generator-25kW-.html. [Accessed: Jan 11, 2021].

[50]   AEDesign, "Solar Invictus 53E," *AEDesign.com.pk.* [Online]. Available: https://aedesign.com.pk/energySolarInvictus53E.html. [Accessed: Jan 3, 2021].

[51]   C. Proudfoot, "RIPASSO CSP," atlasofthefuture.com, Aug 1, 2015. [Online]. Available: https://atlasofthefuture.org/project/ripasso-csp-system/. [Accessed: Jan 3, 2021].

[52]   World Construction Today , "New efficiency world record of Ripasso Energy gives lowest cost for Dish Stirling solar power," *WorldConstructionToday.com.* [Online]. Available: https://www.worldconstructiontoday.com/pressreleases/new-efficiency-world-record-of-ripasso-energy-gives-lowest-cost-for-dish-stirling-solar-power/. [Accessed: Jan 3, 2021].

[53]   A. Buscemi, V. Brano, C. Chiaruzzi, C. Giuseppina, C. Kalogeri, "A validated energy model of a solar dish-Stirling system considering the cleanliness of mirrors," in *Applied Energy,* Elsevier*,* vol. 260, article 114378, Feb 15, 2020, pp. 6-7, doi: 10.1016/j.apenergy.2019.114378.

[54] S. Mraz, "Infinia uses Stirling cycle for solar power and air conditioning," *MachineDesign.com*, Endeavor Business Media, Aug, 2011. [Online]. Available: https://www.machinedesign.com/markets/energy/article/21831691/infinia-uses-stirling-cycle-for-solar-power-and-air-conditioning. [Accessed: Jan 4, 2021].

[55] "PowerDish by Infinia," Infinia Corporation. [Online]. Available: http://www.powerplaysolar.com/PDFs/PowerDish_Brochure.pdf. [Accessed: Jan 4, 2021].

[56] Schlaich Bergermann und Partner, "HelioFocus 500 m² Big Dish – Prototype," *Schlaich Bergermann und Partner*, 2012. [Online]. Available: https://www.sbp.de/en/project/heliofocus-500-m2-big-dish-prototype/. [Accessed: Jan 4, 2021].

[57] S. Mincer, "Heliofocus Solar Technology Dish Unveiled in Israel," *GreenProphet.com,* May 10, 2012. [Online]. Available: https://www.greenprophet.com/2012/05/heliofocus-israel-china-launch/. [Accessed: Jan 4, 2021].

[58] T. Keck, M. Balz, Y. Blumenthal, "Large is Beautiful, Progress of HelioFocus 500 m^2 Dish," in *Energy Procedia*, Elsevier, vol 69, 2015, pp. 1597-1602, ISSN 1876-6102, doi: 10.1016/j.egypro.2015.03.114.

[59] Schlaich Bergermann und Partner, "HelioFocus Dish Demonstration Plant China," *Schlaich Bergermann und Partner*, 2013. [Online]. Available: https://www.sbp.de/en/project/heliofocus-dish-demonstration-plant-china/. [Accessed: Jan 4, 2021].

[60] Zytech Solar, "Zytech CPV 120X Medium Concentration PV," *Zytech Solar*, Zaragoza, Spain. [Online]. Available: http://zytech.es/brochures/5830/.

[61] Arzon Solar, "Universal CPV Module - uModule,", *Arzon Solar*, Seal Beach, CA, USA. [Online]. Available: https://www.arzonsolar.com/cpv-umodule/.

[62] BSQ Solar, "BSQ-D280 HCPV Module Abridged Data Sheet," *BSQ Solar,* Madrid, Spain. [Online]. Available: https://www.bsqsolar.com/products/.

[63] Suncore, "Z10 Combined Heat & Power," *Suncore.* [Online]. Available: http://suncoreus.com/wp-content/uploads/2015/02/Z10_Brochure_2pg.pdf

[64] R. Tanti, "Assessing the Potential of Installing Photovoltaic Panels in Car Parks to Reach 2020 EU Targets," Institute of Earth Systems, University of Malta, 2018. [Online]. Available: https://www.um.edu.mt/library/oar/handle/123456789/39545

[65] M. Farrugia Magro, "Design and Testing of a Low-level Concentrator," Institute for Sustainable Energy, University of Malta, 2015. [Online]. Available: https://www.um.edu.mt/library/oar//handle/123456789/6627.

[66] R. Mangion, M. Muscat, R. Ghirlando, T. Sant, C. Yousif and S. Vural, "Development of a Stirling engine powered by parabolic trough collectors," International Stirling Engine Conference, ISEC 2014, Bilbao. [Online]. Available: https://www.um.edu.mt/library/oar/handle/123456789/26391.

[67] *ArcGIS Desktop 10.6.1.9270.* (2018). ESRI. Redlands, California, USA.

[68] *Google Earth for Microsoft Edge browser.* (2020). Google. [Online]. Available: https://earth.google.com/.

[69] *Google Maps, Satellite, Street View.* (2020). Map of Malta. Google. [Online]. Available: https://www.google.com/maps/place/Malta/. [Accessed: Nov & Dec, 2020].

[70] "OpenStreetMap," *ESRI ArcGIS*, ESRI, Jan 6, 2020. [Online]. Available: https://www.arcgis.com/home/item.html?id=b834a68d7a484c5fb473d4ba90d35e71. [Accessed: Dec 5, 2020].

[71] Saurabh Singh, "Difference between DEM/DTM and DSM," *GIS Resources*, Sept 26, 2013. [Online]. Available: https://www.gisresources.com/confused-dem-dtm-dsm/. [Accessed: Dec 5, 2020].

[72] Malta Information Technology Agency MITA, *Digital Surface Model (DSM) of Malta,* DSM_LIDAR2012.

[73] ESRI, "How solar radiation is calculated," *ESRI ArcGIS for Desktop*. [Online]. Available: https://desktop.arcgis.com/en/arcmap/10.3/tools/spatial-analyst-toolbox/how-solar-radiation-is-calculated.htm. [Accessed: Dec 9, 2020].

[74] ESRI, "Modelling solar radiation," ESRI ArcGIS Pro. [Online]. Available: https://pro.arcgis.com/en/pro-app/tool-reference/spatial-analyst/modeling-solar-radiation.htm. [Accessed: Dec 3, 2020].

[75] *Excel Spreadsheet (2016).* Microsoft Office.

[76] *PV F-Chart Photovoltaic System Analysis version 3.62W.* (1993-202). F-Chart Software. Madison, Wisconsin, USA.

[77] T. Diacono, "How Maltese Households Started Being Charged More For Electricity Without Being Told," *Lovin Malta*, May 7, 2018. [Online]. Available: https://lovinmalta.com/opinion/analysis/how-maltese-households-started-being-charged-more-for-electricity-without-being-told/. [Accessed: Jan 27, 2021].

[78] *EEA 2017 CO2 emission intensity of electricity generation dataset*, European Environment Agency, Feb 13, 2020. [Online]. Available: https://www.eea.europa.eu/data-and-maps/data/co2-intensity-of-electricity-generation. [Accessed: Jan 27, 2021].

BIBLIOGRAPHY

V. Buhagiar, R. Farrugia, E. Scerri and C. Yousif, "Energy Profile for Malta," M.E.E.R.E.A., prepared for the "Renewable Energy for Development" newsletter published by the Stockholm Environment Institute (SEI), August 31, 2017.

"Energy 2020 A strategy for competitive, sustainable and secure energy," Communication from the Commission to the European Parliament, the Council, the European Economic and Social Committee and the Committee of the Regions. [Online]. Available: https://eur-lex.europa.eu. [Accessed: Oct 20, 2020].

"Concentrating Photovoltaics (CPV)," Green Rhino Energy. [Online]. Available: http://www.greenrhinoenergy.com/solar/technologies/pv_concentration.php. [Accessed: Dec 16, 2020].